UNDERSTANDING MOISTURE DYNAMICS IN THE VADOSE ZONE: TRANSCENDING THE DARCY SCALE

A Dissertation

by

NANDITA GAUR

Submitted to the Office of Graduate and Professional Studies of
Texas A&M University
in partial fulfillment of the requirements for the degree of

DOCTOR OF PHILOSOPHY

Chair of Committee,	Binayak P. Mohanty
Committee Members,	Yalchin Efendiev
	Sorin Popescu
	Patricia Smith
Head of Department,	Steve Searcy

December 2015

Major Subject: Biological and Agricultural Engineering

ABSTRACT

Soil moisture forms the interface at which the partitioning of the energy, carbon and water budget for the land-surface occurs. Its variability impacts different fields of application at varying extent scales like agriculture at the field scale, meteorology at the regional scale and climate change assessment at the global scale. However, past literature has focused on understanding soil moisture dynamics at this diverse range of extent scales using soil moisture data at the Darcy support scale which cannot effectively cater to soil moisture dynamics for the current eco-hydrologic models that describe complex heterogeneous domains at remote sensing footprint scales. This dissertation serves to push the envelope of our understanding of soil moisture dynamics and its dependence on land-surface heterogeneity at the coarse remote sensing scales. The research questions answered in this dissertation include 1) determining the dominant land-surface controls of near-surface soil moisture dynamics at scales varying between the Darcy (of the order of a few centimeters) support and satellite footprint scale (25.6 km); 2) generating a framework for quantifying the relationships between antecedent wetness, land-surface heterogeneity and near-surface soil moisture at remote sensing scales and 3) evaluating variability in the root zone moisture dynamics as evaluated through evapo-transpiration estimates at different remote sensing footprint scales. The dominant land-surface factors controlling soil moisture distribution at different scales were determined by developing a new Shannon entropy based technique and non-decimated wavelet transforms. It was found that the land-surface controls on soil moisture vary with hydro-climate and antecedent wetness conditions. In general, the effect of soil was found to reduce with coarsening support scale while the effect of topography and vegetation increased. A novel Scale-Wetness-Heterogeneity (SWHET) cuboid was developed to coalesce the relationship between soil moisture redistribution and

dominant physical controls at different land-surface heterogeneity and antecedent wetness conditions across remote sensing scales. The SWHET cuboid can potentially enable spatial transferability of the scaling relationships for near-surface soil moisture. It was found that results from the SWHET cuboid enabled spatial transferability of the scaling relationships between two similar hydro-climates (Iowa, U.S.A and Manitoba, Canada) under some wetness and land-surface heterogeneity conditions. Evapotranspiration estimates were computed at varying scales using airborne and satellite borne remotely sensed data. The results indicated that in a semi-arid row cropped orchard environment, a remote sensing support scale comparable to the row spacing and smaller or comparable to the canopy size of trees overestimates the land surface temperature and consequently, underestimates evapotranspiration.

DEDICATION

This dissertation is dedicated to my parents

Mrs. Sushma Gaur and Mr.Ripudaman Gaur

ACKNOWLEDGEMENTS

I would like to thank all the people who contributed their time, effort and support that was necessary to make this dissertation a reality.

My deepest gratitude goes to my academic advisor, Dr. Binayak P. Mohanty, for introducing me to the fascinating concept of scale. He went out of his way to make time to discuss any ideas I had and nurture the promising ones to steer my research. Without his passionate guidance, persistent faith in me and my abilities, constant funding for my graduate studies and honest criticism, this research effort was not possible. I would also like to thank my doctoral committee members, Dr. Patricia Smith, Dr. Sorin Popescu and Dr. Yalchin Efendiev who ensured I stayed on track with my dissertation and extended consistent support for all my efforts. A big vote of thanks is also due to all my teachers (especially J.S. Bathh) who during school, undergraduate and graduate studies helped me shape my thoughts and the choice of my career.

I would also like to acknowledge the help and support that all the staff at Texas A&M extended to make this journey smooth, especially David Riggs for promptly addressing all my computer issues and Sonya Stranges for her unselfish interest in my well-being.

I would also like to thank my late paternal grandparents, Mr. Shugan Chand Gaur and Mrs. Shanta Gaur and maternal grandparents, Mr. Tek Chand Vashisht and Mrs. Bharti Vashisht whose love and memories have been a constant source of inspiration. My sincere gratitude goes to my parents, Mrs. Sushma Gaur and Mr. Ripudaman Gaur for instilling in me a sense of wonder about this world and my brother, Vikram Pratap Gaur and sister-in-law, Nitasha Gaur for their constant love and unwavering support throughout the course of this journey. My extended family also deserve a special mention especially my aunts, Shakuntla Sharma and Pushpa Sharma for being inspirational role models and

Sunita Vashisht and Shiva Vashisht for their encouragement. A big thanks to my uncle Mr. Rajan Vashisht for ensuring the seamless success of my student life and Dr. ManMohan Sharma, Mr. Rakesh Vashisht and Mr. Pawan Sharma for encouraging my sense of exploration.

My heartfelt gratitude goes to my best friend, Aditya, who has singularly handled being an unfailing mental and emotional support system and sounding board for all my research ideas. His suggestions and periodic brainstorming sessions with me have greatly improved the quality of my work.

I also wish to acknowledge the unfailing support that my friends Lucy, Shilpa, Prabhkiran and Anna offered by being with me in spirit throughout my journey. I would like to thank my friends- Harini, Ramaa, Kopila, Prakash, Ashok, Champa, Katherine, Deepthi, Li Chao and Zhenlei who made this journey at Texas A&M a joyful experience and Deepa Mohanty, Avha and Shlok for being my family away from home. I would also like to thank everyone at the Vadose Zone Research group especially Raghu, Yongchul, Jonggun, Amor, Naren, Neelam and Samagra for being great colleagues and their assistance through the course of my graduate studies and also Dipankar, Bhavna, Joseph and Sayena who helped me at various points in my graduate life.

I also want to thank and acknowledge Dr. Michael Cosh at USDA and Dr. Andreas Colliander at Jet Propulsion Laboratory for providing me with valuable datasets to complete my dissertation. The funding support from the NASA Earth and Space Science Fellowship is also duly acknowledged.

Above all, I would like to thank the energy that sustains the world and to whom I pledge all my work.

TABLE OF CONTENTS

Page

LIST OF FIGURES

FIGURE Page

LIST OF TABLES

1. INTRODUCTION

Soil moisture is a state variable that describes the water content of the (typically) partially saturated or vadose zone of the land-surface that lies above the ground water table. Due to its strategic position at the interface of the atmosphere and deeper permanently saturated zone, it exerts a large impact on the energy and water budgets of the Earth. In the top few centimeters of soil, it controls the overland flow and infiltration fluxes whereas in the deeper root zone, it influences evapotranspiration and percolation to the groundwater aquifers. It also acts as the carrier for fertilizers, nutrients, and pollutants in the soil. It is thus, an important variable for field-scale agricultural water management, and watershed-scale hydrologic management. In modeling scenarios, it describes the bottom boundary condition for atmospheric models while describing the upper boundary condition for land-surface models. The application of soil moisture in the above mentioned fields differs primarily in terms of the spatial and temporal scale at which it is utilized. Agricultural water management and contaminant transport requires fine scale soil moisture information (of the order of a few meters or finer) whereas land-surface and atmospheric models use moisture estimates at the scale of a few kilometers.

Soil moisture is a highly dynamic variable in the spatial as well as temporal domain. Spatial correlation lengths ranging from 30 m up to 119 km across different time scales have been reported in various studies across the globe (Cosh and Brutsaert, 1999, Ryu and Famiglietti, 2006, Joshi and Mohanty, 2010, Western et al., 1998). In lieu of the strategic location of this variable at the interface of the atmosphere and land-surface and its inherent spatio-temporal dynamic nature, it is essential to continuously monitor and describe soil moisture dynamics at different space-time scales.

1.1 Current Data Collection Practices

Collecting spatially representative soil moisture data continuously and periodically on the ground is expensive and logistically infeasible. Periodic ground based data is only collected using sparsely distributed permanent monitoring stations. This data, though periodic in time, represents a support scale of only a few centimeters and thus, lacks spatial representation. Spatially distributed ground based data on the other hand, is collected during intensive short term soil moisture campaigns like Southern Great Plains (SGP) campaigns- SGP97, SGP 99, Soil Moisture Experiments (SMEX)- SMEX02, SMEX04, Cloud and Land Cover Interaction Campaign- CLASIC07 and Soil Moisture Active Passive Validation Experiment- SMAPVEX12 during which airborne remotely sensed data is also collected. This spatially representative data, however, is limited in the spatial extent scale and also time. In order to periodically measure soil moisture across the globe, spaceborne remote sensing has emerged as a viable tool and has been popular since the past decade. National Aeronautics and Space Administration's (NASA) Advanced Microwave Scanning Radiometer (AMSR-E) which went out of operation in October, 2011, collected surface soil moisture data twice a day starting from 2002. More recently, in 2009, Soil Moisture Ocean Salinity (SMOS) was launched by the European Space Agency (ESA) while NASA's Soil Moisture Active Passive (SMAP, launched in January 2015) is the latest to join the global mission of estimating soil moisture from space. However, the data produced using remote sensing platforms has two major limitations: 1) it gives us information of only near-surface soil moisture, 2) the spatial resolution of the soil moisture outputs is incompatible with most modeling scenarios.

1.2 Limitations in Effectively Utilizing Coarse Scale Soil Moisture Data

Soil moisture movement in the vadose zone has typically been defined using the Richard's equation at the Darcy scale or a homogeneous representative elementary volume (REV)

scale. However, the same equation is extended and used beyond the Darcy scale by defining effective parameters through optimization. Even though, the Richard's equation using these scaled parameters is often useful in defining moisture dynamics at the coarse scale, it unexpectedly fails under different conditions since its conception is not anchored in a theoretical framework. Thus, in order to outline effectively homogeneous REV's at the coarser scale where the scaled Richard's equation may either be applied or a new equation describing water flow at the coarse scale is defined, it is imperative to understand and quantify the factors affecting soil moisture distribution at the coarser footprint scales. Since we are restricted in terms of resolution of soil moisture observations, it is also essential to understand the scaling behavior of soil moisture so that information at one scale can be effectively utilized at another scale.

1.3 Motivation

Soil moisture, like other land surface state variables is dependent upon several geophysical parameters. These geophysical parameters which act as external physical controls of soil moisture are soil, vegetation, topography and meteorological factors. Hydrologists, over the years, have attempted to establish quantitative relationships between these physical controls and soil moisture (Joshi and Mohanty, 2010, Mohanty et al., 2000, Joshi et al., 2011, Famiglietti et al., 1998, Njoku and Entekhabi, 1996). However, it has not yet been possible to come up with a generic relationship because of inherently different heterogeneous study domains. Under varying wetness conditions, the physical controls interact differently to create unique patterns of soil moisture. The effect of physical controls has been shown to be scale dependent and may also change with different hydro-climates since the nature of vegetation, topography, soil type; itself is dependent on the hydro-climate of a region. Keeping in mind the requirement and non-availability of soil moisture data at different spatial scales, a scaling scheme which is reliable and transferable across hydro-

climates is required.

Past scaling studies of soil moisture have either been based on statistical formulations or particular case studies which are non-transferable to other hydro-climatic conditions with varying heterogeneities. Besides statistics, scaling of soil moisture often involves the use of land surface models which are based on the equations developed for the Darcy scale. These equations depend upon the pore sizes based heterogeneity (Fig. 1.1a) in the soil, based on which the hydraulic properties for soil water movement are determined. However, the land surface at coarser footprint scales is more heterogeneous (Fig. 1.1b) and this heterogeneity determines water movement at these scales. In order to generate effective soil moisture scaling schemes which are transferable across locations, the science for soil moisture movement at coarser scales needs to be developed.

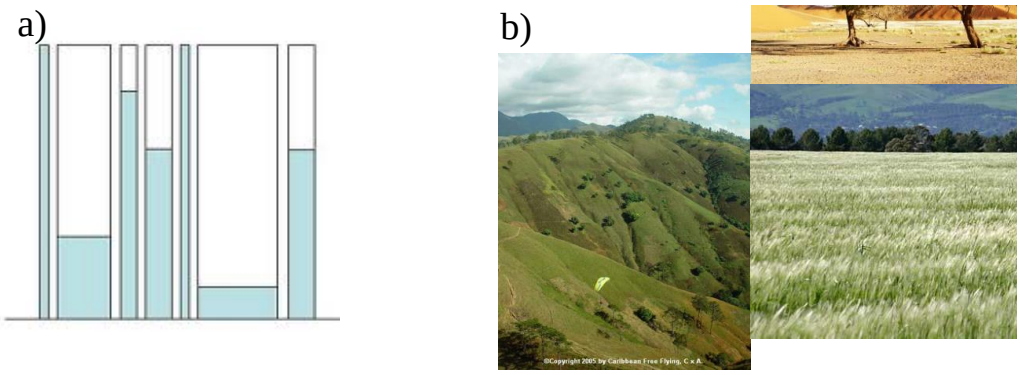

Figure 1.1: a) Heterogeneity at Darcy scale, b) Heterogeneity at coarser scales

1.4 Research Objectives

The overarching objective of this research is to coalesce soil moisture information collected from different platforms at different scales and define scaling relationships for near-surface soil moisture that are rooted in a sound physical framework. Specific research

objectives are given below

1. Determine relationships between physical controls and near-surface soil moisture at different scales and quantify them.

2. Incorporate the determined relationships into a scaling scheme and generate spatially transferable scaling relationships for near-surface soil moisture.

3. Explore moisture dynamics in the root zone, as observed from space, and determine its scaling behavior through estimation of evapotranspiration at different scales.

1.5 Hypotheses

The dissertation evaluates the following two hypotheses.

1. The effect of geo-physical factors on spatial distribution of soil moisture is a function of scale and hydro-climate.

2. It is possible to characterize regions based on heterogeneity and hydro-climate and create data based scaling functions (without the use of existing physical models), which are transferable in space.

The dissertation addresses the objectives of this research in the following seven chapters.

Chapters II and III of this dissertation address the first objective. Chapter II is focused on determining the most dominant physical control of soil moisture at the point and airborne (0.8 x 0.8 km) footprint scale for two different hydro-climates. This has been achieved by introducing a new entropy based scheme which combines the use of easily available categorical information of physical factors with quantitative soil moisture information to potentially establish hierarchy of physical controls dominance on soil moisture.

Chapter III is focused on describing the spatial extent and quantified effect of physical factors on soil moisture redistribution at multiple remote sensing footprint scales (1.6 to 25.6 km) and three different hydro-climates. This has been done by employing 2-dimensional non-decimated wavelet transform on spatial soil moisture redistribution and physical signals in a novel way to determine spatial scale based dominance of physical factors on soil moisture.

Chapter IV and V address the second objective. Chapter IV incorporates the findings of objective 1 to describe a spatially transferable scaling cuboid (Scale-Wetness-Heterogeneity (SWHET) cuboid) for soil moisture redistribution for three different hydro-climates. The novelty of this cuboid is that it incorporates the scale specific dynamic effects of static physical factors on soil moisture redistribution. The scheme is potentially transferable to areas with varying heterogeneity within the same hydro-climate. The resulting scheme can also be used to validate footprint scale soil moisture data.

Chapter V describes the generation of a downscaling scheme for soil moisture. The technique is based on the SWHET cuboid developed in Chapter IV.

Chapter VI addresses the third objective. Remote sensing based evapotranspiration (ET) estimates obtained from an airborne sensor (very fine spatial resolution) have been compared with those obtained from a satellite borne sensor. This study was conducted over partially vegetated areas which compound the problem of estimating ET from space.

Chapter VII concludes the dissertation along with a description of the potential impact of this research as well as future directions for extending the field of study.

2. EVOLUTION OF PHYSICAL CONTROLS FOR SOIL MOISTURE IN HUMID AND SUB-HUMID WATERSHEDS[1]

2.1 Synopsis

The co-variability of soil moisture with soil, vegetation, topography and precipitation are linked by physical relationships. The influence of each of these interdependent physical controls on soil moisture spatial distribution depends on the nature of heterogeneity present in the domain and evolves with time and scale. This paper investigates the effect of three physical controls - topography (slope), vegetation (type) and soil (texture) on soil moisture spatial distribution in the Little Washita and Walnut Creek watersheds in Oklahoma and Iowa, respectively at two support scales. Point support scale data collected from four soil moisture campaigns (SMEX 2002, SMEX 2003, SMEX 2005 and CLASIC 2007) and airborne scale data from three soil moisture campaigns (SGP 1997, SGP 1999 and SMEX 2002) were used in this analysis. The effect of different physical controls on the spatial mean and variability of soil moisture was assessed using Kruskal-Wallis and Shannon entropy, respectively. It was found that at both (point and airborne) support scales, non-uniform precipitation (forcing) across the domain can mask the effect of the dominant physical controls on soil moisture distribution. In order to isolate land surface controls from the impact of forcing, we removed the effect of precipitation variability. After removing the effect of precipitation variability, it was found that for most soil moisture conditions, soil texture as opposed to vegetation and topography is the dominant physical control at both the point and airborne scales in Iowa and Oklahoma. During a very wet year (2007), however, the effect of topography on soil moisture spatial variability overrides the

[1]Reprinted with permission from, 'Evolution of physical controls for soil moisture in humid and sub-humid watersheds' by Gaur, N., and B. P. Mohanty (2013) Water Resour. Res., 49, 1244-1258, doi:10.1002/wrcr.20069, Copyright 2013 John Wiley and Sons, Inc.

effect of soil texture at the point support scale. These findings are valuable for developing any physically based scaling algorithms to up- or down-scale soil moisture between point and watershed scale in the study watersheds in humid and sub-humid regions of the Great Plains of USA. These results may also be used in designing effective soil moisture field campaigns.

2.2 Introduction

Soil moisture is a dynamic state variable. This dynamic behavior may manifest itself in long term changes in mean soil moisture of an area on a yearly basis which are of interest to climate modelers or very short daily time scales wherein a change in soil moisture may cause convective storms (Taylor et al., 2012). Thus, in order to address the effects of soil moisture variability in hydrological and meteorological processes, it is very important to identify and understand the spatial and temporal variability of soil moisture and quantify it.

The temporal and spatial patterns of soil moisture are dependent on a set of physical controls. These physical controls have been identified primarily as precipitation, soil, vegetation and topography (Famiglietti et al., 1999; Entin et al., 2000; Mohanty and Skaggs, 2001, Albertson and Montaldo, 2003, Teuling and Troch, 2005, Joshi and Mohanty, 2010). The physical controls interact to create certain spatial and temporal patterns of soil moisture. Due to the interdependent nature of these physical controls, it is often impossible to isolate their individual effects on soil moisture distribution. Numerous studies have been undertaken to understand the controls that these factors assert over soil moisture spatial distribution (Famiglietti et al., 1999, Mohanty et al., 2000a,b, Joshi and Mohanty, 2010) and their temporal persistence (Mohanty and Skaggs, 2001, Jacobs et al., 2004, Joshi et al., 2011). The use of geostatistical analysis has been a popular choice for investigating the dominance of physical controls. Using geostatistical techniques, in Tarrawarra catch-

ment in Australia, Western et al., (1998) showed that the degree of wetness of top 30 cm of soil moisture affect spatial distribution of soil moisture. In a mixed vegetation pixel with relatively homogeneous topography and soil type, Mohanty et al., 2000a showed that variable land cover, land management and micro-heterogeneity affect soil moisture distribution. Yet in another study pixel with uniform vegetation, Mohanty et al., 2000b showed the influence of topography in spatio-temporal arrangement of surface soil moisture. Using airborne remote sensing data, Cosh and Brutsaert, (1999) showed that soil type strongly affects the soil moisture variability. Ryu and Famiglietti (2006) observed that within regional scale, soil texture and vegetation control the smaller scale correlation whereas larger scale correlations are controlled by precipitation.

The other popular technique that has been used to study the dominant controls for soil moisture is the Empirical Orthogonal Functions (EOFs) (Preisendorfer and Mobley, 1988, Kim and Barros, 2002, Jawson and Niemann, 2007, Joshi and Mohanty, 2010). Kim and Barros (2002) used the EOF technique to explore the relationship between physical controls and soil moisture spatial structure over a 40 km x 250 km region across Southern Great Plains. They observed that topography dominated the spatial distribution of soil moisture during and after a rainfall event. Soil hydraulic properties controlled spatial variability above field capacity while vegetation controlled soil moisture distribution during drydown. In another study for the same region, Jawson and Niemann (2007) showed that soil texture, topography and land use, describe spatial soil moisture patterns with soil texture influencing the spatial and temporal distribution by the maximum amount. In an agricultural watershed in Iowa, Joshi and Mohanty (2010) showed that topography, rainfall, and soil texture have mixed effects on soil moisture distribution at watershed and regional scale whereas vegetation parameters namely vegetation water content has very limited influence at both scales.

2.2.1 Heterogeneity, Scale, and Soil Moisture Measurements

All past studies suggest that the presence of spatial heterogeneity in any kind of physical control induces a variation in observed soil moisture spatial distribution even under same precipitation input. Also, studies showed that under different wetness conditions, various physical controls interact differently (Joshi and Mohanty 2010). The effect and dominance of physical controls may also vary with different hydroclimates, since vegetation type, topographic features, and soil morphology intricately depend on the hydroclimate of a region. Thus, along with investigating the spatial distribution of soil moisture across a domain, it is also equally essential to explore the nature of heterogeneity of its different physical controls. The importance of effectively representing land surface heterogeneity for a broader understanding of the effect of scale on soil moisture has also been emphasized by Western et. al (2002). A brief description of how heterogeneity and soil moisture distribution are related to the scaling triplet (Bloschl and Sivapalan, 1995) i.e. support, extent and spacing is described below.

2.2.1.1 Support Scale

1. **Point Scale:** At the point scale, soil moisture is measured using gravimetric method, Time Domain Reflectrometry (TDR) etc. These measurement techniques have the support size of a few square centimeters. At the centimeter scale, the measurements made are very sensitive to the pore sizes in the soil. Soil moisture measurements taken a few centimeters apart may differ greatly if a macropore in the soil is encountered as opposed to soil matrix. Thus, the heterogeneity which may affect the soil moisture distribution that is obtained from the point observation scale is the soil structure. Soil structure is often a difficult quantity to quantify. However, since the formation of soil structure is itself controlled by the soil texture, and the nature of roots and organic lifeforms (earthworms etc.) present in the soil system, it can be

quantified to some extent using these other measureable ancillary parameters.

2. **Airborne Scale:** The usual airborne scale in past field experiments (e.g., Southern Great Plain Hydrology Experiment 1997, Soil Moisture Experiment, 2002, 2003) has been of the order of 800m x 800m. Airborne remote sensing of soil moisture attributes one soil moisture value to a large heterogeneous pixel (800m X 800m). At this large support scale, the heterogeneity in terms of soil pore sizes may no longer influence the measurements since the effect gets averaged out. However, each pixel has an intrinsic characteristic heterogeneity comprised of soil, vegetation and topography, which is different from its adjoining pixel and is interacting to create a soil moisture distribution within the pixel. Thus, in order to understand the underlying dynamics of soil moisture distribution at the remote sensing footprint scale, it is important to characterize the heterogeneity observed at this support scale. Pixels may differ in vegetation type, relief, and soil texture, that may be characterized using topographic indices (e.g., slope, aspect), soil properties (e.g., soil texture, bulk density), and vegetation attributes (e.g., vegetation type, Leaf Area Index, Normalized Difference Vegetation Index).

2.2.1.2 Extent Scale

When delineating a physical control as dominant, it is also important to mention the extent scale of the measurements. The rainfall, which according to past studies has the major influence on soil moisture, observed over a larger extent may be more variable. The rainfall heterogeneity observed at a watershed scale may be different from the heterogeneity observed at the regional and continental scale. Past studies have demonstrated that the influence of different physical attributes changes at different wetness conditions (Joshi and Mohanty, 2010). Thus, increasing the extent scale in a scaling study can change the wetness conditions observed in the domain. This can influence the apparent dominant

physical controls of soil moisture for domains of different sizes. On the other hand if the extent scale is limited, there is a loss of large scale features (Western et. al, 2002).

2.2.1.3 Spacing Scale

The spacing at which observations are taken determines the heterogeneity captured. If the spacing is too large it may not capture the soil moisture dynamics for a given extent at a particular observation scale. Thus, in order to describe the soil moisture dynamics of an area adequately, the spacing of observations should be such that it describes the heterogeneity of the entire extent. Western et al. (2002) also pointed out a loss of detail in the small scale features if a higher spacing is used. Measurement spacing along with the support scale may thus be considered to be a control of the level of detail of soil moisture dynamics that can be resolved at a particular scale.

2.2.1.4 A New Dimension for the Scaling Triplet- Time

Besides the spatial scales which control the representation of heterogeneity in an area, the time scale also holds utmost importance in assessing the dominance of physical controls of soil moisture. Heterogeneity on the land surface itself is dynamic and is governed by time. An agricultural watershed may be more dynamic than a natural terrain. It is highly likely that during different times in a plant's growth cycle or throughout the course of the year, the hierarchy of dominance that physical controls exert over soil moisture spatial distribution may change with the changing heterogeneity. Thus, it is very important to specify and work with the time scale when discussing the spatial physical controls of soil moisture. The time scale may itself be split into support (time over which a given reading is averaged), spacing (time between two readings) and extent (time span of the experiment).

In addition to the understanding of how scale may impact heterogeneity and soil moisture distribution, it is equally essential to understand the physical processes that influence

soil moisture distribution at various scales. A brief discussion is given below.

1. **Effect of Soil:** Soil texture is based on a range of composition of sand, silt and clay. These quantities together are indicative (to some extent) of the soil structure and its hydraulic properties. Soil texture determines the pore sizes in the soil or alternatively the water holding capacity of the soil. The hydraulic properties of soil determine the downward hydraulic conductivity of a soil, the matric potentials that the soil may create to impede the flow of water through the soil and also the plant available water content.

2. **Effect of Vegetation:** Vegetation may impact the downward as well as upward vertical flow of water. Vegetation may reduce the impact of a precipitation event by interception. Different vegetation types lead to different amounts of interception, throughfall and stemflow, thus, affecting the input of water to the ground surface. Also, vegetation affects the upward flow of water through the process of transpiration. Different rooting structures will lead to different amount of water uptake. The effect of vegetation on soil moisture spatial distribution can be considered to be most dynamic.

3. **Effect of Topography:** Topography usually affects spatial redistribution of water under saturated conditions. Water tends to move from a higher potential to lower potential and thus, flows along a path determined by the slope of the area. Topography also determines the aspect of an area, and based on the varying amount of sunlight available the evapotranspiration occurring on different aspects may vary. Thus, the water loss on different portions of topography might be different.

The primary objective of this study is to assess the effect of spatially heterogeneous physical controls on soil moisture spatial distribution under different wetness conditions

for two watersheds with different hydroclimates. The evolution of dominance of the soil moisture physical controls at point and airborne scales for (1) Walnut Creek, Iowa agricultural watershed, and (2) Little Washita, Oklahoma watershed has been investigated using Kruskal Wallis analysis and the concept of entropy to respectively assess the effect of physical controls on the mean and variance of soil moisture across a watershed.

2.3 Study Area and Data Description

2.3.1 Study Area

Walnut Creek Watershed, Iowa: The Walnut Creek watershed (WC) is located in Boone and Story counties in Iowa. The region is characterized by humid climate with an average annual precipitation of 818 mm. The majority rainfall in this region occurs from April through September which is also the growing season in this agricultural watershed. The topography of the watershed is fairly flat. Owing to the comparatively young geologic development, the watershed is poorly drained and consists of low depressional areas or 'potholes' which are hydrologically unconnected. The main crops grown in the watershed are corn and soybean. The estimated evapotranspiration through the growing season varies approximately between 1-9 mm/day and 3-8 mm/day for corn and soybean respectively (Geli, 2012).

Little Washita Watershed, Oklahoma: The Little Washita watershed (LW) spreads over parts of Caddo, Canadian and Grady counties in Oklahoma. The climate is sub-humid with an average annual precipitation of 795 mm. It receives bulk of its rainfall in May, June, September and October. The average potential evapotranspiration over these months is about 6.3 mm/day (Mohseni et. al., 1998). This watershed has a significantly rolling topography with an average elevation of 400 m and a maximum relief of 183 m. Surface runoff in the watershed is generally towards the east. The water bearing aquifers underlying the watershed contribute to the Little Washita river and seepage has been observed

along portions of the channel in the central region. (Liew and Garbrecht, 2003).

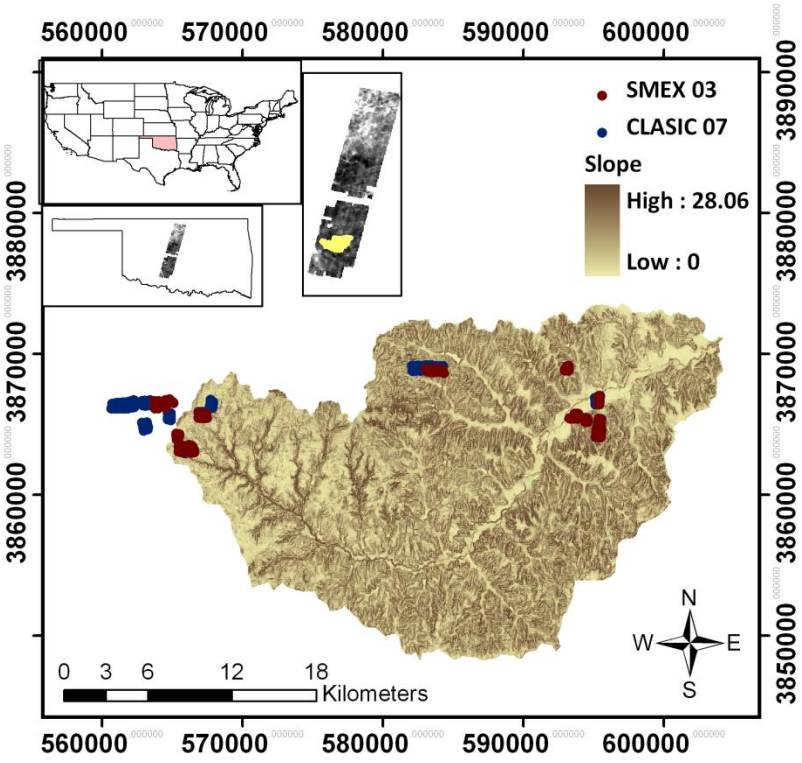

Figure 2.1: Slope and point scale soil moisture data collected in Oklahoma

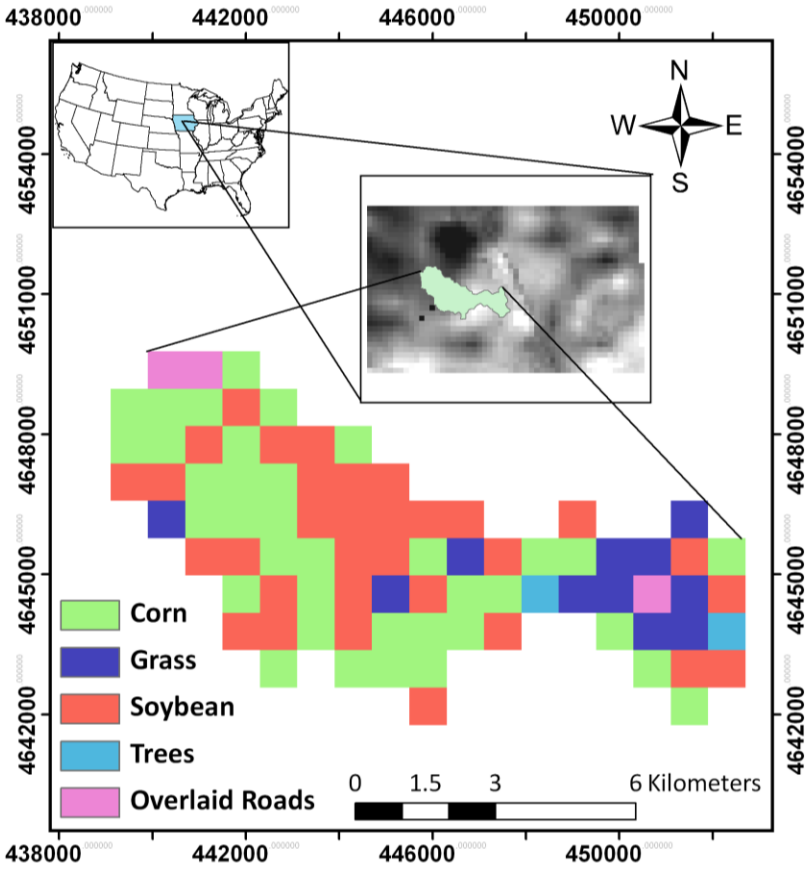

Figure 2.2: LULC data in Walnut Creek watershed, Iowa

2.3.2 Data

The soil moisture dataset for the watersheds were obtained from National Snow and Ice Data Center located at, http://nsidc.org/data/amsr_validation/soil_moisture /index.html. The point support scale soil moisture measurements for top 5 cm depth were taken using an impedance-based probe, namely Time Domain Reflectometers (TDR) (ML2 probes with HH2 data loggers of Delta-T Inc.; http//www.delta-t.co.uk) and were calibrated gravimetrically for the specific sites. Point scale data for Little Washita watershed, Oklahoma (Figure 2.1) was obtained from the Soil Moisture Experiments in 2003 (SMEX 03) and Cloud and Land-Surface Interaction Campaign in 2007 (CLASIC 07). Point scale data for Walnut Creek watershed, Iowa was obtained from the soil moisture sampling conducted during 2002 (SMEX02) and 2005 (SMEX05). Point support scale soil moisture measurements (100 m apart) were taken at 14 points in each of the fields chosen to monitor the hydrology of the watershed. At each of the 14 points in the Walnut Creek agricultural watershed, 3 readings were taken- one on the furrow, one on the slope of the furrow and the third one on the crop row. In the Little Washita watershed for the pasture cover, three replicated samples were taken within a 1-m diameter sampling area at the 14 sampling locations. In addition to ground-based point sampling, soil moisture was retrieved from airborne Electronically Scanned Thinned Array Radiometer (ESTAR) (Jackson, et al. 1999) during the Southern Great Plains Hydrology Experiments in 1997 and 1999 and Polarimeteric Scanning Radiometer (PSR) (Bindlish, 2006) during 2002 respectively. A brief description of the various soil moisture campaigns is given in Tables 2.1, 2.2 and 2.3.

Vegetation attributes for Iowa (Figure 2.2) were obtained during the field experiments and DEM (National Elevation Dataset, NED, 30m resolution) was used to create the slopes for the watersheds. The slope map at the 800 m resolution was constructed after aggregating the elevation data at 30 m to 800 m. The soil texture information has been obtained

from SSURGO (30 m resolution). Soil maps of the Walnut Creek and Little Washita watersheds in Iowa and Oklahoma are shown in Figures 2.3 and 2.4, respectively The soil moisture variability observed over the two watersheds (at the airborne scale) is shown in Figure 2.5, 2.6 and 2.7.

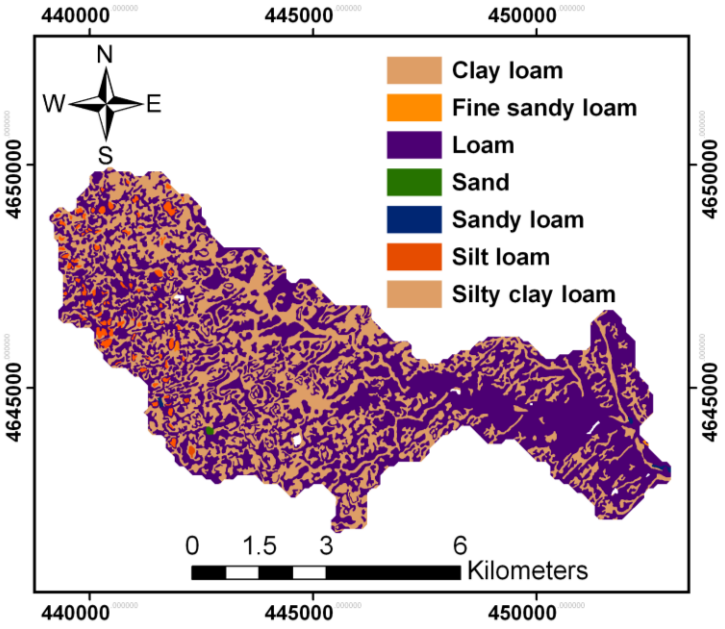

Figure 2.3: SSURGO based classified soil map of Walnut Creek watershed, Iowa

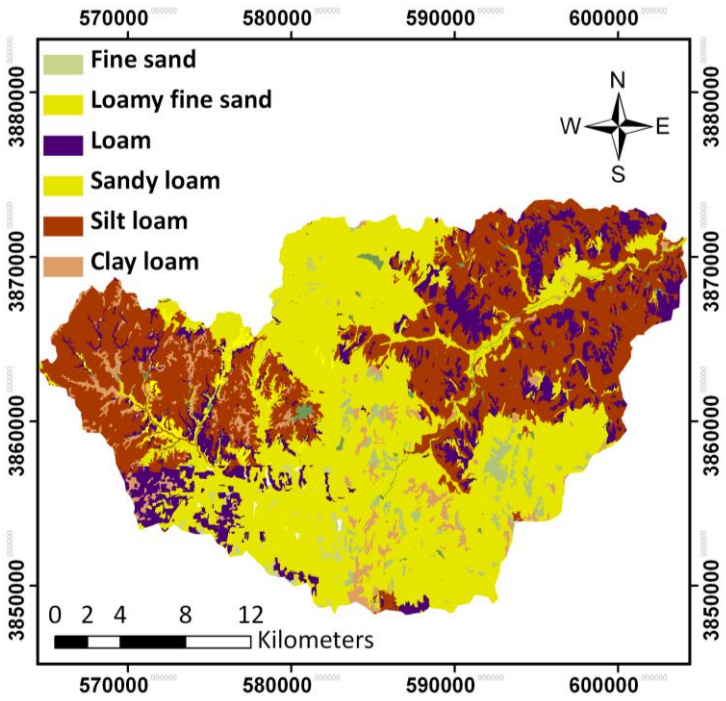

Figure 2.4: SSURGO based classified soil map of Little Washita watershed, Oklahoma

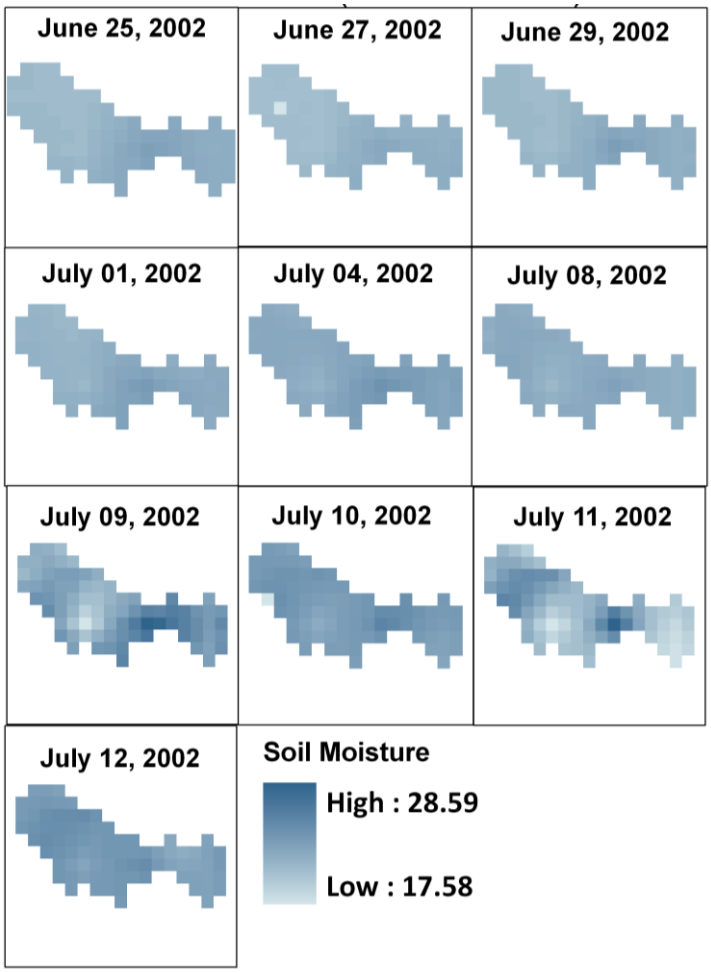

Figure 2.5: Airborne soil moisture maps for Walnut Creek watershed, Iowa

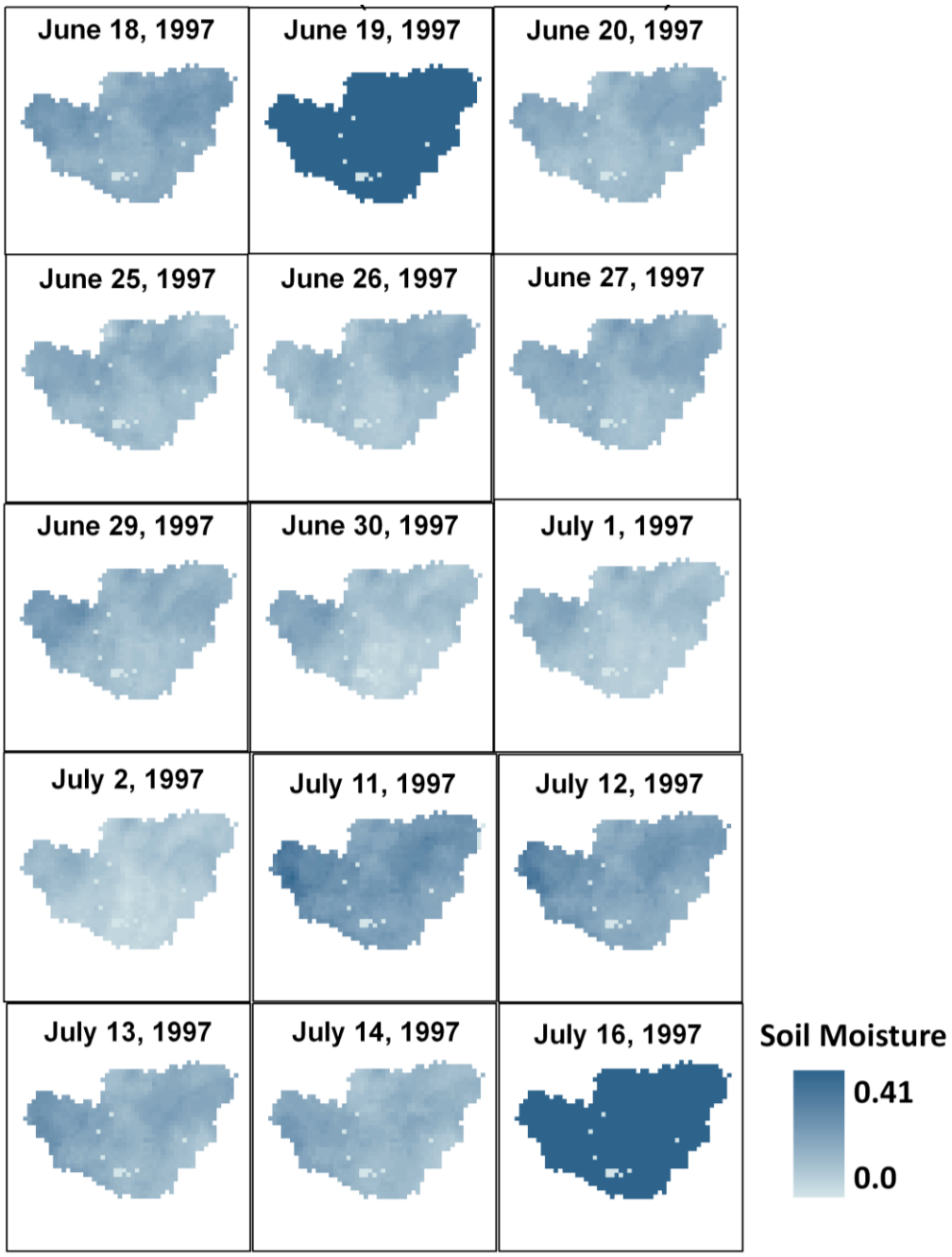

Figure 2.6: Airborne soil moisture maps for Little Washita watershed (1997)

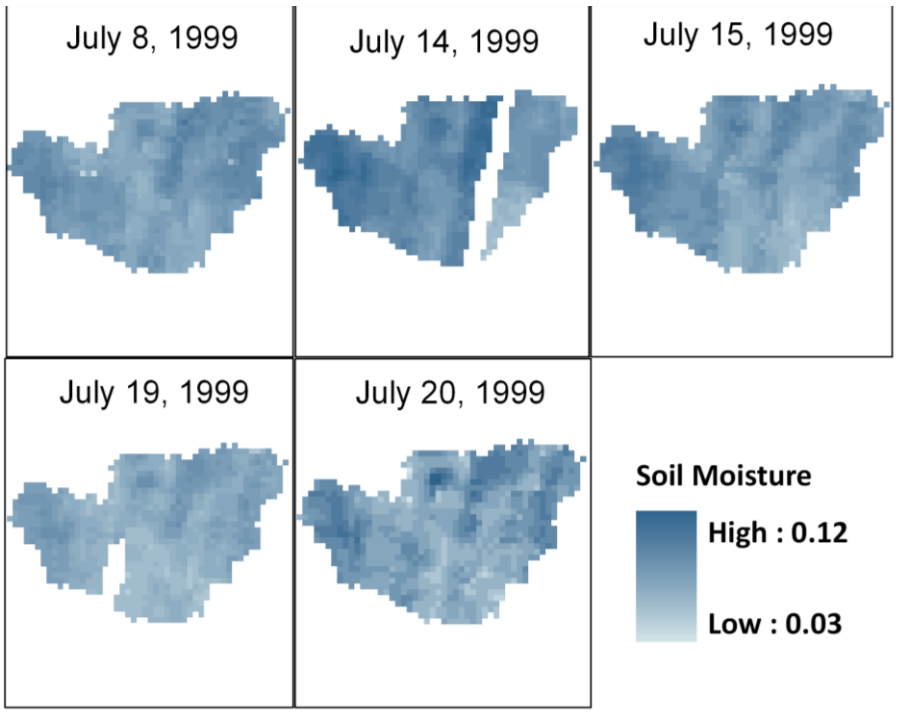

Figure 2.7: Airborne soil moisture maps for Little Washita watershed (1999)

2.4 Methodology

2.4.1 Kruskal-Wallis

The first step in assessing the dominance of a particular physical control is to check whether its inherent heterogeneity leads to an effective separation of mean soil moisture within a classification. This was done using the Kruskal-Wallis test on the mean soil moisture. This test is the non-parametric equivalent of the Analysis of Variance test and is used to distinguish between the difference in means of 2 or more distributions. The null hypothesis for this test was, H_N.: There is no difference in the median soil moisture grouped by 'a', where 'a' represents the categories in a particular classification. This test was conducted to compare the separability between mean soil moisture values of different categories within a classification.

Table 2.1: Overview of the various soil moisture campaigns

Campaign	Location	Duration	Support Scale	Measuring instrument
SGP 97	OK	June 18-July 18, 1997	Airborne (800 m x 800 m)	ESTAR
SGP 99	OK	July 8- July 20, 1999	Airborne (555 m x 450 m)	ESTAR
SMEX 02	IA	June 25- July 12, 2002	Point, and Airborne(800 m x 800 m)	TDR and PSR
SMEX 03	OK	July 2- July 17, 2003	Point	TDR
SMEX 05	IA	June 13- July 4, 2005	Point	TDR
CLASIC 07	OK	June 11- July 6, 2007	Point	TDR

2.4.2 Shannon Entropy

The next step was to assess the variability in the data which is done using Shannon entropy. Shannon entropy (Shannon, 1948) has been a popular technique for investigating spatial variability in the field of hydrology (Mishra et al., 2009; Mogheir et al., 2004; Phillips, 2001 etc.) However, to the best of the authors' knowledge, this is the first study to use the entropy technique to understand the dominance of physical controls on soil moisture spatio-temporal variability. The strength of this technique lies in its effective simplicity to incorporate the effect of dependent or independent physical controls (categorical or numerical) on soil moisture spatial distribution. It can be used on datasets of a short or long length. However, in order to use this technique it is essential to isolate the parameters (physical controls) whose effect we want to assess on soil moisture spatial distribution.

Shannon entropy (I) (Shannon, 1948, 2001) is a statistical quantity representing a measure of the information that may be extracted from a system or analogously the uncertainty that the system comprises of. Entropy for a system with a state random variable, V, is formulated as

Table 2.2: Details of number of data points used for the support scale analysis

Campaign	Classification	Min/Max number of points /day used in the analysis	No. of bins used
SMEX03	*Total*	139-204	
	Based on Soil Type		
	Loam	10-13	3
	Silt Loam	90-133	6
	Sandy Loam	39-63	4
	Based on topographic position		
	Hilltop	55-91	3
	Slope	30-40	5
	Valley	54-78	4
CLASIC07	*Total*	101-112	
	Based on Soil Type		
	Loam	14-17	3
	Silt Loam	44-54	5
	Sandy Loam	34-43	5
	Based on topographic position		
	Hilltop	19-20	3
	Slope	49-56	4
	Valley	31-36	5
SMEX02	*Total*	244-278	
	Based on Soil Type		
	Loam	41-48	5
	Clay Loam	195-230	9
	Based on vegetation		
	Corn	148-184	10
	Soybean	83-94	7
SMEX05	*Total*	286-321	
	Based on Soil Type		
	Loam	155-176	10
	Clay Loam	125-145	8
	Based on vegetation		
	Corn	170-190	9
	Soybean	111-132	8

Table 2.3: Details of number of data points used for the airborne scale analysis

Campaign	Classification	Min/Max number of points /day used in the analysis	No. of bins used
SGP97	*Total*	601	
	Based on Soil Type		
	Loam	68	5
	Silt Loam	313	11
	Sandy Loam	220	9
	Based on topographic position		
	Hilltop	119	6
	Slope	371	10
	Valley	111	6
SGP99	*Total*	473-532	
	Based on Soil Type		
	Loam	76-80	5
	Silt Loam	214-268	10
	Sandy Loam	183-184	8
	Based on topographic position		
	Hilltop	94-107	6
	Slope	298-334	10
	Valley	81-91	6
SMEX02	*Total*	64	
	Based on Soil Type		
	Loam	7	2
	Clay Loam	57	5
	Based on vegetation		
	Corn	31	3
	Soybean	33	4

$$I_V(p_1, p_2, ..., p_n) = -\sum p_i \log_2 p_i$$
$$V : n \in N \tag{2.1}$$

$$\sum_{i=1}^{n} p_i = 1 \tag{2.2}$$

p_i: probabilities of occurence of realizations of V

I_V, entropy of the system, is representative of the uncertainty of the random variable or the unresolved information in the random variable. However, instead of a unique value of uncertainty, all systems possess a range of uncertainty, which depends on the probability values associated with the set N chosen to represent the random variable. This range of uncertainty is quantified by a range of entropy values of the system. By addition of information to this system in terms of either constraints, like specifying the moments of the random variable etc., the range of uncertainty and correspondingly the range of entropy of the system reduces. In other words, with each addition of independent information to a system, the system goes from being stochastic (with a range of uncertainty) to being deterministic (i.e. possessing a unique probability distribution). The entropy of a completely determinate system is zero.

Entropy is an extensive quantity and unlike energy does not follow the conservation laws. In order to express the combined uncertainty of two or more independent random variables, their respective entropy values may be added. However, if the random variables are dependent on each other, this dependence must be accounted for as 'transinformation', T(A,B), i.e., the amount of information common to both sets of random variables. The joint information or entropy, I(A,B) of this system of random variables is calculated as shown in equation 2.3. For two independent random variables, 'T(A,B)' is zero. This

concept of transinformation can be extended to more than two variables as well.

$$I(A,B) = I(A) + I(B) - T(A,B) \tag{2.3}$$

2.4.2.1 Entropy as a Tool to Assess Physical Controls of Soil Moisture

As discussed above, entropy of a system of random variables will decrease with addition of information. The information which explains more uncertainty in the data will have a lower value of entropy of the random variable (Paszto, et al., 2009). This property of entropy forms the basis of this study.

In this study, the random variables under consideration are point and airborne measurements of soil moisture. The addition of information to the random variable is done in the form of classification of the soil moisture data. These soil moisture values are classified under different categories based on the physical controls present at the location of the measurement. These categories are 'soil type' and 'vegetation type' for the agricultural watershed in Iowa, and 'soil type' and 'topographical location' for the natural terrain in Oklahoma. The classification type which leads to a lower entropy explains the maximum uncertainty in the random variable. The factor on which the lowest entropy classification is based can be considered to be the most dominant physical control in terms of controlling soil moisture variability.

Despite the availability of various attributes to represent the various physical controls like hydraulic conductivity, percent sand, percent silt and percent clay etc. for soil, Normalized Difference Vegetation Index (NDVI), Leaf Area Index (LAI), vegetation type etc. for vegetation, and slope, aspect, elevation etc. for topography, broad classification categories namely soil type, vegetation type and topographic location were chosen. This was done in order to incorporate easily available categorical information and retain the individual identities of each physical control along with each classification being representative

of the properties of the physical control. For example, 'soil type' gives a fair idea about the range of hydraulic conductivity, infiltration and evaporation behavior of a soil. Similarly, 'vegetation type' is representative of the root zone and root water uptake, plant percentage cover on land, LAI, etc. for landuse and landcover. There may be other factors like plant health which may not be represented in an adequate way under this classification scheme but we assumed that plant health at the extent scale may be excluded as a heterogeneous factor. 'Topographical location' was determined based on the location of a sampling point on the slope. This classification scheme adequately represents most of the attributes of topography like elevation and slope. It does not however represent aspect which may be an important attribute for soil moisture variation. But considering the moderate relief of the area under consideration, aspect will not influence the soil moisture distribution significantly. The different classification categories used in this study are provided in Tables 2.4 and 2.5. The choice of these parameters for describing the heterogeneity was made based primarily on their suitability for representing the key landscape features and also on the ease of obtaining such categorical data.

Table 2.4: Classification categories for Walnut Creek, Iowa

Classification Type	Categories
Soil Type	Loam, Clay Loam
Vegetation Type	Corn, Soybean

1. **Marginal Entropy Calculation for Soil Moisture:** We arranged the soil moisture sm^k_d values , where, d (days): 1,2,....d; and k (number of soil moisture values 1,2,....n_0, day wise to calculate entropy values for each day separately. Using the Scott's algorithm (Scott, 1979) of optimal binning, frequency histograms for each

Table 2.5: Classification categories for Little Washita, Oklahoma

Classification Type	Categories
Soil Type	Loam, Silt Loam, Sandy Loam
Topography position	Hilltop, Valley, Slope
(Slope: 0-1.5%, flow accumulation: 0)	Hilltop
(Slope: 0-1.5%, flow accumulation: >0)	Valley
(Slope: 1.5-14%, flow accumulation: >0)	Slope

day were calculated. According to this algorithm, the bin-width (h) in the daily frequency histograms is defined as

$$h = 3.49 s n_0^{\frac{-1}{3}} \tag{2.4}$$

h: bin width

s: standard deviation of daily soil moisture

The average value of 'h' across the duration of the campaign was chosen as the representative bin width for a particular campaign. A probability, p_i is assigned to each bin and calculated as

$$p_i = \frac{n_i}{n_0} \tag{2.5}$$

n_i: number of observations in the i^{th} bin

Then we substituted p_i in eq. 2.1 to find out daily marginal entropies.

2. **Joint Entropy Calculation for Each Classification:**Soil moisture values were classified under different categories as mentioned in Tables 2.4 and 2.5. A joint probability mass function (pmf) was constructed for soil moisture values in different categories. The steps for constructing a joint pmf with two variables are given be-

low. A joint pmf for three variables can be constructed along the same lines. It is important to note here that this method may become computationally intensive with increasing number of categories in a classification scheme.

The soil moisture values in one category (sm_j) under a classification were paired up with soil moisture values in the other category (sm_m) within the same classification to form unordered pairs on a daily basis (for example loam and sandy loam category under soil classification).

$$(sm_j, sm_m), \quad j = 1,2,...,J \qquad m = 1,2,....M$$

A contingency table representing the relative frequencies, f_i, was used to calculate the probabilities as given in eq. 2.6. The bin sizes for the two categories under the classification were decided based on eq. 2.4.

$$f_i = p(sm_j, sm_m) = \frac{n_{jm}}{n_0}, \quad j = 1,2,...,J \qquad m = 1,2,....M \tag{2.6}$$

n_{jm}: number of observation in the j^{th} (from category 1) and m^{th} (from category 2) bin

Substituting $p(sm_j, sm_m)$ in eq. 2.1, the joint entropies were obtained. This joint entropy of the dataset correspond to I(A,B) in equation 2.3.

2.4.3 Bootstrapping

In order to achieve statistically significant daily results, bootstrapping was employed to get multiple samples for each category in a classification. Bootstrapping enables the use of the sample data at hand as a population from which random samples may be drawn. Random sampling with replacement was done within each category. Equal number of data points were employed in each bootstrapping routine with 40 samples being created for each category. These results were used to compute the joint pmf and to identify the uncertainty range of the entropy values (represented by error bars).

2.4.4 Effect of Precipitation

As mentioned above, if the extent scale is large enough and precipitation varies across the extent, the effect of precipitation may mask the actual effect of different physical land surface controls on soil moisture. In order to remove the effect of precipitation, the entire computation was repeated for soil moisture anomalies. In order to compute soil moisture anomalies at the point support scale, the mean soil moisture values of every field in the entire study domain were computed. These means were subtracted from the soil moisture readings collected in each respective field. At the airborne scale, the soil moisture values were linearly detrended to obtain the anomalies. Linear detrending was done by linearly regressing a straight line through the soil moisture values plotted against its spatial location and then subtracting the regressed value from the actual soil moisture value. The entire coding for the analysis was done using MATLAB.

2.5 Results and Discussion

This section is divided into 2 sub-sections. The first part discusses the Kruskal-Wallis results and the second part discusses the entropy results. Each sub-section is further divided into 2 parts- 1) Point Scale and 2) Airborne Scale. The two analyses comprehen-

sively describe the effect of different physical controls of soil moisture on its spatial-temporal distribution. Kruskal-Wallis compares the mean soil moisture of different distributions whereas the entropy based analysis compares the variability observed in the distributions.

2.5.1 Comparison of Means: Kruskal-Wallis Based Analysis

Point Scale: Year 2005 (SMEX05) was relatively wetter than 2002 (SMEX02) in Iowa. In Oklahoma, CLASIC07 during 2007 was very wet whereas 2003 (SMEX03 campaign) was very dry. In addition, SGP97 in Oklahoma was an average year whereas SGP99 again was very dry.

Table 2.6 contains the p-values of Kruskal-Wallis. From the p-values calculated for 2002 (Iowa), we see that soil texture, for the most part partitioned the mean soil moisture at a significance level of 0.05 whereas vegetation type was not as effective on the wetter days (DOY 187 onward). Soil texture was consistently capable of separating mean soil moisture from DOY 176 to DOY 186. These days corresponded to low soil moisture values. On DOY 188, the mean soil moisture for the watershed increased from 0.15(V/V) to 0.21(V/V) because of a precipitation event and neither soil texture nor vegetation type induced an effective partition of mean soil moisture. A failure for either of the two classifications inducing a mean difference in soil moisture indicates an interaction of soil and vegetation or an extraneous factor besides the two, which is dominating under these conditions. However, during a similar increase from 0.15(V/V) to 0.28 (V/V) on DOY 192, soil texture (but not vegetation) was capable of discerning a difference in mean soil moisture. This can be attributed to the difference in the antecedent soil moisture conditions that prevailed in the watershed. Before the precipitation event on DOY 188, the antecedent soil moisture conditions were very low whereas after the precipitation event on DOY 192, the antecedent moisture conditions were relatively higher. This indicates that when the crop is

water stressed on account of limited soil moisture availability, the interaction between the vegetation and soil increases and jointly they control the soil moisture spatial distribution. Physically, this may refer to two competitive forces acting within the soil: (1) matric potential of soil that tries to hold the water in the soil pores and (2) suction potential of plant roots which tries to withdraw water from the soil pores. However, when the antecedent moisture conditions are high, suction forces of plant roots do not compete for near-surface soil moisture since the deeper root zone is not water stressed. The density of roots is higher in the slightly deeper root zone and thus, observing the principle of minimum energy requirement, plants would preferentially take water from the deeper zone. Thus, we observe that after the second precipitation event, soil texture, which determines the water holding capacity of soil pores, effectively partitions mean surface soil moisture which could be due to more infiltration to the lower layers.

In 2005, which was a relatively wetter year, we found that vegetation was slightly more capable of discerning a difference in near surface soil moisture. Corn and soybean have very different canopy structures. Corn has a very dense canopy and leads to greater interception as opposed to soybean which offers little to no interception. This holds true for the later half of the campaign when the canopies are fully developed. Also, it could be attributed to the difference in infiltration properties of the soil under these (corn vs. soybean) canopies, as rooting structure and organic content play an important role in the development of infiltration properties of the soil (Mohanty et al., 1994, DasGupta et al., 2006). On DOY 172, after a precipitation event, vegetation (p-value<0.05) partitioned the mean soil moisture more than soil texture (p-value = 0.3992). This is somewhat different from 2002. However, it is important to keep in mind that SMEX02 (DOY 176 - 193) and SMEX05 (DOY 164 - 185) captured different portions of the growth cycle of corn and soybean. DOY 172 in 2005 fell in the growing cycle of corn and soybean and thus the water requirements were considerably more than in 2002, when we see more dominance

Table 2.6: p-values for Kruskal-Wallis test, Walnut Creek watershed, Iowa (point scale)

DOY	Mean volumetric soil moisture (%)	Soil	Vegetation
2002		p-value	p-value
176	0.1	<0.0001*	0.0273*
177	0.1	0.0091*	0.0002*
178	0.09	0.0291*	0.0081*
182	0.07	0.0481*	0.0001*
186	**0.14**	**0.0068***	**0.0006***
187	**0.15**	**0.0921**	**0.2650**
188	**0.21**	**0.0874**	**0.2986**
189	0.18	0.0008*	0.8908
190	0.15	0.0086*	0.0807
192	**0.28**	**0.0013***	**0.2168**
193	0.26	<0.0001*	0.9502
2005			
166	0.24	0.0011*	<0.0001*
167	0.21	0.0112*	<0.0001*
168	0.2	0.0082*	<0.0001*
169	0.18	0.3068	<0.0001*
170	0.17	0.0346*	0.1354
171	0.16	0.3759	0.0101*
172	**0.2**	**0.3992**	**0.0296***
176	0.17	0.6679	0.2436
177	**0.32**	**0.0002***	**<0.0001***
178	0.27	0.0198*	<0.0001*
181	**0.32**	**<0.0001***	**<0.0001***
182	0.26	0.0351*	<0.0001*
183	0.23	0.0007*	<0.0001*
184	0.2	0.5525	<0.0001*

* represent a significant difference in means with a significance level of 0.05.
The shaded rows represent that a rainfall event preceded the DOY

of soil texture. This implies that in an agricultural watershed, the effect of vegetation on soil moisture dynamics is highly dependent on the crop growth stage. Another interesting observation is that if we compare the effect of soil texture and vegetation on soil moisture means during the same stages of the crop growth cycle, we observe very different effects. In 2005, except for a brief exception of DOY 170 and DOY 176, vegetation continued to exert an effect on the partitioning of soil moisture means in contrast to what was observed in 2002. This can again be explained by referring to the antecedent soil moisture conditions. 2002 was a comparatively drier year with a larger range of soil moisture. The root zone vegetation dynamics (phenology) were probably very different in 2002 as compared to 2005. Thus, in addition to crop growth stage, the antecedent wetness conditions in the study domain exert a large influence on effect of different physical controls on soil moisture spatial distribution. On DOY 176, neither vegetation nor soil texture displays a partitioning of soil moisture mean. Hysteresis in soil moisture variability, previously been reported at the field scale by Teuling et. al., 2007 and Ivanov et. al., in 2010, may possibly be another contributor to this behavior.

Table 2.7 contains the p-values for Little Washita, Oklahoma. Interestingly for Oklahoma, at the point scale, soil texture remained dominant throughout in the wet as well as dry year. There could be two possible explanations for this behavior. The first could be the soil texture is dominating and is the only factor responsible for deciding the separation of mean soil moisture. The other possible explanation could be that such a small support scale is insufficient to represent a topographical position. But irrespective, this finding may prove to be highly useful for conducting future field campaigns.

Airborne Scale: During SMEX02 campaign in Iowa, at the 800m x 800m scale, the p-values of vegetation based Kruskal-Wallis test were on some occasions much lower than the p-values of soil texture based Kruskal-Wallis test (Table 2.8). On DOY 182, the soil moisture values rose up to 0.20 V/V and then consistently remain above it. During this

Table 2.7: p-values for Kruskal-Wallis test, Little Washita watershed, Oklahoma (point scale)

DOY	Mean volumetric soil moisture (%)	Soil	Topography
2003		p-value	p-value
183	0.129	<0.0001*	0.0608
184	0.117	<0.0001*	0.4389
185	0.108	<0.0001*	0.3529
186	0.096	<0.0001*	0.1101
187	**0.103**	**<0.0001***	**0.2992**
2007			
160	0.271	<0.0001*	0.081
161	0.247	<0.0001*	0.3963
162	**0.283**	**<0.0001***	**0.1725**
163	0.259	<0.0001*	0.1166
164	0.242	<0.0001*	0.3791
168	**0.326**	**<0.0001***	**0.3673**
169	0.304	<0.0001*	0.2835
170	0.291	<0.0001*	0.2835
174	**0.297**	**<0.0001***	**0.1953**

* represent a significant difference in means with a significance level of 0.05. Since there were three classifications, a Bonferroni correction was applied bringing the actual level of significance testing to 0.016 (0.05/3) for each individual comparison The bold face rows represent that a rainfall event preceded the DOY

period, vegetation showed lower p-values on all days with the exception of DOY 190 and 191. p-value indicates the level of confidence that we have in the results that the two means are equal to each other or come from the same distribution. However, neither soil texture nor vegetation type partitions the mean soil moisture quite effectively with the exception of DOY 193 where vegetation emerges as the dominant factor. This could imply that soil-vegetation interaction effects are more important when observing soil moisture at a coarser scale than their individual effects. A heterogeneity factor comprising of both soil and vegetation together may be needed to effectively represent soil moisture heterogeneity in the Walnut Creek agricultural watershed region. The analysis could also be indicative of a type II statistical error since the number of data points was relatively low.

Table 2.8: p-values for Kruskal-Wallis test, Walnut Creek watershed, Iowa (airborne footprint)

DOY	Mean volumetric soil moisture (%)	Soil	Vegetation
2002		p-values	p-values
176	0.18	0.8213	0.8772
178	0.16	0.6437	0.9625
180	**0.18**	**0.8213**	**0.8561**
182	**0.2**	**0.7388**	**0.3041**
185	**0.23**	**0.788**	**0.4319**
189	0.21	0.4451	0.2507
190	**0.23**	**0.6749**	**0.8351**
191	**0.27**	**0.5687**	**0.8984**
192	**0.35**	**0.6749**	**0.1525**
193	0.28	0.372	0.0053*

* represent a significant difference in means with a significance level of 0.05. The shaded rows represent that a rainfall event preceded the DOY

Contrary to the results from the agricultural watershed in Iowa, soil texture in Little Washita, Oklahoma, partitioned mean soil moisture effectively at the airborne scale (Table

2.9). Topography also displayed an effective partitioning of mean soil moisture on most days. The interesting point to note here is that during SGP97, on DOY 178, there was a small precipitation event wherein the soil moisture rose from 0.132 V/V to 0.151 V/V. Despite the precipitation event topography failed to partition the mean soil moisture even though soil continued to do so. On the other hand on DOY 192, when the soil moisture value rose from 0.080 V/V to 0.227 V/V, topography was able to show an effective partitioning in mean soil moisture. This was true even for DOY 197 wherein topography and soil type both showed an effective partitioning of mean soil moisture. This result also shows that there exist certain precipitation amount thresholds wherein the influence of topography on soil moisture means begins. During SGP99, which was a considerably drier year, soil texture partitioned soil moisture mean more effectively than topography. Even though the airborne and point scale data were taken in separate years, soil texture dominance at both scales is noteworthy.

This analysis also showed another important feature. Walnut Creek watershed is an agricultural watershed with considerable vegetation heterogeneity usually absent in a natural watershed like Little Washita. The p-values in Little Washita for the Kruskal-Wallis tests based on soil and topography followed similar patterns for the most part across time as opposed to those in Walnut Creek watershed, where soil and vegetation dominated at different times. This may imply a stronger correlation between soil type and topography (slope) in comparison to correlation between vegetation type and soil texture, which is more dynamic in nature. This could also suggest that for a similar spatial extent, the absence of (dynamic) vegetation based heterogeneity leads to more predictable soil moisture dynamics as observed by Albertson and Montaldo (2003).

Table 2.9: p-values for Kruskal-Wallis test, Little Washita watershed, Oklahoma (airborne footprint)

DOY	Mean volumetric soil moisture (%)	Soil	Topography
1997		p-values	p-values
1997		p-values	p-values
169	0.188	<0.0001*	0.0157*
170	0.173	<0.0001*	0.0639
171	0.147	<0.0001*	0.5906
176	0.138	<0.0001*	0.0868
177	0.132	<0.0001*	0.3856
178	**0.151**	**<0.0001***	**0.501**
180	0.143	<0.0001*	0.0012*
181	0.106	<0.0001*	0.0002*
182	0.104	<0.0001*	0.0007*
183	0.08	<0.0001*	0.0054*
192	**0.227**	**<0.0001***	**<0.0001***
193	0.202	<0.0001*	<0.0001*
194	0.16	<0.0001*	<0.0001*
195	0.141	<0.0001*	<0.0001*
197	**0.17**	**0.9108**	**<0.0001***
1999			
189	0.097	<0.0001*	0.036*
195	**0.118**	**<0.0001***	**0.6542**
196	0.097	<0.0001*	0.0067*
200	0.075	<0.0001*	0.1364
201	0.076	<0.0001*	0.2705

* represent a significant difference in means with a significance level of 0.05. Since there were three classifications, a Bonferroni correction was applied bringing the actual level of significance testing to 0.016 (0.05/3) for each individual comparison The shaded rows represent that a rainfall event preceded the DOY

2.5.2 Evolution of Physical Controls Dominance: Entropy Based Analysis

Entropy analysis using raw soil moisture data from various field campaigns explains the control that the geophysical parameters exert over the soil moisture variability across a watershed. Watershed is a relatively large spatial extent and different parts of the watershed may receive different amounts of rainfall. Since dominance of physical controls changes under different wetness conditions (as discussed in the previous section), it is possible that dominant physical controls across the watershed may not be the same. In order to remove the effect of variable precipitation from the analysis, the entropy computation was done on soil moisture anomalies (computed as explained in 2.4.4).

The marginal entropy values using daily soil moisture anomalies were plotted against the daily mean soil moisture in Figures 2.8 and 2.1. Marginal entropies refer to the entropies computed for all the soil moisture values grouped together (without any classification). For the point scale entropy values in Walnut Creek agricultural watershed in Iowa, we observed that entropy (or variability) is maximum when the soil moisture was in the intermediate range (i.e., neither too high nor too low). In the Little Washita natural Watershed, Oklahoma, the entropy values were slightly higher during the dry year 2003 (SMEX03) as compared to the wet year 2007 (CLASIC07). At the airborne scale in Walnut Creek watershed, in line with past research findings (Rodriguez- Iturbe et al., 1995, Western and Bloschl, 1999), we observed that the entropy (and consequently the variability) was lower than at the point support scale. However, in the Little Washita watershed, even though airborne data from SGP97 showed slightly lower entropy than that observed at the point support scale, data from SGP99 showed otherwise.

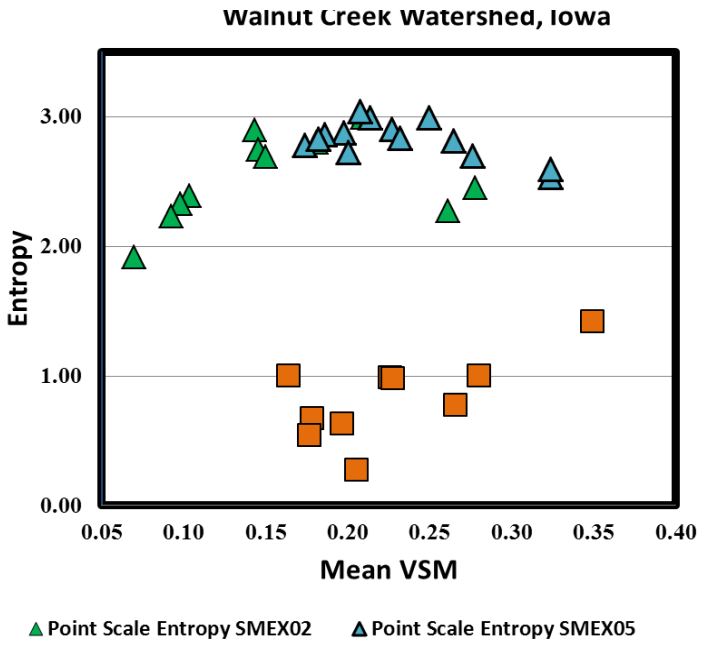

Figure 2.8: Mean volumetric soil moisture v/s Entropy for Walnut Creek watershed, Iowa

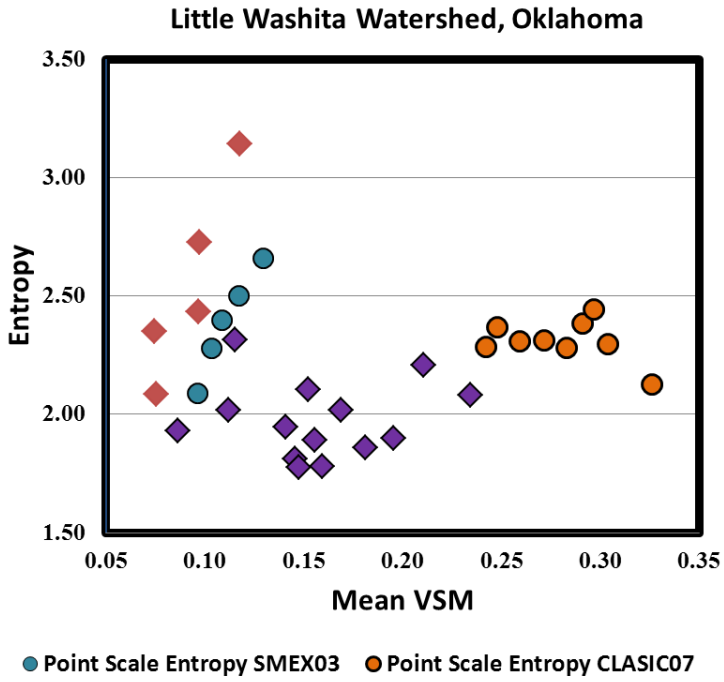

Figure 2.9: Mean volumetric soil moisture v/s Entropy for Little Washita watershed, Oklahoma

The joint entropy values calculated based on soil moisture anomalies and different classifications are provided in Figures 2.10 and 2.11 (point scale) and Figures 2.12 and 2.13 (airborne scale). Joint entropies refer to the entropy values computed based on a particular classification scheme. These values represent the mean entropy values based on the bootstrapping result. In Iowa, a comparison of mean soil moisture for the watershed between two years reveals that 2005 was a wetter year as compared to 2002 (Figures 2.14 and 2.15).

Correspondingly, we observed that even though the marginal entropy values were similar for the years 2002 and 2005 (Figure 2.8), the joint entropy values based on the soil and vegetation classification were higher for 2005 (Figure 2.10). The same however, cannot be said for the Little Washita watershed, OK, where the dry (SMEX03) and the wet (CLASIC07) years show a similar range of joint entropies based on the soil and topography based classifications (Figure 2.11). This analysis also shows that the inclusion of a vegetation based heterogeneity leads to an increase in variability of soil moisture during wet conditions, also consistent with the findings of Albertson and Montaldo (2003).

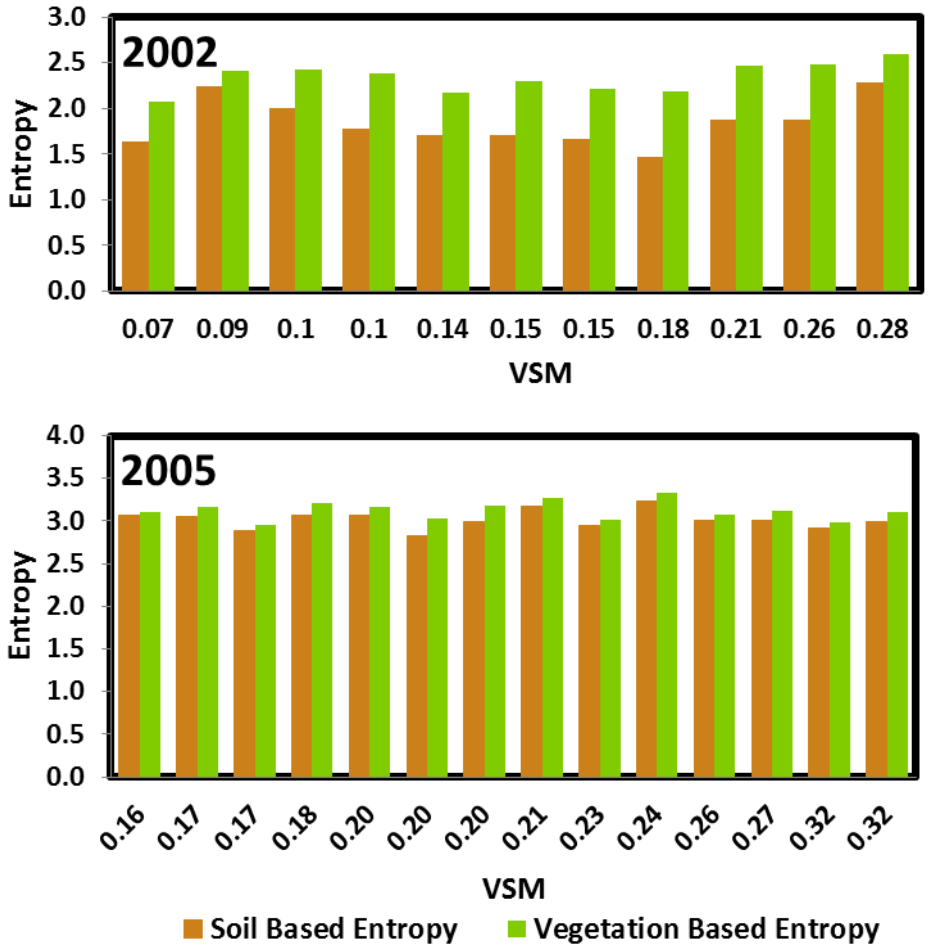

Figure 2.10: Point scale joint entropy values based on soil and vegetation for Walnut Creek watershed, Iowa

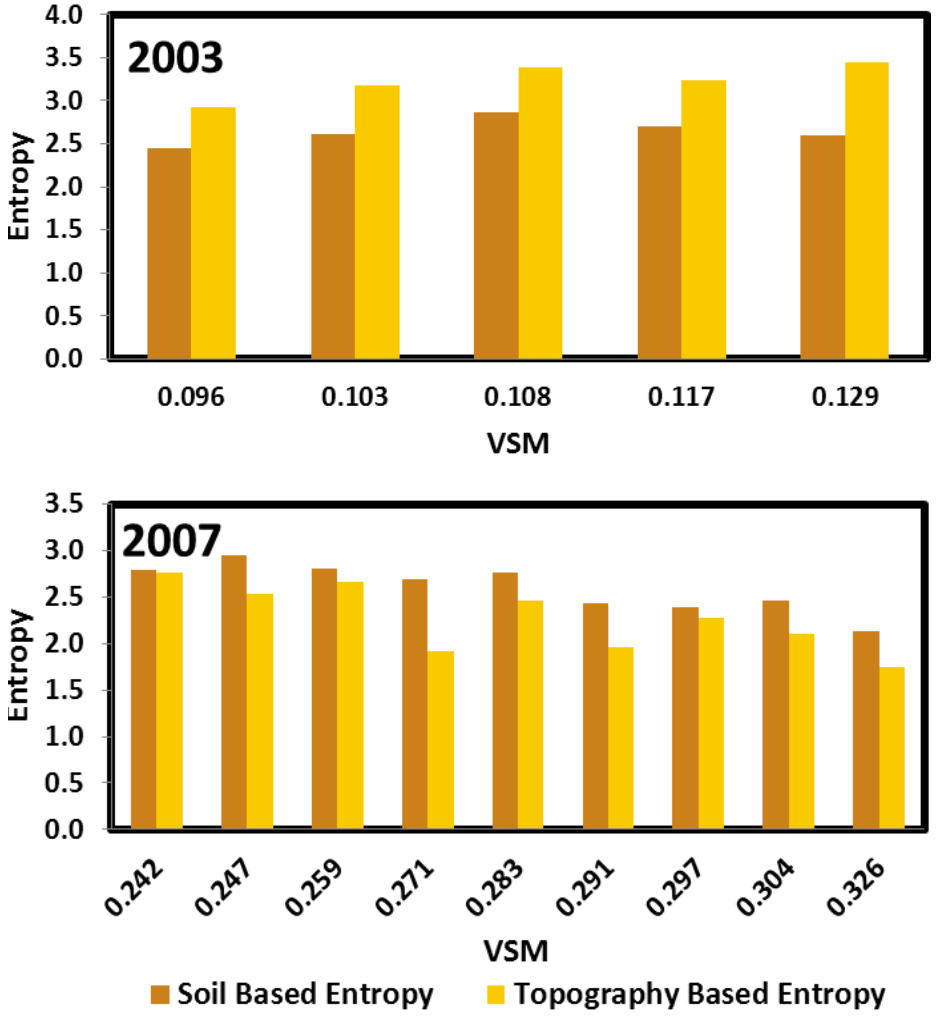

Figure 2.11: Point scale joint entropy values based on soil and topography for Little Washita watershed, Oklahoma

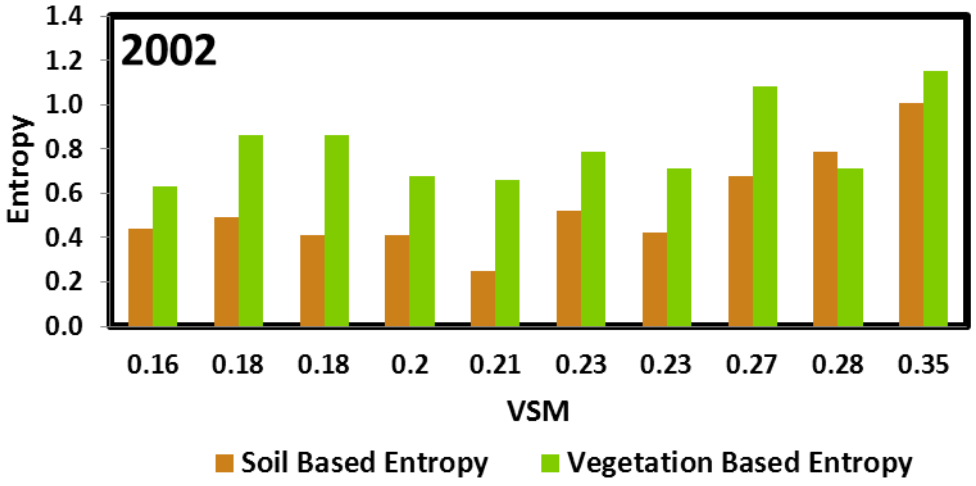

Figure 2.12: Airborne scale joint entropy values based on soil and vegetation for Walnut Creek watershed, Iowa

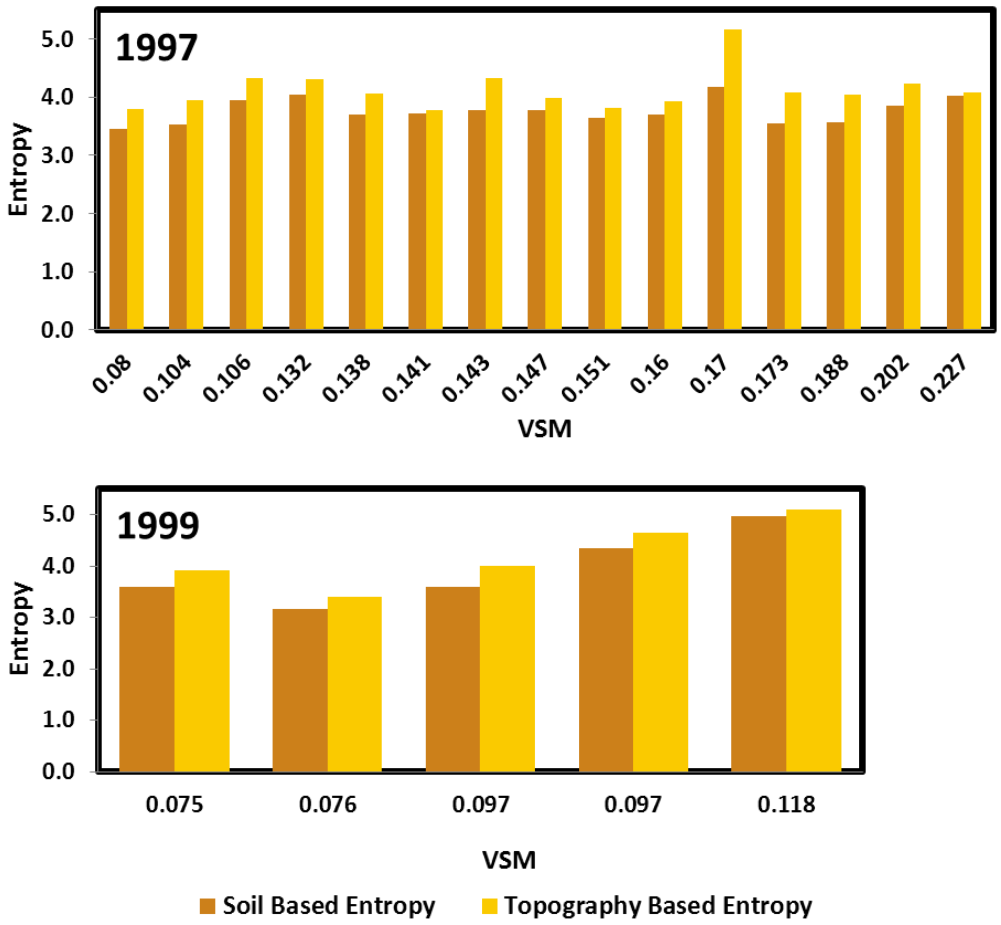

Figure 2.13: Airborne scale joint entropy values based on soil and topography for Little Washita watershed, Oklahoma

At the airborne scale, as compared to the point support scale, we see a lowering of the joint entropy values in Iowa (Fig. 2.12 and 2.13). This implies that at the airborne scale, soil texture and vegetation type (as a heterogeneity index) perform better than at the point scale. For Oklahoma, even though the marginal entropy values for airborne scale followed a similar range (Fig 2.9) when compared with the point scale values, the joint entropy values show a marked increase (Fig. 2.11 and 2.13). This means that the soil and topography based classifications do not represent soil moisture variability well at this scale.

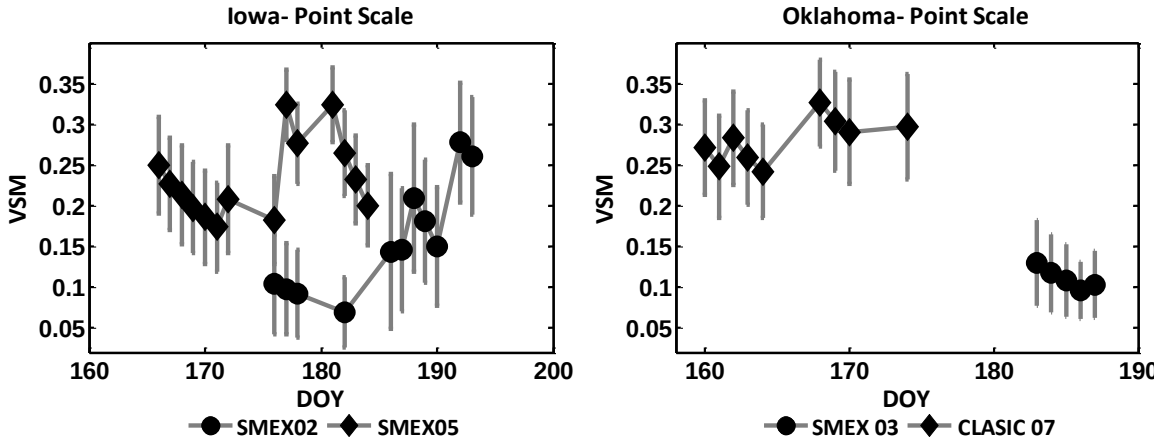

Figure 2.14: Time series of mean soil moisture for point support scale. The whiskers represent 1 standard deviation.

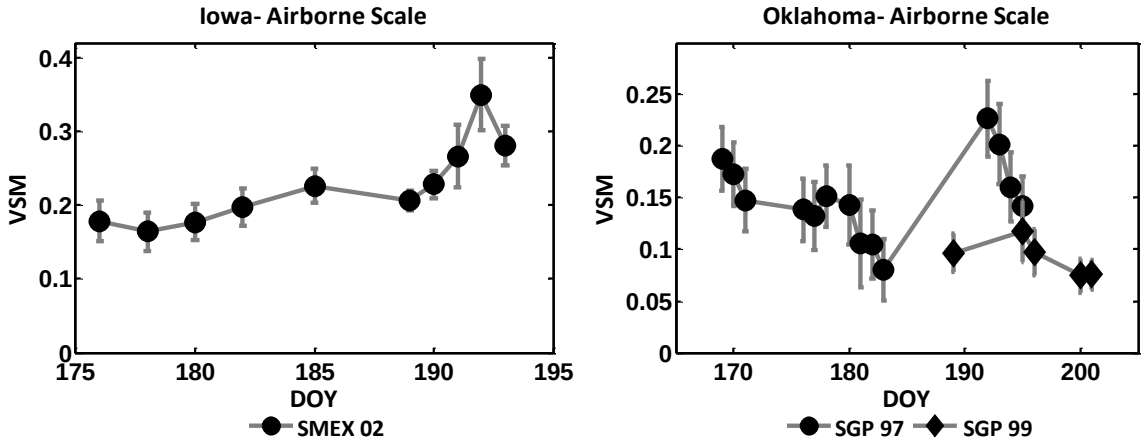

Figure 2.15: Time series of mean soil moisture for airborne footprint Scale. The whiskers represent 1 standard deviation.

The differences between the joint entropy values based on the different classification schemes were computed and the difference between the two (Δ Entropy) was evaluated (Figures 2.16, 2.17, 2.18 and 2.19). For Oklahoma, (Δ Entropy) represents difference between soil based and topography based entropy. For Iowa, (Δ Entropy) represents difference of soil based and vegetation based entropy. We would also like to point out that the exclusion of transinformation between the entropies based on the different classifications has not been computed separately in the analysis. However, this does not take away the credibility of the analysis, since we worked with the entropy difference and not the absolute entropy values to ascertain the dominant physical control.

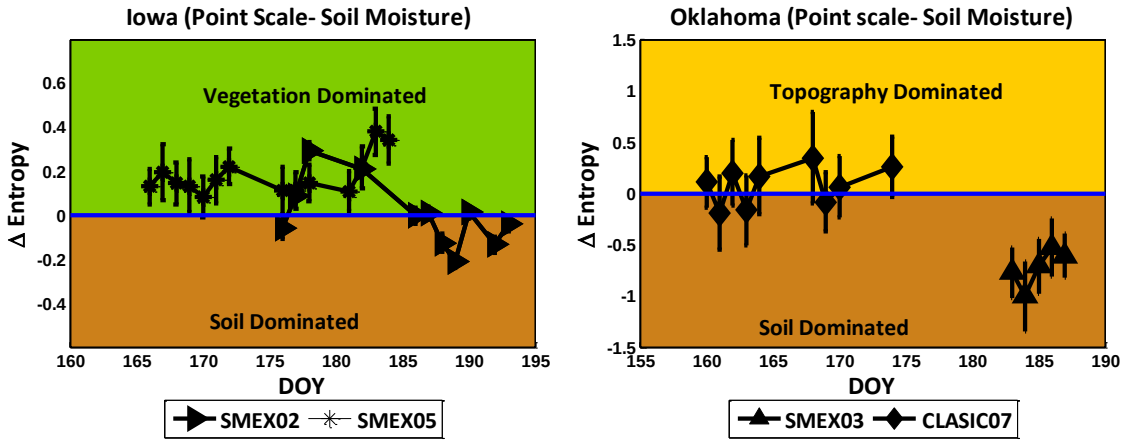

Figure 2.16: Time series of entropy difference (raw soil moisture) for point support scale. The error bars represent 1 standard deviation from the bootstrapping result. For Iowa: Δ Entropy = soil based entropy – vegetation based entropy, For Oklahoma: Δ Entropy = soil based entropy – topography based entropy

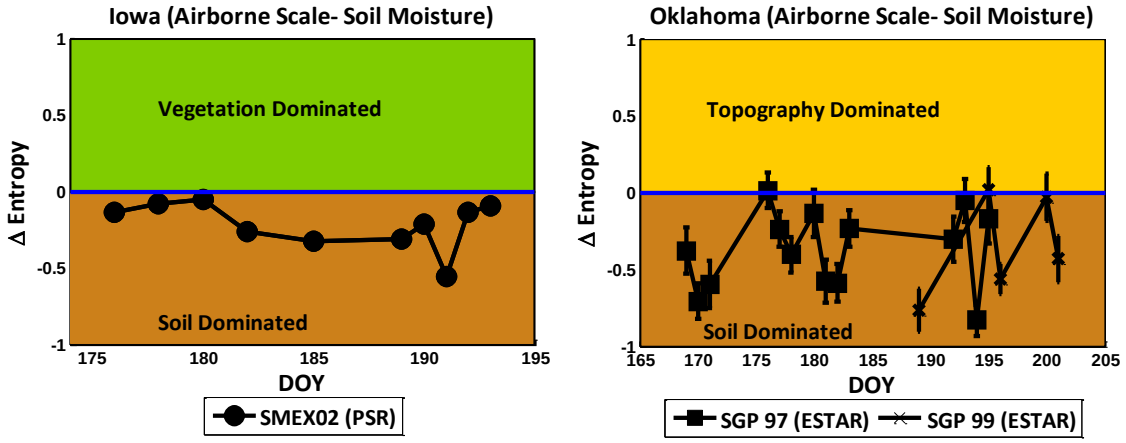

Figure 2.17: Time series of entropy difference (raw soil moisture) for airborne support scale. The error bars represent 1 standard deviation from the bootstrapping result. For Iowa: Δ Entropy = soil based entropy – vegetation based entropy, For Oklahoma: Δ Entropy = soil based entropy – topography based entropy

Point Scale: In Iowa, using the raw soil moisture data at the point support scale (Figure 2.16), we observe that during the relatively wet SMEX 05 year, vegetation appeared to dominate the soil moisture spatial distribution. However, during SMEX 02, the controls shifted between soil and vegetation at precipitation events (as marked by an increase in soil moisture, Figures 2.14 and 2.15). This was also consistent with the mixed results obtained using the Kruskal-Wallis analysis where 2002 showed mixed effects. However, this could be a result of the different amounts of rainfall that occurred over different parts of the watershed. After removing the effect of rainfall (Fig. 10), we observed that across both the years, soil texture was explaining more of the variability in the data. Though the difference between the soil and vegetation based entropy evolved with time, soil texture gave us more information about the spatio-temporal distribution at the point support scale.

The soil moisture conditions in Oklahoma represented two extremes of the wetness spectrum. 2003 was very dry whereas 2007 was very wet. Using the raw soil moisture data, we observe that soil was the dominant physical control in 2003 as opposed to the dynamic evolution of dominant physical controls evident in 2007. However, after removing the effect of precipitation from the analysis, we discovered that soil still dominated the spatio-temporal distribution of soil moisture in 2003 whereas only topography based dominance was evident in 2007. This analysis reinforces the diagnosis that variable rainfall across the watershed can lead to misleading results. For the dry year, 2003, excluding the effect of rainfall did not have any effect on the analysis. The dominant physical control was soil texture. However, in the wet year, 2007, despite the fact that topography was unable to effectively partition the mean soil moisture (Kruskal-Wallis), it still explained more variability (entropy) in soil moisture spatial distribution than soil. A clear dominance of one factor is difficult to outline in this case.

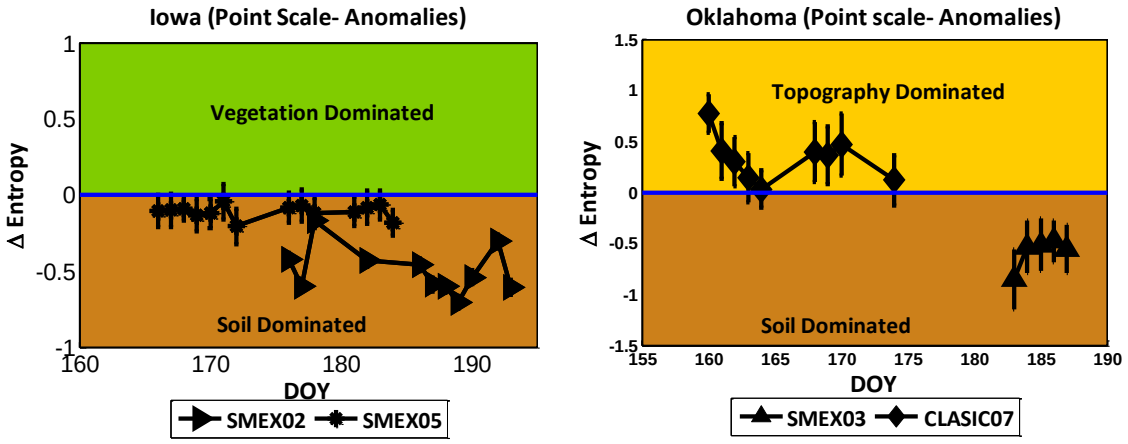

Figure 2.18: Time series of entropy difference for point support scale. The error bars represent 1 standard deviation from the bootstrapping result. For Iowa: Δ Entropy = soil based entropy – vegetation based entropy, For Oklahoma: Δ Entropy = soil based entropy – topography based entropy

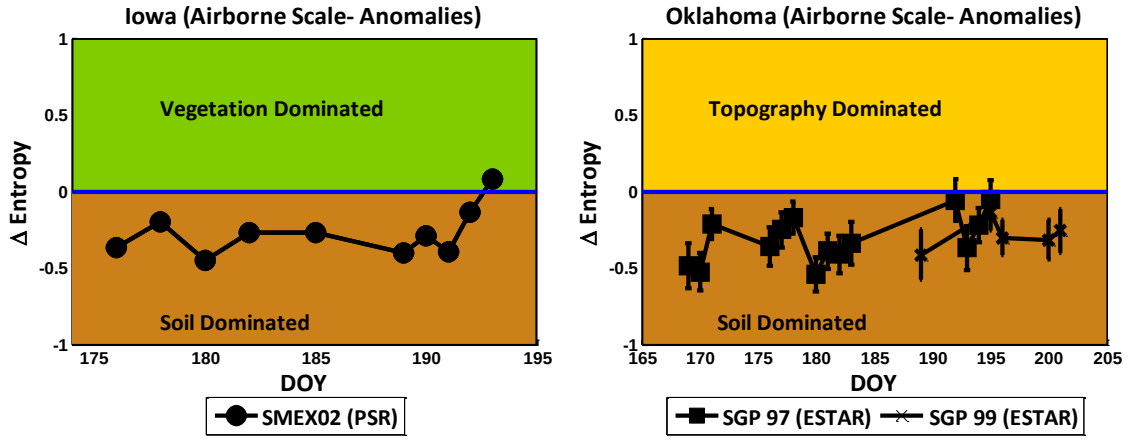

Figure 2.19: Time series of entropy difference for airborne support scale. The error bars represent 1 standard deviation from the bootstrapping result. For Iowa: Δ Entropy = soil based entropy – vegetation based entropy, For Oklahoma: Δ Entropy = soil based entropy – topography based entropy

Airborne Scale: In Iowa, 2002, soil texture is dominant. Even though the magnitude of âĹĘ Entropy changed after removing the effect of precipitation, the analysis did not change much. The same was observed in Oklahoma in 1997 and 1999. Soil texture was the dominant physical control and the analysis result did not change much after removing the effect of precipitation. These results were consistent with Cosh and Brutsaert, (1999) who showed that soil is the most plays the most dominant role in controlling the spatial variability of soil moisture. However, it cannot be said that soil texture would be the most dominant factor of spatio-temporal distribution of soil moisture in Iowa, since, it did not partition the mean soil moisture effectively. In Oklahoma on the other hand, soil texture can be called the most dominant physical control of soil moisture. It should also be noted that retrieval algorithms utilize vegetation (land cover, single scattering albedo and vegetation water content) and soil information (soil texture) when estimating soil moisture (Bindlish et. al, 2006). The effect of slope is not considered in radiometer based soil moisture retrievals. This result may be an artifact of the structure of the retrieval algorithm itself. From the above entropy based analysis, we saw a change in the interaction between the physical controls before and after removing the effect of precipitation for the point support scale but not so much for the airborne scale. It can be deduced that the effect of variability of precipitation across the extent is more pronounced when the support scale is smaller.

2.6 Conclusions

In this study we investigated the evolution of dominance of different physical controls on spatial distribution of soil moisture across time for Walnut Creek watershed, Iowa and Little Washita watershed, Oklahoma. The two watersheds were located in different hydroclimates and had distinctly different inherent heterogeneity. Walnut Creek watershed in Iowa is an agricultural watershed in a humid climate with heterogeneity in the form

of vegetation and soil type. The Little Washita watershed in Oklahoma is a more natural watershed in a sub-humid environment with heterogeneity existing in the form of topography and soil type. The analysis was conducted at two levels. The Kruskal-Wallis based analysis formed the primary step and assessed the applicability of the physical controls in causing a separation in mean soil moisture due to the heterogeneity observed in the particular physical control. We found that in the Walnut Creek watershed, the broad classifications of vegetation type and soil type, served to explain differences in soil moisture well. Soil texture performed slightly better in 2002 whereas vegetation performed better in 2005. However, at the airborne scale, neither soil nor vegetation served as good representatives of heterogeneity. In Little Washita watershed, on the other hand, soil and topography (slope) performed relatively well at both the point and airborne scale. Soil texture partitioned mean soil moisture to a greater extent at both scales.

The second level of analysis comprised of assessing the partitioning the variability of soil moisture by the physical controls which was done by computing the entropy values. At the point scale, we found that in Iowa soil texture partitioned soil moisture variability across both the years. However, in Little Washita, the two years showed different results. In the dry year soil texture showed better partitioning of soil moisture whereas in the wet year, topography showed better partitioning. At the airborne scale, soil texture showed an effective partitioning of soil moisture variability for both the watersheds. However, this may be an artifact of the structure of the soil moisture retrieval algorithm itself.

We also found that given the same extent scale, variable precipitation is more liable of effecting the apparent interactions of physical controls with data observed at a smaller support scale. An important take home message from the study is that during a field campaign while collecting ground based data, it is very important to collect representative samples from different vegetation and soil types in agricultural watersheds since they jointly control the soil moisture spatial distribution. In the absence of vegetation based heterogeneity

in the watershed, soil textures based heterogeneity seems to yield more control on soil moisture spatial distribution as opposed to topography. However, since the nature of heterogeneity controls the spatial distribution of soil moisture, this result must be restricted to watersheds with similar heterogeneity.

3. LAND-SURFACE CONTROLS ON NEAR-SURFACE SOIL MOISTURE DYNAMICS: TRAVERSING REMOTE SENSING FOOTPRINTS

3.1 Synopsis

In this new era of remote sensing based hydrology, a major unanswered question is how to incorporate the impact of land-surface based heterogeneity on footprint scale soil moisture in understanding the hydrologic cycle. The answer to this question becomes twice complicated since 1) soil moisture dynamics that vary with (support, extent and spacing) scale are dependent on land-surface based heterogeneity and 2) land-surface based heterogeneity itself is scale specific and varies with hydro-climate/regions. Land-surface factors such as soil, vegetation and topography affect soil moisture dynamics by redistributing the available soil moisture on the ground. In this study, we determined the contribution of these physical factors on the redistribution of near-surface soil moisture across a range of remote sensing scales varying from airborne remote sensor footprint (1.6 km) to a satellite footprint scale (25.6 km). Two-dimensional non-decimated wavelet transform was used to extract the support scale specific information from the spatial signals of the land-surface and soil moisture variables. The study was conducted in 3 hydro-climates: humid (Iowa), sub-humid (Oklahoma) and semi-arid (Arizona). It was found that the dominance of soil on soil moisture dynamics typically decreased as we went from airborne scale to satellite footprint scales whereas the influence of topography and vegetation increased with increasing support scale for all three hydro-climates. The distinct effect of hydro-climate was identifiable in the soil attributes dominating the soil moisture dynamics. It was found that the near-surface soil moisture dynamics in Arizona (semi-arid) can be more attributed to the clay content which is effective limiting parameter for evaporation whereas in the humid and wet Oklahoma, % sand (limiting parameter for drainage) was the dominant

attribute of soil. The findings from this study can provide a deeper understanding of the impact of heterogeneity on soil moisture dynamics and the consequent improvement of hydrological models operating at footprints scales.

3.2 Introduction

Near-surface soil moisture dynamics refer to the variations in near surface soil moisture. They govern (1) partitioning of the energy and water budget, (2) triggers for runoff on the land surface or infiltration into the deeper layers after rainfall depending on the antecedent moisture conditions, (3) modulation of groundwater recharge rates and contaminant transport to the groundwater and (4) bottom boundary condition for climate models and top boundary condition for watershed hydrology and agricultural production models. However, the apparent soil moisture dynamics can vary widely with the spatial and temporal scale of measurement of soil moisture (Bloschl and Sivapalan, 1995; Gaur and Mohanty, 2013) which can be varied based on the scaling triplet, i.e., support, extent, and spacing scale (Bloschl and Sivapalan, 1995). The advent of a remote sensing (RS) era in hydrology has led to increased availability of data over larger extents, coarse remote sensing supports (footprints) and regular spacing whereas our understanding of soil moisture dynamics (Richard's equation, Richard (1931) has been based on soil moisture data collected at smaller extents, Darcy support scale and irregular spacing. In order to exploit the full potential of soil moisture estimation from space and enable transfer of knowledge of soil moisture dynamics between scales, it is essential to understand soil moisture dynamics from a remote sensing (support, spacing and extent) scale perspective. The other important factor governing soil moisture dynamics at the RS footprint is the hydro-climate of the region. The hydro-climate of a region determines the amount of input water (in terms of precipitation) to any region and discounting tectonic activity or nature of parent rock material, it also represents the nature of landscape forming agents (like precipitation,

temperature extremes observed in a region etc.). For example, an arid hydro-climate (like deserts) will be dry and will typically have poorly formed coarser sandy soils since a major weathering agent (water) is available in low quantity. Likewise, the vegetation density is also determined by the precipitation amount, temperature etc. while many topographic features (rills etc.) may also be generated as a result of long term impact of channeling of precipitation. Since soil type, vegetation (type, density etc.), topography and precipitation history control soil moisture dynamics (Mohanty and Skaggs, 2001; Gaur and Mohanty, 2013), it can be hypothesized that dynamics of soil moisture are hydro-climate specific.

Past literature has focused extensively on correlations between physical factors and soil moisture using geostatistics. This has enabled scientists to evaluate their effect on soil moisture at varying extent and spacing scales but fixed support scale (typically Darcy). Ryu and Famiglietti (2006) used ground based soil moisture data (Darcy support scale) to propose that small scale correlations were controlled by soil and vegetation properties whereas large scale correlations could be attributed to precipitation (Joshi and Mohanty, 2010). Cosh and Brutsaert (1999) demonstrated a soil based control on soil moisture distribution which was also corroborated by Gaur and Mohanty (2013). Soil moisture distribution has also been shown to be influenced by variable land cover, land management, micro-heterogeneity (Mohanty et al., 2000a) and topography (Mohanty et al., 2000b; Burt et al., 1985; Western et al., 1999). Oldak et al. (2002) computed soil moisture variograms with data collected at 400 m support scale and compared them with those of rainfall and soil texture. They associated soil moisture variability observed in Oklahoma at 10 km to soil texture and larger scale dynamics to precipitation variability. However, only a few studies have discussed soil moisture variability by varying support scales (RS footprints) and have mostly been limited by the scales and/or hydro-climates being analyzed. Jawson and Niemann (2007) described the influence of soil texture, topography and land-use on soil moisture patterns using soil moisture data collected at 800 m support scale for a re-

gion in Oklahoma and described that percent sand is most closely related to soil moisture variability. Joshi and Mohanty (2011) used data collected at the 800 m support scale in Iowa and argued that rainfall, topography, and soil texture have maximum effect on soil moisture distribution with limited influence of vegetation. Gaur and Mohanty (2013) used data from Oklahoma and Iowa at 800 m support scale to show a soil texture based control on soil moisture variability.

Considering the lack of and need for studies regarding the effect of varying support scales on the relationship between soil moisture and heterogeneity, the primary objective of this study was to determine the hierarchical dominance of land-surface (soil, vegetation and topography) factors on soil moisture across remote sensing support scales varying from 1.6 km (airborne) to 25.6 km (satellite) for 3 hydro-climates. The extent and spacing scale for the study was fixed at regional extent and regular spacing while the support was varied to extract support scale specific information from the spatial signal of the physical variables using 2-dimensional non-decimated wavelet transform. A number of attributes were chosen to represent soil, vegetation and topography for a comprehensive evaluation of the land-surface factors. To the best of the authors' knowledge, this is the first study addressing the physical controls of near-surface soil moisture across such a wide range of support scales.

3.3 Study Area and Data

3.3.1 Climatology

The study has been conducted in 3 separate regions representing different hydro-climates (Figure 3.1). The first region lies in Arizona. The climate in this region is classified as semi-arid hot climate (climate classification BSh, Ackerman (1941)). This climate typically receives 25.4 cm of precipitation but not more than 76.2 cm annually. Precipitation is caused by cyclonic fronts and the water balance displays a deficit (output

> input) throughout the year. The potential evaporation during the growing season is between 101.6- 127 cm (NOAA technical report NWS 33, 1982). The second region is in Iowa. The climate in the region is classified as moist climate with severe winter (climate classification Dfa). The potential evaporation during the growing season is 76.2 cm. The third study area is in Oklahoma and is characterized as sub-tropical climate (climate classification Cfa). The climate in the region remains humid throughout the year. The summers are hot and long while the winters are cool and short. Frontal precipitation from cyclonic storms dominates in winters which are replaced by convectional precipitation during summer. The potential evaporation during the growing season is between 91.4- 101.6 cm. The water budget for Oklahoma typically is a surplus. In case a deficit exists, it does not last beyond 2-3 months.

3.3.2 Data

The heterogeneity in topography, soil, and vegetation was described using various attributes for a comprehensive analysis. Topography was represented by elevation (DEM), slope (degree) and flow accumulation, soil was represented by percent clay and percent sand, while leaf area index (LAI) was used to represent vegetation. The elevation data was obtained from the National Elevation Dataset (Gesch, 2009). Slope (calculated in degrees) and flow accumulation were derived from the same elevation dataset using ArcGIS (ESRI). Percent sand and clay values were obtained from Soil Geographic (STATSGO) Data Base for the Conterminous United States (Miller and White, 1998). LAI was extracted from the 4-day composite MODIS product (NASA Land Processes Distributed Active Archive Center). Statistics describing site characteristics have been given in 3.1. Airborne volumetric soil moisture data (Figure 3.2 and 3.3) for Iowa and Arizona was collected during Soil Moisture Experiments in 2002 (SMEX02) and 2004 (SMEX04) respectively, using the Polarimetric Scanning Radiometer, PSR (Bindlish et al., 2006, 2008) at 800 m X 800

m spatial resolution. The data for Oklahoma (Figure 3.4) was collected in 1997 (Southern Great Plains (SGP) 1997 hydrology experiment) using the Electronically Scanning Radiometer (Jackson, et al. 1999) at 800 m X 800 m spatial resolution. The soil moisture data comprises a wide range of soil moisture conditions (Figure 2) that are representative of the typical soil moisture conditions in the regions during the growing season. The airborne soil moisture data was validated against the corresponding field averages of the ground based soil moisture data that was collected simultaneously. Thus, the moisture retrieval algorithm used does not bias the interpretation of the results in this study.

3.4 Methodology

Land-surface based physical factors (also referred to as physical factors or physical controls in the study) mainly affect soil moisture dynamics by redistributing the available moisture in the land surface. Moisture redistribution or changes in soil moisture content in a region over a given period of time, takes place as a result of infiltration/drainage (primarily dependent on soil type) or evapo-transpiration (dependent on vegetation, soil and topography) from within a pixel and also sub-surface/overland flow (dependent on soil and topography) between pixels etc. Since each process causing redistribution has its own associated time scale, a redistributed soil moisture signal sampled over different time scales may reveal a dominance of different physical processes. Thus, moisture redistribution at a fixed time scale (representative of RS data) was selected as the variable for evaluating controls of physical factors on footprint scale soil moisture dynamics. The magnitude of soil moisture redistribution is also a function of antecedent moisture conditions and depends on whether the domain is undergoing drying or wetting as evident by hysteresis observed in past studies (Teuling et. al., 2007; Ivanov et. al., 2010; Gaur and Mohanty, 2013). Thus, in order to study the effect of land-surface factors on soil moisture dynamics in isolation, the effect of antecedent soil moisture from the moisture redistribution spatial signal

was removed. We generated pixel based daily (in some cases, once in 2 days or bidiurnal) moisture redistribution images. The daily (and bidiurnal) scale was selected keeping in mind that most satellite based soil moisture data is typically available once every day. The influence of physical factors on moisture redistribution was computed in terms of their areal extent of dominance and the average magnitude of moisture redistribution they cause. The areal extent was evaluated by comparing the spatial patterns of the redistribution signal with the patterns of different land-surface based physical factors. It was assumed that if a physical factor contributed to moisture redistribution, the spatial pattern of moisture redistribution would reflect the spatial pattern of the same physical factor. For example, the spatial patterns of vegetation would match that of moisture redistribution if evapotranspiration was the dominant process causing redistribution. The results were analyzed for drying and wetting conditions separately to account for any large scale hysteresis. The computational details of the methodology are given below.

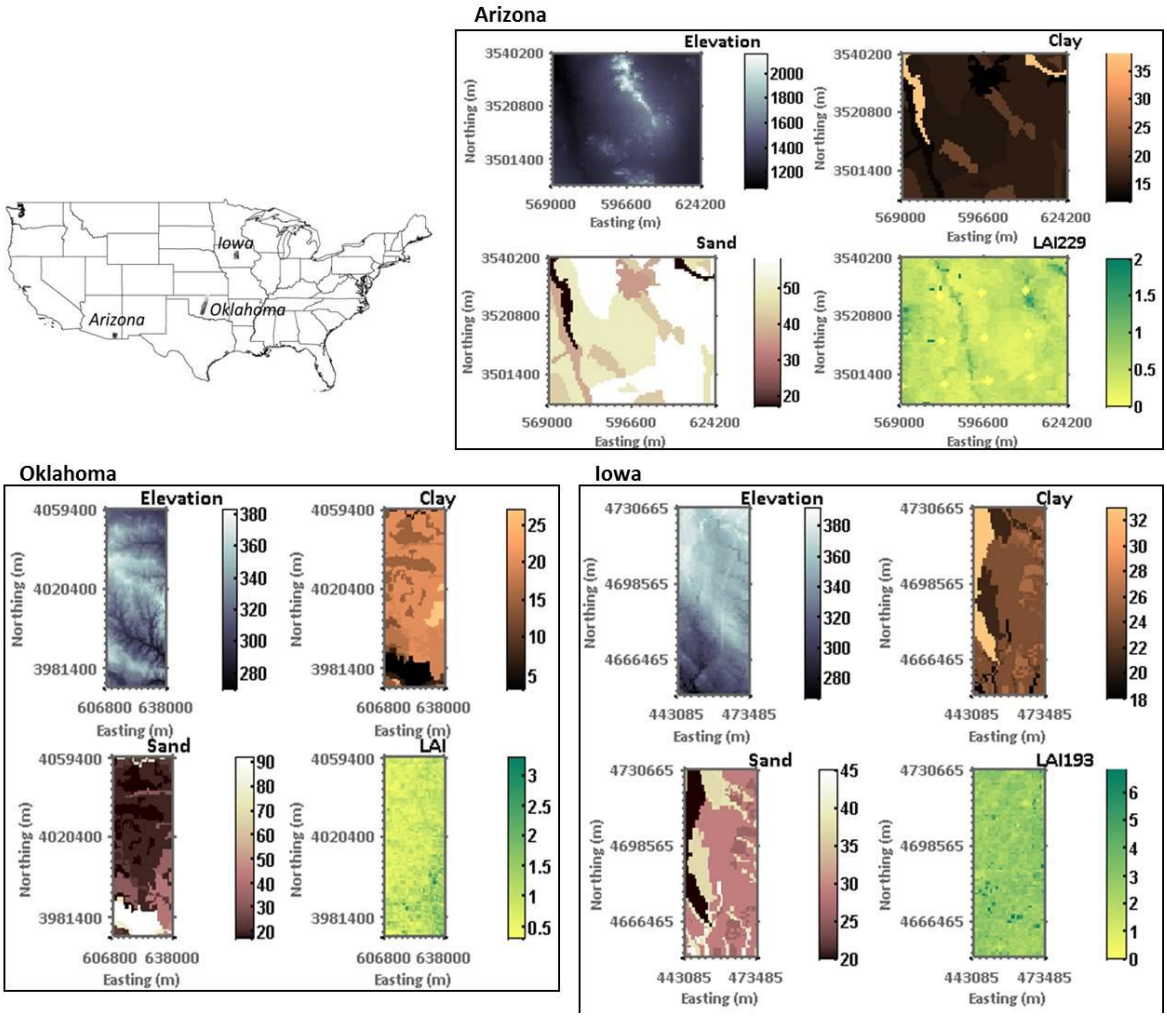

Figure 3.1: Locations of the various study areas along with the heterogeneity that the regions are composed of.

Table 3.1: Metrics of properties representing different physical factors for semi-arid (Arizona), humid (Iowa) and sub-tropical (Oklahoma) regions.

Phys. Factor	Max	Min	Average	CV**	Median
Elevation					
Arizona	2155	1074	1365.96	0.11	1335
Iowa	391.63	266.95	342.85	0.07	350.51
Oklahoma	383	269.99	328.32	0.06	327.67
Clay					
Arizona	38	12	16.64	0.28	16
Iowa	33	18	24.76	0.14	24
Oklahoma	27	3	16.83	0.33	19
Sand					
Arizona	58	17	50	0.19	49
Iowa	45	20	29.92	0.19	29
Oklahoma	92	17	31.51	0.72	20
Slope					
Arizona	17.22	0.03	1.61	1.22	1.05
Iowa	1.36	0	0.24	0.66	0.21
Oklahoma	1.53	0.01	0.35	0.59	0.31
Flow Acc.					
Arizona	1339	0	21.6	3.97	2
Iowa	129	0	4.37	2.58	0
Oklahoma	701	0	10.23	3.81	0
LAI					
Arizona	1.8	0	0.46	0.45	0.5
Iowa	6.8	0.1	2.62	0.33	2.5
Oklahoma*	3.3	0.3	0.96	2.68	0.9

* LAI data for Oklahoma was taken from the year 2004 since MODIS data was not available in 1997. Since Oklahoma is mostly natural grasslands which remain almost same across the years, datasets from different years with similar rainfall was considered.

**CV represents coefficient of variation

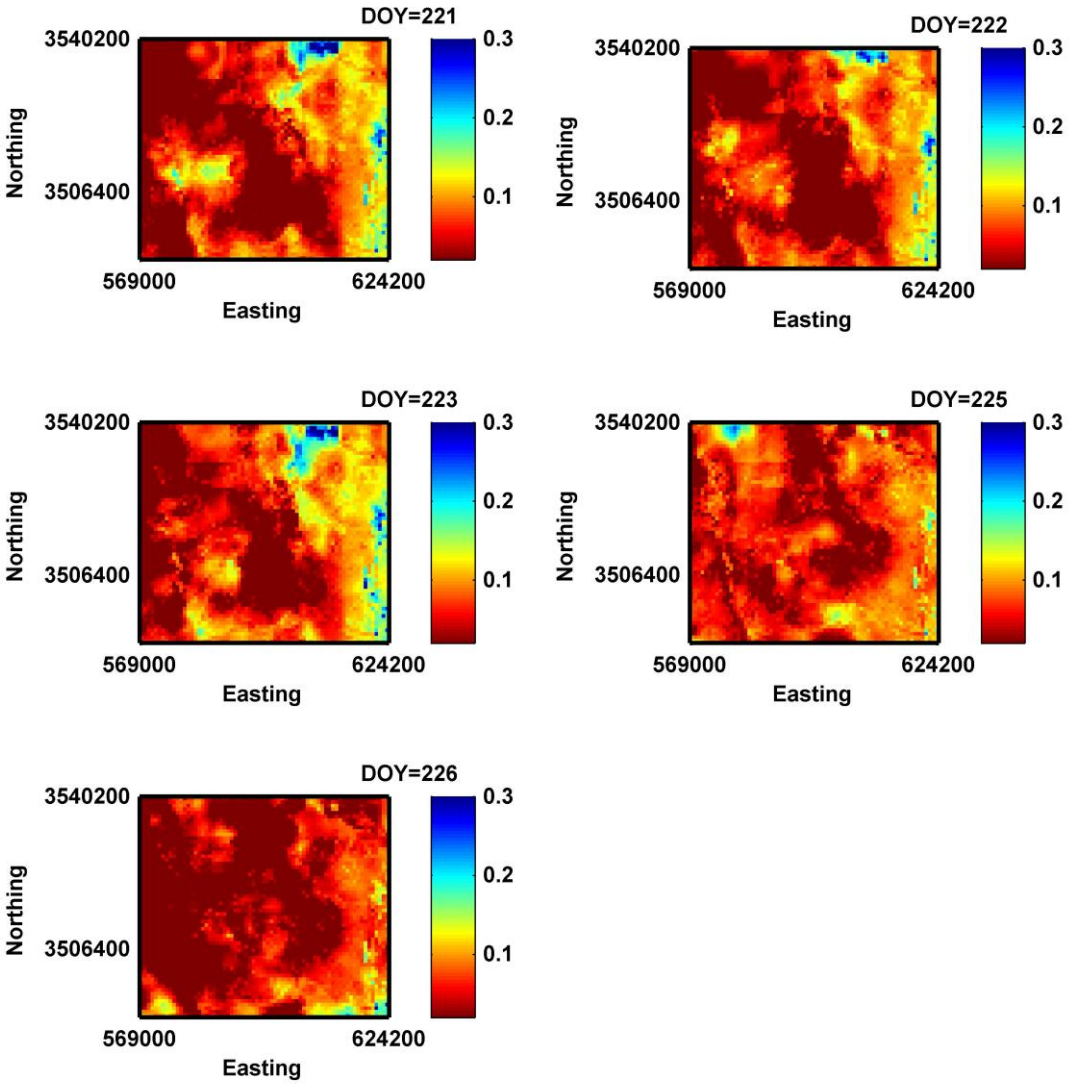

Figure 3.2: Soil moisture maps for Arizona

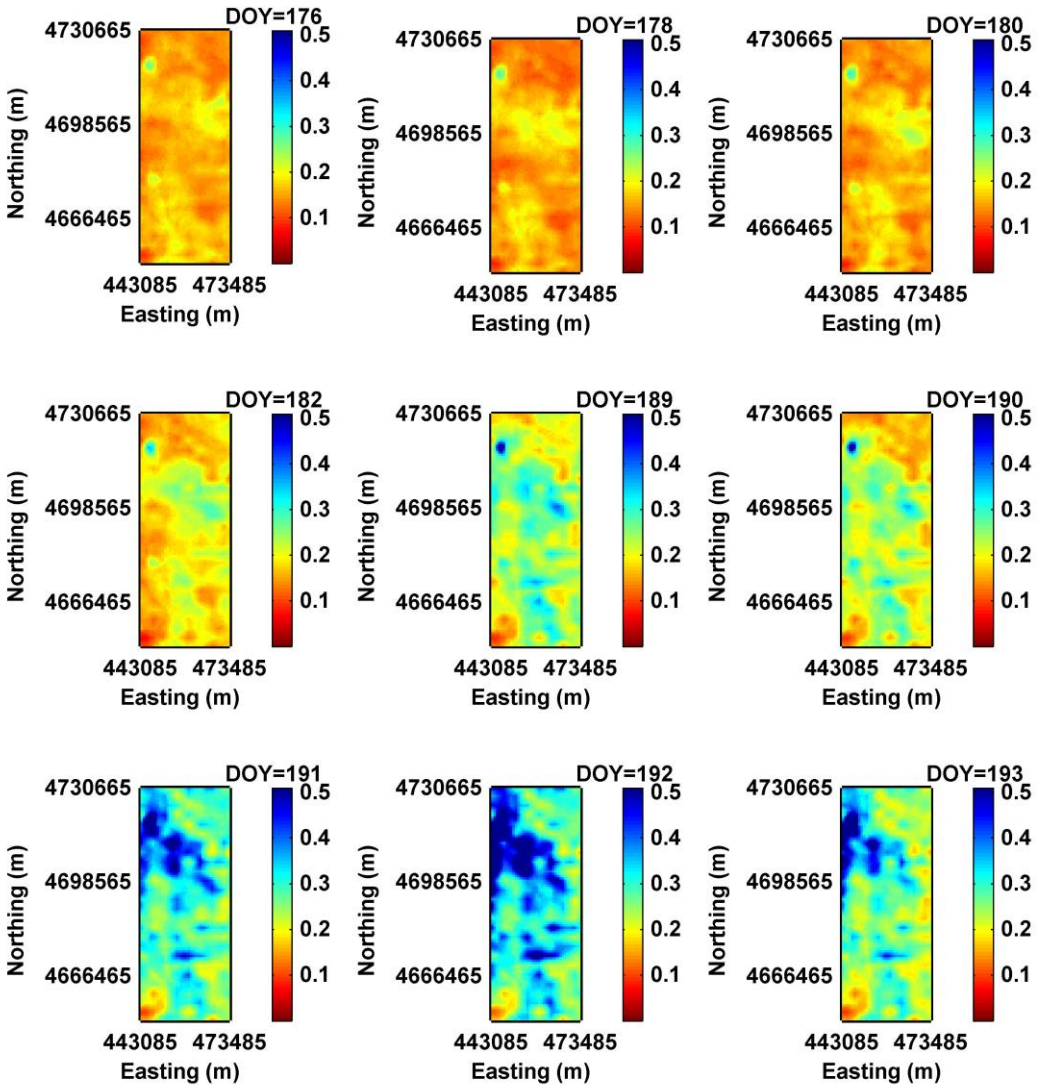

Figure 3.3: Soil moisture maps for Iowa

Using the soil moisture data for each region, soil moisture redistribution (eq. 3.1 and eq. 3.2) values were computed. Soil moisture data was collected at irregular time intervals. Thus, the redistribution values represent soil moisture redistribution over time scales ranging from 1-2 days depending on the duration between two consecutive airborne remote sensing data collection days (Table 3.2).

$$\Delta SM_t = sm_t - sm_{t-1(t-2)} \tag{3.1}$$

where,

ΔSM_t = redistributed soil moisture for day, t (before correction for antecedent soil moisture)

sm_t = soil moisture for day, t

$$\Delta SM_{norm,t} = \frac{\Delta SM_t}{SM_{ant}} \tag{3.2}$$

$\Delta SM_{norm,t}$ = value of soil moisture redistribution at a pixel after correction for antecedent moisture

SM_{ant} = antecedent soil moisture at the pixel

Figure 3.5 shows a monotonic decreasing relationship between antecedent soil moisture and moisture redistribution. Thus, in order to evaluate the significance of different geophysical factors on moisture redistribution in isolation from the effect of antecedent moisture, the redistribution values were normalized using antecedent moisture values for each pixel (eq. 3.2)

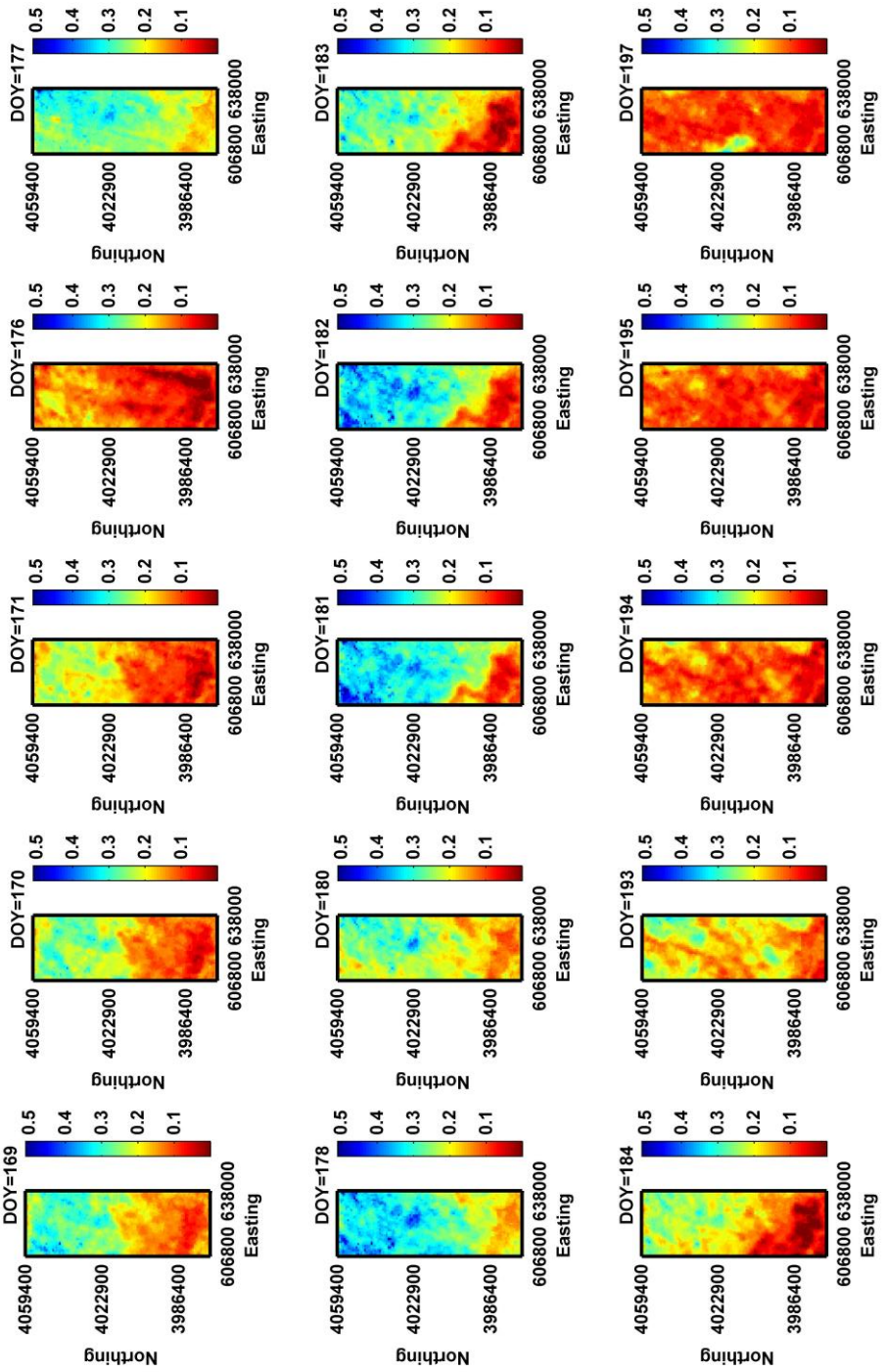

Figure 3.4: Soil moisture maps for Oklahoma

Table 3.2: Days of year (DOY) data was available for and the time and spatial scales at which the wetting/drying dynamics were analyzed

Region	Data availability (DOY)	Time scales analyzed (days)	Spatial support scale (km)	Data dimension (pixels)
Arizona	221-223,225-226	1-2	1.6, 3.2, 6.4, 12.8	4340 (62x70)
Iowa	176,178,180,182,185 189-193	1-2	1.6, 3.2, 6.4, 12.8	3900 (100x39)
Oklahoma	169-171,176-178,180-184, 193-195,197	1-2	1.6, 3.2, 6.4, 12.8	4440 (111x40)

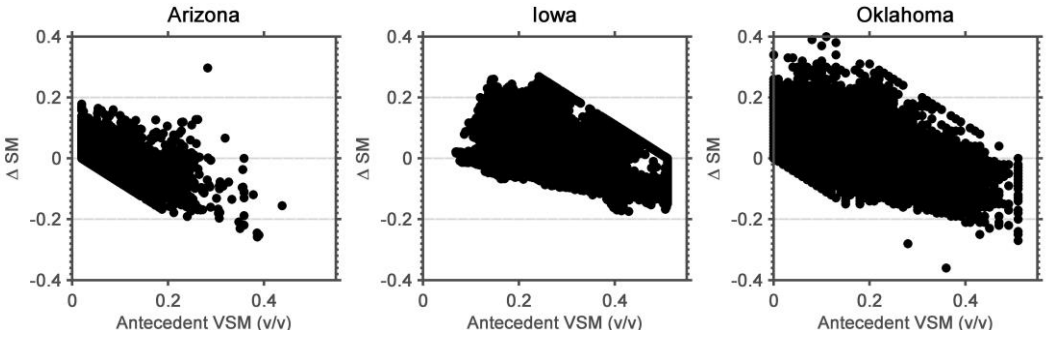

Figure 3.5: Plot of observed ΔSM given antecedent soil moisture conditions

3.4.1 Wavelet Analysis

In order to extract support scale based information from the images comprised of the moisture redistribution values as well as the physical factors, two- dimensional non-decimated wavelet (NDWT) analysis was used. Wavelet analysis has proved to be a powerful tool in understanding geophysical data (Kumar and Foufoula-Georgiou, 1997, Si and Zeleke, 2005). Wavelets are wave like functions, ψ(x), defined at a location 'x' which oscillate about the x-axis and satisfy three criteria 1) $\int_{-\infty}^{\infty} \psi(x)dx = 0$ i.e. zero mean value , 2) $\int_{-\infty}^{\infty} |\psi(x)|^2 dx = 1$ i.e. finite energy, and 3) compact support i.e. non-zero value over a narrow interval. Once a particular formulation of the mother wavelet, ψ(x), is fixed, it is (dilated) and translated over a given signal (eq. 3.3) and the resultant variations serve as

basis functions $\psi_{s,u}(x)$ to represent the given signal.

$$\psi_{s,u}(x) = \frac{1}{\sqrt{s}}\psi(\frac{x-u}{s}) \tag{3.3}$$

s = scaling parameter which controls the dilation

u = location of wavelet used for translation across the signal

NDWT is a discrete wavelet transform. For a discrete wavelet transform (DWT), any signal $f(x)$ is decomposed (eq. 3.4) into wavelet coefficients, $W_{s,u}$ for each scale (s) and location (u), through wavelets. Simply explained a wavelet coefficient, $W_{s,u}$, represents the degree of similarity between the wavelet at the scale 's' and at location determined by 'u' and the signal at the same location. The higher the wavelet coefficient, greater is the similarity

$$W_{s,u} = \sum f(x)\psi_{s,u}(x) \tag{3.4}$$

The basis functions in the case of a DWT scale up in a dyadic series represented by eq. 3.5. The largest scale of the basis function is restricted by the length of the dataset.

$$\psi_{s,u}(x) = 2^{\frac{s}{2}}\psi(2^s x - u) \tag{3.5}$$

s = 1,2,...

The mother wavelet chosen for our study was the Haar wavelet represented by eq. 3.6. A Haar wavelet was chosen given its suitability in soil moisture applications in literature (Das and Mohanty, 2008).

$$\begin{aligned} \psi_{s,u}(x) &= 1 \quad 0 \leq x < 0.5 \\ &= -1 \quad 0.5 \leq x < 1 \\ &= 0 \quad otherwise \end{aligned} \tag{3.6}$$

We performed a 2-dimensional NDWT on our spatial data. A 2-D wavelet transform is a wavelet transform performed twice- once on the rows and once on the columns. It produces horizontal, vertical and diagonal details and an approximation (Figure 3.6). The approximation represents the original signal after the details at support scale range,'s', have been removed from the signal. While running wavelet analysis, each wavelet transform is conducted on the approximation of the next finer scale range (Figure 3.6). Thus, after running the wavelet analysis over all possible scales, the result is a set of details at all scales 'S' and a signal approximation (A_S). The horizontal details are obtained by passing high pass-low pass (HP-LP) filters, vertical details by passing LP-HP and diagonal details are obtained by passing HP-HP filters over the domain. The hyphenated combination indicates the vertical-horizontal direction in which filters are moved. The set of all wavelet coefficients ($\tilde{W}_s$) at a particular scale, s, represents the 'details' in the signal at that particular scale. NDWT is associated with zero phase filter and is translation invariant. It thus results in images of the wavelet coefficients which can be perfectly aligned with the original signal (Percival and Walden, 2000) and reduces error in interpretation resulting from the sampling scheme/starting point of the data. For more mathematical details on NDWT, the readers are referred to Percival and Walden (2000). The NDWT wavelet analysis on our dataset was carried out using the waveslim package (Whitcher, 2012) in the statistical software package R version 3.0.1.

Wavelets analysis (like Fourier analysis) is computed in the frequency domain of the

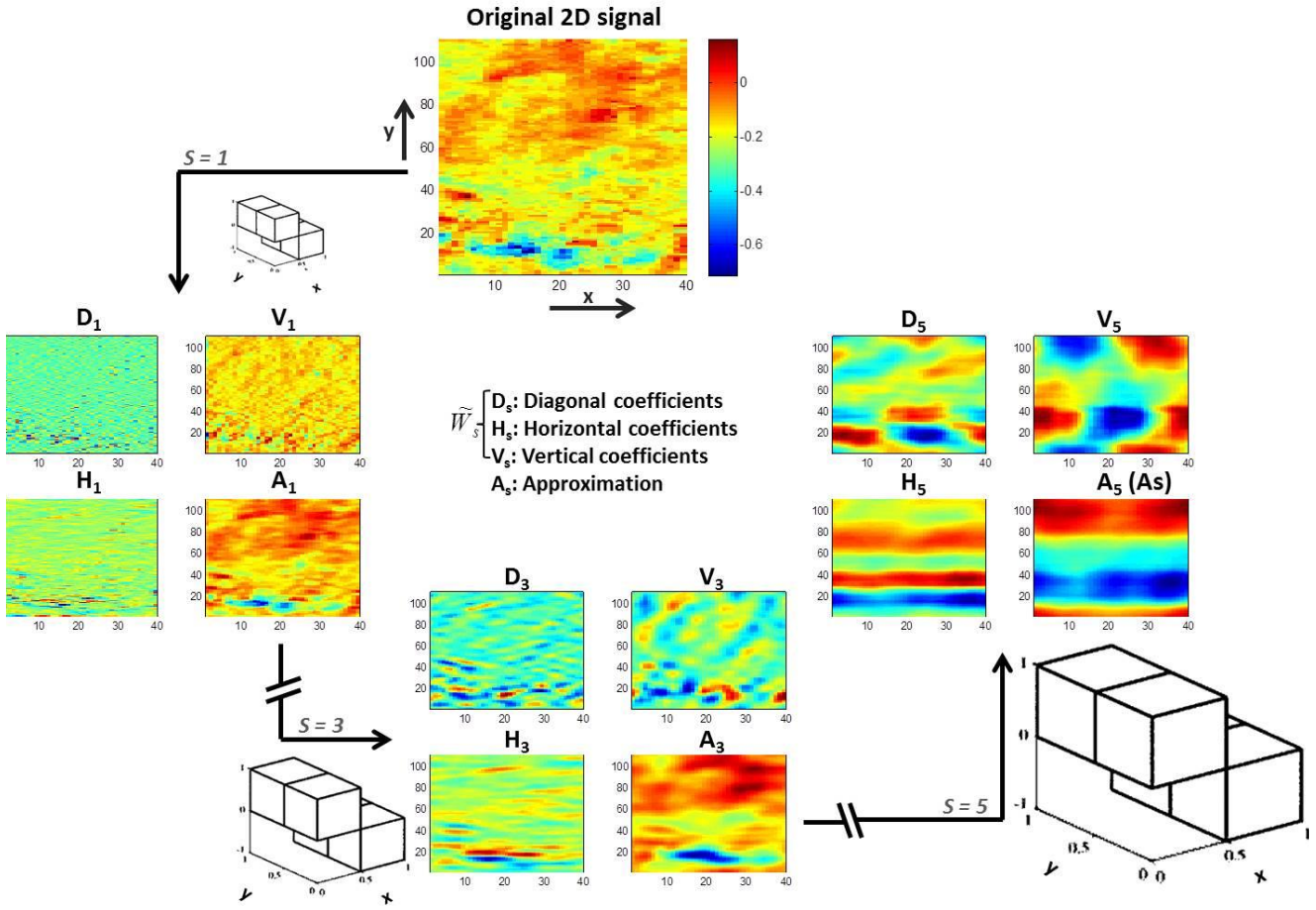

Figure 3.6: Diagrammatic representation of non-decimated wavelet analysis. A dilated (scaled) HAAR wavelet is run on each subsequent approximation of the previous scale to obtain (H,V,D details). Some scales have been omitted for brevity.

(in this case, spatial) signal and provides information of the range of support scales corresponding to different frequency bands. In the given study, the dataset was analyzed over 4 support scale ranges (1.6 - 3.2 km, 3.2 - 6.4 km, 6.4 - 12.8 km, 12.8 - 25.6 km) that represent corresponding ranges of spatial frequency. The scale ranges have been referred to by their lower scale limit in the results and discussion.

A useful property of NDWT is that it divides the total variance of the signal, $\sigma(f(x))$ into the components of variance associated with different support scales. The total variance of the signal can be reconstructed by simple addition (Percival et al., 2011) as explained in eq. 3.7.

$$\sigma(f(x)) = \sum_{S} \sigma(\tilde{W}_s) + \sigma(A_S) \tag{3.7}$$

$\sigma(f(x))$ is defined as the statistical variance $=\Sigma\frac{(f(x)-\overline{f(x)})^2}{n-1}$, where $f(x)$ is the moisture redistribution variable, $\overline{f(x)}$ is the sample mean and n is number of realizations of the variable. $\sigma(\tilde{W}_s)$ or the global wavelet spectrum is the variance contributed by support scale range, s, to the variance of the signal,$\sigma(f(x))$, which can also be obtained by adding the variance of the detail wavelet coefficients (horizontal, vertical and diagonal) at each support scale range. Thus, wavelets can characterize a non-stationary spatial/temporal dataset at different support scales (coarser than the scale of the original signal).

In the given study, the global wavelet spectrum was modified (eq. 3.8) to understand the percentage of variance ($\sigma_{global}(\%)$) contributed by a particular support scale range to the total variance of moisture redistribution signal

$$\sigma_{global}(\%) = \frac{\sigma(\tilde{W}_s)}{\sigma(f(x))} x100 \tag{3.8}$$

3.4.2 Pattern Matching

The contribution of different physical factors to soil moisture redistribution was computed in terms of its areal extent of influence and the magnitude of moisture redistribution associated with the physical factor.

The spatial patterns of the physical factor were matched with the patterns of the moisture redistribution signal at different support scales. The areal extent of impact was determined by calculating the total area at which pattern matches between the physical factor and $\Delta SM_{norm,t}$ were observed. A successful match in the pattern of $\Delta SM_{norm,t}$ and the physical factor was computed by equating the wavelet spectrum ($W^2_{s,norm}$) of the two signals for each spatial support scale. Location specific wavelet spectrum values that differed by less than 0.005, were considered to display a similar pattern at the particular location. Prior to comparison of the wavelet spectrum of the physical factors and $\Delta SM_{norm,t}$, the wavelet coefficients for all set of images were normalized (eq. 9) with mean of 0 and standard deviation of 1. The mean and standard deviation for normalizing the coefficients were calculated after removing the outliers. The outliers were determined and removed using eq. 10.

ΔSM (redistributed near-surface soil moisture) and geophysical control attributes have different ranges. The values of their wavelet coefficients are thus influenced by this varying range in data. Thus, after calculating wavelet coefficients for ΔSM and physical factors, the wavelet coefficients were normalized (eq. 3.9) to transform them to a normal distribution with mean of 0 and standard deviation of 1. The mean and standard deviation for normalizing the coefficients were calculated after removing the outliers. The outliers were determined using eq. 3.10.

$$W_{s,norm} = \frac{W_s - \frac{1}{k}\sum W_s}{\sqrt{(\frac{1}{k}\sum (W_s - \frac{1}{k}\sum W_s)^2}} \tag{3.9}$$

k = number of pixels in the domain

$$\begin{aligned} \hat{W}_{s,outlier} = W_s &> \frac{1}{k}\sum W_s + 2\sqrt{(\frac{1}{k}\sum(W_s - \frac{1}{k}\sum W_s)^2} \\ = W_s &< \frac{1}{k}\sum W_s - 2\sqrt{(\frac{1}{k}\sum(\hat{W}_s - \frac{1}{k}\sum W_s)^2} \end{aligned} \tag{3.10}$$

Eq. 3.11 was then used to determine the areal extent of influence of the physical factors (e.g., soil, topography and vegetation) on $\Delta SM_{norm,t}$ at different support scale ranges.

$$C_{f,s} = \frac{N_{f,s}}{N_{\sum f,s}} x100 \tag{3.11}$$

where $C_{f,s}$ = percent contribution of physical factor, f at a specific support scale range, s;

$N_{f,s}$ = number of pattern matches of a specific physical factor, f, at a specific support scale range, s

$N_{\sum f,s}$ = total number of pattern matches observed for all physical controls at a particular support scale range, s.

The magnitude of controls ($M_{f,s}$) of each physical factor, f, at scales, s, was computed by evaluating the mean of$\Delta SM_{norm,t}$ for the pixels where a pattern match between the physical factor, f and $\Delta SM_{norm,t}$ was observed (eq. 3.12).

$$M_{f,s} = \frac{1}{N_{f,s}} \Sigma_{N_{f,s}} \Delta SM_{norm,t} \tag{3.12}$$

3.5 Results and Discussion

$\Delta SM_{norm,t}$ was computed over 1- or 2-day intervals. The 2-day interval soil moisture redistribution values were calculated when the soil moisture data was not collected daily because of rain events or logistic reasons. Table 2 provides the details of available data

for each study region. The $\Delta SM_{norm,t}$ computed for day of year (DOY) 225 (in Arizona), DOY 178, 180, and 182 (in Iowa) and DOY 180, and 197 (in Oklahoma) represent soil moisture redistribution computed over 2 day periods.

3.5.1 Analysis of Variance of $\Delta SM_{norm,t}$

The variance of a soil moisture signal is dependent on the support scale it is sampled at (Bloschl and Sivapalan, 1995). The total variance of the original$\Delta SM_{norm,t}$ signal represents the variance in soil moisture dynamics at the 0.8 km support scale which contains information of scales at and coarser than 0.8 km (restricted by extent of data). The variance within the 0.8 km support scale has been averaged within the dataset and cannot be represented by this data. The NDWT based analysis divides the variance of the original spatial signal (0.8 km support scale) into variance contributed by different spatial support scale ranges i.e., 1.6- 3.2, 3.2-6.4, 6.4-12.8, and 12.8- 25.6 km. Figure 3.7 shows the percent contribution ($\sigma_{global}(\%)$, eq. 3.8) of each support scale to the total variance of spatial $\Delta SM_{norm,t}$ signal. The daily variance signals showed typical increasing trend up to 6.4 km spatial resolution for all days in Iowa and a few days in Arizona and Oklahoma (Figure 5).

Qualitatively, the trend of scale based variance does not appear to be related to the antecedent moisture conditions (Figures 3.2, 3.3 and 3.4) since both trends (i.e increasing and decreasing till 6.4 km) occur for dry as well as wet days. These results may on the other hand be qualitatively related to the spatial patterns of the land-surface factors (Figure 3.1). Iowa has a smoothly varying gradient in elevation with elevation being higher in the northern part of the region whereas lower in the southern part of the region. The elevation in Arizona on the other hand has a high elevation band in the middle of the domain which radiates to lower elevations while Oklahoma has a rolling topography. Likewise, the soil patterns in Iowa are not 'patchy' unlike Oklahoma which shows higher variation in % sand at shorter distances. Similar variations can be seen in the soil pattern in Arizona albeit

at slightly larger distances than Oklahoma. The higher heterogeneity in the patterns of land-surface factors at coarser scales potentially causes the variability in the soil moisture dynamics to be higher as the support scale is coarsened in Iowa (beyond 6.4 km). Arizona and Oklahoma which are more locally heterogeneous than Iowa show mixed effects with no consistent pattern in the global wavelet spectrum (Figure3.7 a and c).

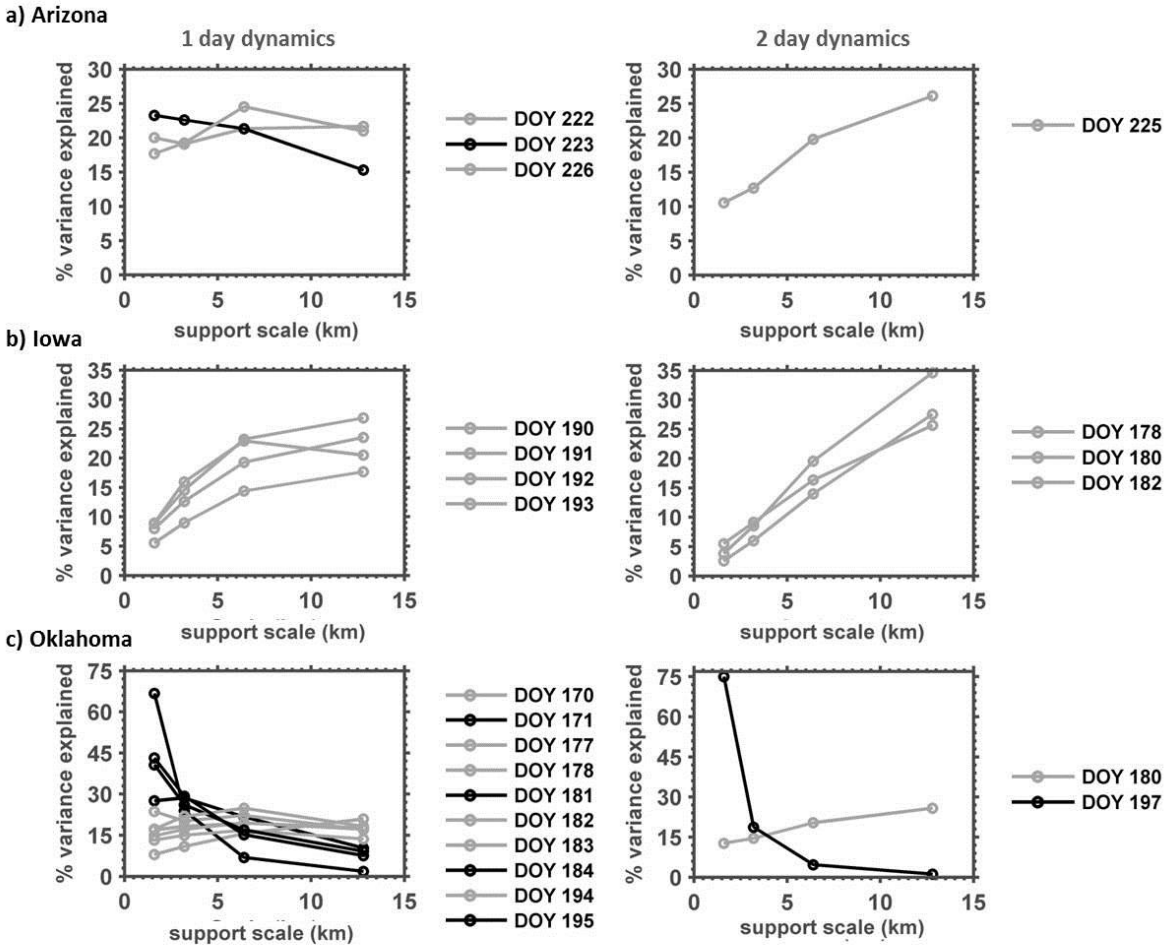

Figure 3.7: Graphs depict percent of the total variance observed in the soil moisture change signal at different scales for a) Arizona, b) Iowa and c) Oklahoma. 1-day and 2-day dynamics represent soil moisture change observed at 1 day and 2-days' interval, respectively. Black line represents declining trend, while grey line represents increasing trend

At homogeneous Darcy scale, antecedent wetness conditions and the stage at which imbibition or drying is initiated determine moisture dynamics of soil. However, this part of the analysis indicates that at remote sensing footprints, heterogeneity and the organization (co-variablity) of land-surface heterogeneity has a greater control over the soil moisture dynamics. The relationship between landscape heterogeneity and moisture dynamics has been discussed in detail in the subsequent sections.

3.5.2 Scale Based Contribution of Physical Factors

The scale based contribution of the physical factors to soil moisture redistribution was evaluated as a function of their areal extent (eq. 3.11) of influence and the relative magnitude of their effect (eq. 3.12) on soil moisture redistribution. The analysis was conducted separately for drying and wetting conditions to account for large scale hysteresis.

3.5.2.1 Areal Extent of Controls, $C_{f,s}$

The patterns observed in different physical factors and $\Delta SM_{norm,t}$ signals were matched for the three study regions. A sample diagrammatic representation of locations of pattern match between moisture redistribution patterns and % sand values is shown in Figure 3.8. Figures 3.8 a and b depict the normalized wavelet coefficients of$\Delta SM_{norm,170}$ (Oklahoma) and % sand respectively while Figure 3.8 c depicts the locations of the pixels where a pattern match between the two was observed. The white pixels correspond to the central location of the wavelet at which a pattern match was observed. The area of these white pixels was consolidated (eq. 3.11) to estimate $C_{f,s}$ (Figure 3.9). The contribution of soil (% sand and % clay) remains high (and typically maximum compared to other factors) in all three hydro-climatic regions while maintaining a decreasing trend as we go higher in scale (Figure 3.9). The trend for contribution of topographical and vegetation factors, on the other hand, increases with increasing scale. Specifically in Arizona, at 12.8 km, the effect of topography and vegetation becomes equivalent/ slightly greater than soil. Also

in Oklahoma, vegetation becomes more dominant than soil beyond 3.2 km. These factors are analyzed in greater detail below.

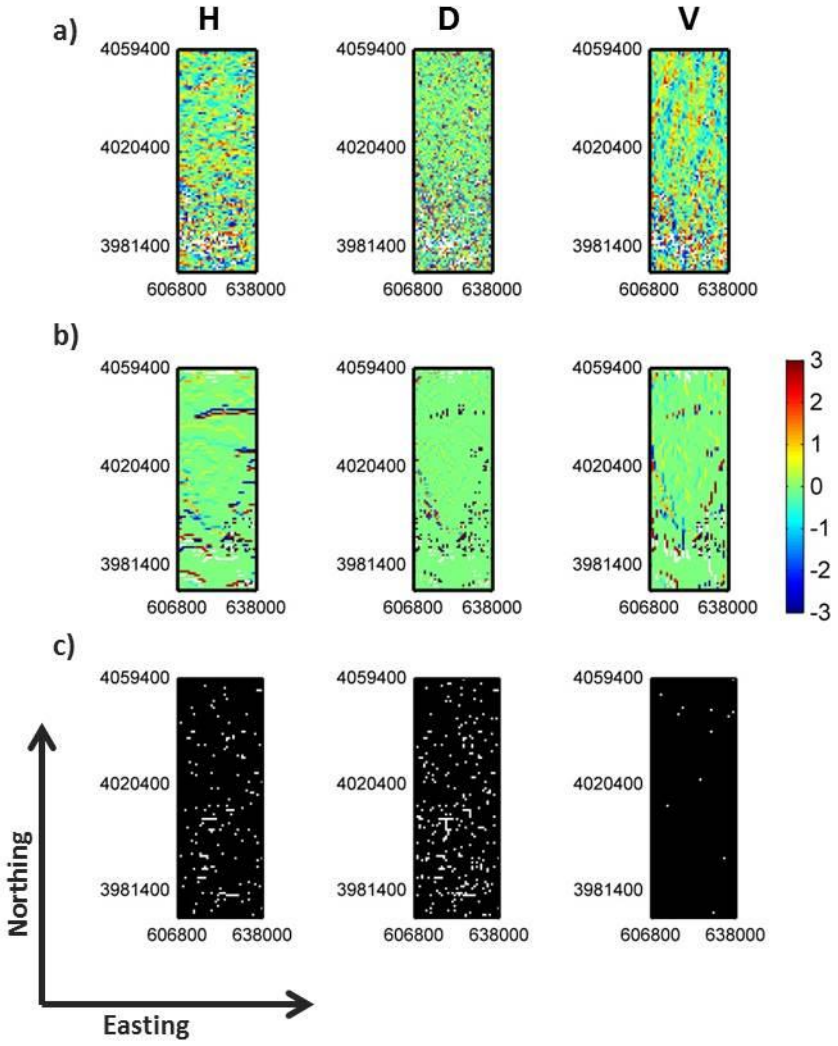

Figure 3.8: a) Normalized wavelet coefficients (Horizontal (H), Vertical (V) and Diagonal (D)) for soil moisture redistribution (DOY 170), b) for % sand, c) Locations of pattern match (white pixels), in Oklahoma at 1.6 - 3.2 km scale

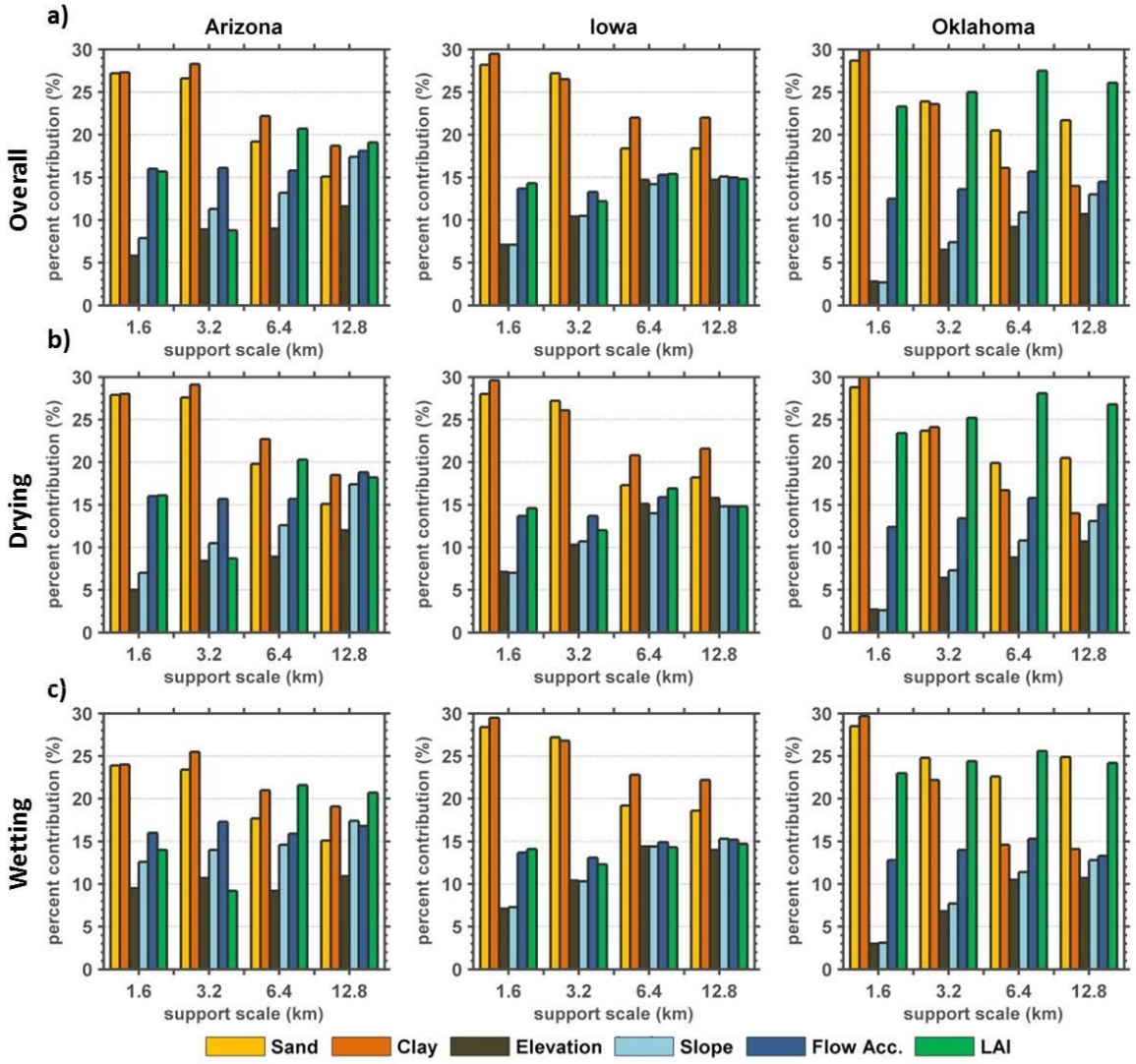

Figure 3.9: Relative contribution of different physical controls to soil moisture redistribution observed in Arizona, Iowa and Oklahoma, a) all pixels, b) drying pixels, and c) wetting pixels.

1. **Soil Factors**

Percent clay and sand: The percentage of clay and sand together define the infiltration capacity of the domain at the land surface. Since they comprise the primary factors determining the pore sizes and structure of the soil in which water is being held, they also affect the rate of evaporation from the soil. Significant association between soil based factors and soil moisture change is evident in all three regions. Higher clay content can be related to higher water holding capacity of the soil. It also slows down infiltration and hinders drainage. In contrast, sand promotes increased infiltration. The spatial distribution of sand and clay across the study scales also determine infiltration vs. evaporation patterns (Nachshon et al., 2011; Zhu and Mohanty, 2002; Mohanty and Zhu, 2007).

The contribution of % clay on soil moisture variability is higher than that of % sand in Arizona and in Iowa (except for the 3.2 km scale), whereas in Oklahoma % sand contributes more than % clay (except for the 1.6 km scale). This is true for drying as well as wetting scenarios. Arizona is semi-arid and receives very little rainfall. Under these conditions, any moisture that is held in the soils is held by the small pores represented by % clay as opposed to % sand. The greater pattern association with % clay in Arizona represents that the evaporation is the dominant process of water redistribution as opposed to drainage of free water (Zhu and Mohanty, 2002). Despite being a sandy region, the water dynamics in Arizona are controlled (limited) by the clay content in the soil. In case of Iowa, which is primarily a cultivated region that receives higher precipitation than semiarid Arizona, soil moisture patterns match well with both % sand and % clay. This indicates that both processes (evaporation and drainage) occur in this region to cause redistribution of moisture. Iowa is a cropped land planted with soybean and corn. The canopies of the two

crops (during initial period of growth) allow bare soil exposure to the sun. Thus, the top soil made porous by plant roots enables infiltration (represented / limited by % sand) whereas the landcover promotes water losses (represented / limited by % clay) through evapotranspiration. Oklahoma is a wet and sub-humid region and the major losses to the near-surface soil moisture are due to drainage represented / limited by % sand. Thus, the influence of soil texture on soil moisture redistribution is directly linked to the hydro-climate and wetness condition of a region.

2. **Topographic Factors**

   Elevation, slope and flow accumulation: Elevation is the basic topographic factor from which a number of heterogeneity representing parameters (slope, flow accumulation etc.) may be derived. Elevation patterns can relate to soil moisture patterns for different reasons (Coleman and Niemann, 2013). It may cause steep potential gradients thus, influencing moisture redistribution. Large elevation differences induce differences in evapotranspiration patterns (Goulden et al., 2012). Slope can strongly influence water distribution through overland flow or aspect based drying. Flow accumulation represents the tendency of the region to accumulate water (concavity) and thus, the water holding capacity. This may lead to localized infiltration and evaporation.

   Figure 3.9a shows that the behavior of topography (elevation, slope and flow accumulation) with scale is similar for all three hydro-climates i.e. its percent contribution increases with support scale. In the relatively natural (anthropogenically unaltered) and topographically more complex (undulating terrain) regions, Oklahoma and Arizona, flow accumulation has a higher contribution than slope and elevation, whereas the trend is different for Iowa where elevation takes a higher precedence at coarser scales (6.4 km and coarser).

Overall, we observe that Arizona and Oklahoma behave similarly whereas the behavior of moisture dynamics in Iowa is different. Oklahoma and Arizona are topographically more complex than Iowa which has a relatively smoothly varying north to south gradient (Figure 3.1). Even though the absolute values of elevations in Iowa and Oklahoma are similar, the pattern association for the two regions is very different. This implies that the spatial patterns of elevation dictate the effect of elevation on soil moisture redistribution. Oklahoma is rolling and thus, the concavity of the domain remains an important factor whereas the slope in Iowa is more uniform and therefore the effect of concavity of the domain becomes lesser than elevation as we go higher in scale. The contribution of slope is slightly higher for the wetting pixels than drying pixels in Oklahoma and Arizona (Figures 3.9b and c). The contribution of elevation is only marginally different during wetting and drying. The higher contribution of slope in the two regions during wetting signifies the occurrence of overland flow in Oklahoma and even in the precipitation limited Arizona. However, in Iowa, the trend is different with elevation showing higher contribution for the drying pixels. The contribution of elevation in Iowa also becomes equivalent to or larger than other topographical factors at the coarser scales (6.4 km and coarser). This signifies two important points. First, elevation influences drying more than wetting and second, irrespective of the precipitation dynamics, in topographically less undulating regions, the contribution of topography on soil moisture spatial distribution is more dominated by the elevation of a pixel. On the other hand in topographically complex (undulating) regions, flow accumulation and slope form better representative parameters of topography for describing soil moisture spatial dynamics.

3. **Vegetation Factors**

Leaf area index: Leaf area can affect soil moisture loss through transpiration and

limit the amount of input water through interception and evaporation of intercepted water on the leaf. It can also direct water flow into the soil through stem flow. The association between LAI patterns and moisture was significant in all 3 regions. The percentage of pattern matches, show a general increasing trend with scale. In Oklahoma, vegetation becomes the most spatially dominant factor at support scale 3.2 km and above. Iowa is an agricultural region with crops of different LAI. Arizona is split among cropland, shrub land, and grass land while Oklahoma is mostly grassland with some agriculture. The significance of vegetation in Iowa is slightly more in the drying pixels as compared to wetting pixels implying more transpiration losses as opposed to differential interception of rain water by the varied plant types (Fig. 3.9b and c). Similarly, Oklahoma also displays a higher contribution of vegetation in the drying scenario. In the sparsely vegetated Arizona, the trend is opposite with higher vegetation contribution for wetting pixels. It signifies a dominance of processes like interception and leaf evaporation from intercepted water.

3.5.2.2 Effect of Physical Factors on Magnitude of $\Delta SM_{norm,t}, M_{f,s}$

Figure 3.10 shows the mean of the absolute values of $\Delta SM_{norm,t}$ (eq.3.12) observed in regions where the pattern matches between various physical factors and $\Delta SM_{norm,t}$ were observed. The range and maximum value of $\Delta SM_{norm,t}$ were higher for the wetting pixels than the drying pixels (Figure 3.10). The higher variability of the $\Delta SM_{norm,t}$ during wetting can be attributed to higher variability in rainfall input to the system which leads to higher variations in soil moisture. Arizona and Oklahoma also showed larger ranges of $\Delta SM_{norm,t}$ whereas they were smaller in Iowa. This partly occurred since there were no heavy precipitation events in Iowa and also the moisture conditions in Iowa did not become extremely dry (Figure 3.5). It was also observed that topography showed significantly greater contribution in Arizona. Mixed effects are observed in Iowa with soil and topography creating

higher $\Delta SM_{norm,t}$ at different scales. Likewise in Oklahoma, topography and soil create higher $\Delta SM_{norm,t}$. These results also reveal that the physical factors which had lower spatial influence (in terms of areal extent) on soil moisture redistribution (Figure 3.9), may have greater influence on the amount of moisture redistribution that takes place and can thus; greatly alter the water budget in the limited spatial regions where they are important. It is worthwhile to note that the magnitude of vegetation effect was typically low in all 3 regions.

3.5.3 Overall Ranking Scheme

In order to characterize the overall effects of the physical factors on soil moisture distribution and provide a general guideline for the three hydro-climates, the physical factors were ranked based on the magnitude of controls (Figure 3.10a) and areal extent of controls (Figure 3.9a). Equal weight was given to both the components and the hierarchy of physical factors on defining near surface soil moisture distribution was evaluated. Results are depicted for the three study regions in Figure 3.11. A lower numerical rank implies greater overall control of the physical factor on soil moisture at a particular scale. In Arizona, soil (or specifically % clay), is the most dominant land-surface factor at the 1.6 - 3.2 km support scale range, while topography (slope) and vegetation (LAI) become more dominant at 3.2-12.8 km and 6.4-25.6 km support scale range respectively. Soil remains the most dominating factor in Iowa consistently with % sand being most dominant at the 1.6 - 3.2 km support scale range beyond which % clay becomes most dominant. As in Arizona, we observe that soil (% sand) is dominant at the relatively finer support scales (1.6 - 6.4 km) while vegetation becomes most important between 3.2 - 25.6 km support scale range in Oklahoma. Topography exerts little dominance at the finer scales and moderate dominance at the relatively coarse support scales.

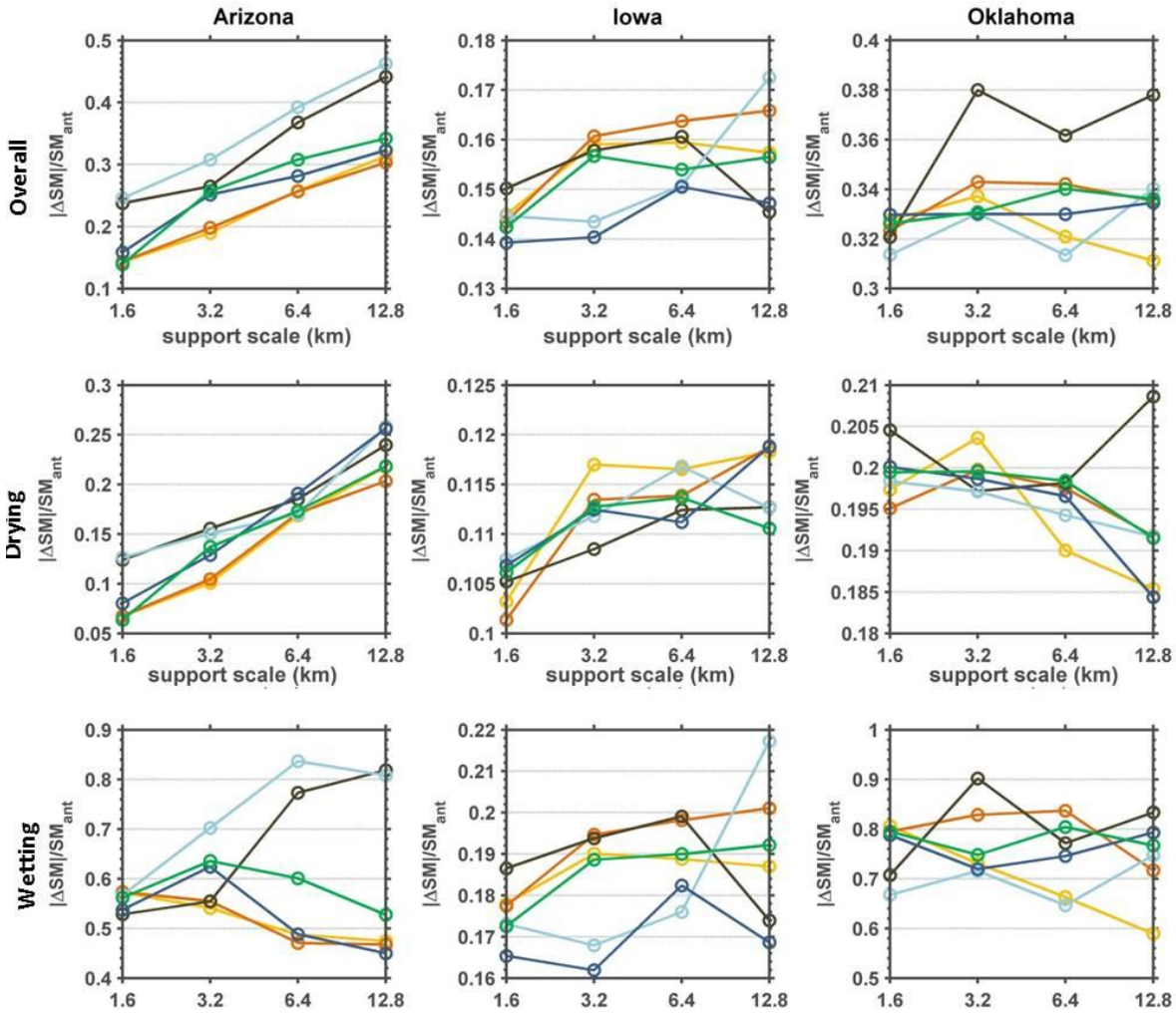

Figure 3.10: Mean redistributed moisture gradients observed in regions where pattern matches with % sand, % clay, elevation, slope, flow accumulation and LAI are observed for a) dry, b) normal and c) wet antecedent conditions during drying and wetting of the domain.

3.5.4 Investigating Antecedent Moisture Based Thresholds

Processes that control moisture movement in the soil surface are generated by the amount of water in the domain and the heterogeneity comprised of different geophysical factors in the domain. In order to investigate the presence of threshold antecedent moisture values at which different physical factors (and thus related hydrologic processes) become dominant, the antecedent soil moisture conditions of the pixels at which different geophysical factors become dominant (pattern matched locations) were compared using the Wilcoxon rank sum (WRS) tests. WRS test is the non-parametric equivalent of the t-test and assesses a difference in the distribution of the ranks of the ordered observations as opposed to their actual values. The physical factors which showed maximum overall control (Figure 3.11) on moisture redistribution values were chosen to represent soil, topography and vegetation attributes. The median values for the same attributes are provided in Table 3.3. Figure 3.12 shows the antecedent soil moisture distribution of the regions where the particular physical factor was found important while the WRS significance results are provided in Table 3.4. We observe that there are statistically significant differences in the antecedent moisture distribution of topography when compared to soil and vegetation in Arizona whereas in Iowa, there are no statistically significant differences/thresholds observed. In Oklahoma, the effect of soil is significantly different from topography at all scales and from vegetation at 3.2-25.6 km support scale range. The typical accuracy of soil moisture retrieval from microwave brightness temperature has been reported to be between 2 - 5% VSM (Narayan et al., 2004; Bolten et al., 2003; Njoku et al., 2002). Thus, any median moisture difference < 0.02 may reflect retrieval errors (Table 3.3). The difference between the median values of antecedent moisture values of the regions where different physical factors dominate is relatively small in Oklahoma and within the error range. In Arizona on the other hand, we observe that differences are more than

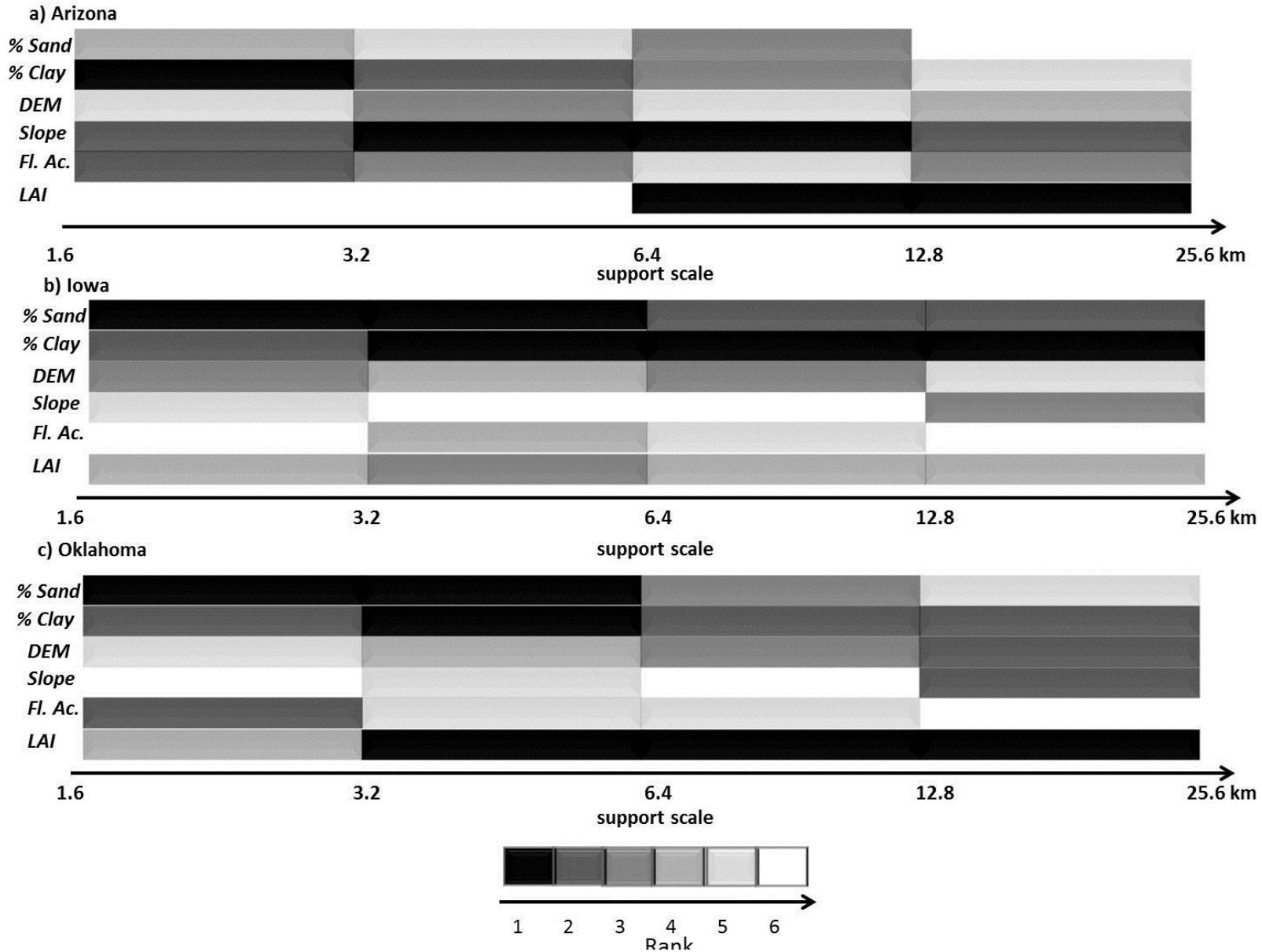

Figure 3.11: Hierarchy of effect of physical factors on near-surface soil moisture distribution

the remote sensing measurement error. This implies that at remote sensing footprint scales, antecedent moisture based thresholds at which the controls switch from one land-surface factor to the other may be effectively identified only in some regions.

Table 3.3: Median of the antecedent moisture values of the regions at which a pattern match between the given physical factors and moisture redistribution was observed.

Median antecedent moisture				
Support scale	1.6 km	3.2 km	6.4 km	12.8 km
ARIZONA				
Soil (Clay)	0.021	0.073	0.093	0.076
Topography (Elevation)	0.099	0.100	0.085	0.060
Vegetation (LAI)	0.020	0.068	0.078	0.077
IOWA				
Soil (Clay)	0.214	0.208	0.210	0.210
Topography (Elevation)	0.215	0.212	0.202	0.203
Vegetation (LAI)	0.209	0.205	0.205	0.204
OKLAHOMA				
Soil (Sand)	0.170	0.180	0.170	0.230
Topography (Elevation)	0.180	0.180	0.170	0.190
Vegetation (LAI)	0.170	0.170	0.150	0.180

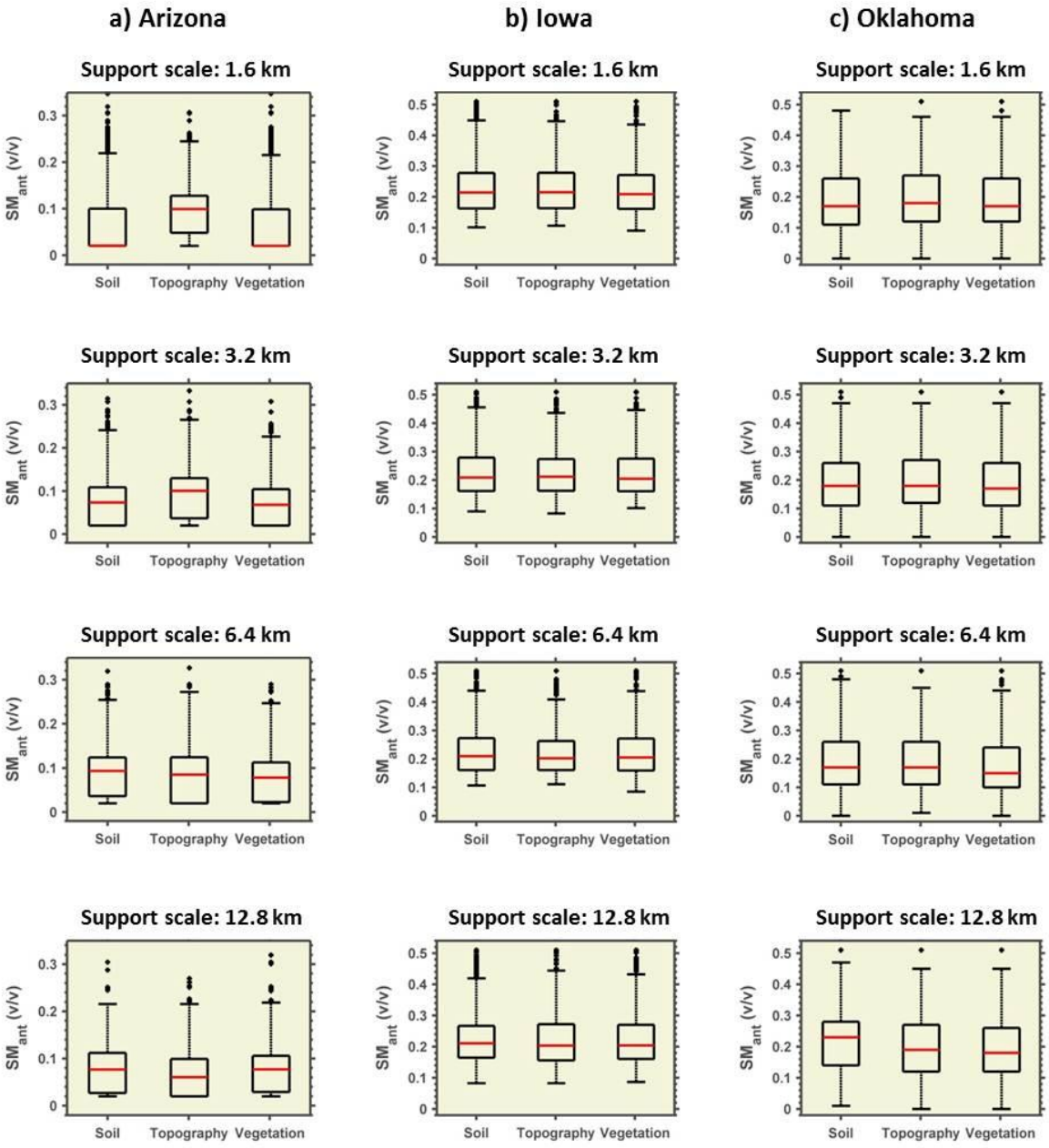

Figure 3.12: SM_{ant} distribution of regions where soil, topography and vegetation are dominant

Table 3.4: Significance results of Wilcoxon rank sum (WRS) test marking the existence of a threshold value. 'x' represents a WRS result significant at 95%.

Soil and Topography				
Region/Scale	1.6 km	3.2 km	6.4 km	12.8 km
Arizona	x	x	x	x
Iowa	-	-	-	-
Oklahoma	x	x	x	x
Soil and Vegetation				
Arizona	x	-	x	-
Iowa	x	-	-	-
Oklahoma	-	x	x	x
Topography and Vegetation				
Arizona	x	x	x	x
Iowa	-	-	-	-
Oklahoma	x	x	x	-

3.6 Conclusions

In this study, non-decimated wavelet analysis was used to assess the influence of land-surface based physical factors, namely, soil (% sand, % clay), topography (elevation, slope, flow accumulation) and vegetation (leaf area index) on soil moisture redistribution at remote sensing footprint scales varying from 1.6 km to 25.6 km. The original soil moisture signal was observed at 0.8 km. The contribution of the different physical factors was computed in terms of areal extent of influence of the physical factor and the magnitude of moisture redistribution associated with it to define their hierarchical control on soil moisture dynamics. The hierarchy was defined for coarse spatial support scales but fine (daily) temporal spacing scales which are typical of remotely sensed soil moisture data. It was determined that the influence of physical factors on soil moisture redistribution at remote sensing footprints varies across different hydro-climates and scales. Soil remains the dominant physical factor in Iowa across all scales whereas the topography and vegetation are the dominant physical controls in Arizona starting at 3.2 km and 6.4 km,

respectively. In Oklahoma, on the other hand, soil is the dominant factor at 1.6- 3.2 km but vegetation becomes more dominant thereafter. The effect of hydro-climate was also identifiable in the soil attributes dominating the soil moisture dynamics. It was found that the near-surface soil moisture dynamics in Arizona (semi-arid) can be more attributed to the clay content which is effective limiting parameter for evaporation whereas in the humid and wet Oklahoma, % sand (effectively limiting drainage) was the dominant attribute of soil. Antecedent moisture based thresholds at which the effect of different physical factors becomes significant were also found to be hydro-climate specific and found to exist only in Arizona.

This study is yet limited by the regional extent, hydro-climates and also time period (growing season) analyzed. However, it provides a direction for understanding hydro-climate based dependence of near-surface soil moisture on physical factors. These findings can assist in developing more effective physically based soil moisture scaling schemes and in the improvement of processes in large scale hydrological models.

4. ON VALIDATING FOOTPRINT SCALE SOIL MOISTURE AT DIFFERENT SUPPORT, SPACING, AND EXTENT SCALE

4.1 Synopsis

The launch of the soil moisture estimating satellites like Soil Moisture Active Passive (SMAP), Soil Moisture Ocean Salinity (SMOS), and Advanced Microwave Scanning Radiometer (AMSR2) has launched hydrology into an era where the use of footprint scale soil moisture (SM) in numerous hydrological and eco-hydrological applications is becoming the norm. Depending on the spatial resolution required, a directly observed or scaled remotely sensed soil moisture value is typically needed. However, the validation of such observed or scaled footprint scale products is severely limited because of the scale discrepancy between footprint scale soil moisture and observed ground based data that is typically used to validate soil moisture products. Scale discrepancy poses a problem in validation because of the difference in land-surface heterogeneity encompassed between the two scales. In this study, we propose a data-driven, scale appropriate scheme that can be used to validate footprint scale soil moisture. The designed scheme generates the spatial variance structure of footprint scale moisture redistribution as a function of a scale appropriate dominant physical factor on which soil moisture redistribution depends. The scheme was developed for a variety of heterogeneous conditions found in 3 regions (Arizona, Iowa and Oklahoma) with different hydro-climates and 3 footprint scales (0.8 km, 1.6 km and 3.2 km). Our results indicate that the spatial variance of moisture redistribution can be effectively modeled as a function of the most dominant physical control (minimum mean R^2 = 0.8 and maximum mean RMSE = 0.119) in each case. In order to make the validation scheme potentially transferable to regions with heterogeneity that is different from the data used, the validation scheme was extended by exploiting the relationship between soil

moisture, scale and heterogeneity through a conceptualized scale-wetness-heterogeneity (SWHET) cuboid. The SWHET cuboid is described by a wetness index, scale index and a newly defined heterogeneity index which can adequately quantify the land-surface heterogeneity across scales. The proposed SWHET cuboid can potentially serve as a look-up graph to model the spatial variance of footprint scale moisture redistribution as a function of the dominant physical controls. The within region validation of the cuboid resulted in rmse values <0.002 in all three regions. The concept can potentially be temporally and spatially transferable to larger footprint scales and hydro-climates.

4.2 Introduction

The increased and periodic availability of soil moisture (SM) observations from satellites like Soil Moisture Ocean Salinity (SMOS), Advanced Microwave Scanning Radiometer (AMSR) and NASA's Soil Moisture Active Passive (SMAP), has led to the possibility of using soil moisture to initialize and calibrate a variety of hydrological models (Wanders et al., 2014, Sutanudjaja et al., 2014, Montzka et al., 2011, Santanello et al., 2007). Large scale hydrological or climate models typically require soil moisture products at remote sensing footprint scales which may or may not match the observed footprint scales. A variety of scaling algorithms are available to generate such soil moisture products (Shin and Mohanty, 2013, Crow et al., 2000, Piles et al., 2011, Merlin et al., 2012, Merlin et al., 2008). However, the validation of soil moisture at remote sensing footprints (scaled or observed) is challenging due to a lack of accurate and representative ground based data.

Past studies have typically used ground based darcy scale soil moisture data from intensive soil moisture campaigns to ascertain the efficacy of their scaled or observed soil moisture product. The major drawback of such validation schemes is the scale discrepancy between the remote sensing footprint and ground based observation data. Remotely sensed soil moisture data is collected over global extent scales, regular spacing scales

(sampling interval of satellites) and typical support scales ranging from 25-60 km. The ground based data on the other hand is available for regional extent scales, highly irregular spacing scales (often only 1 or less per remote sensing pixel) and at support scales of the order of a few centimeters. This scale discrepancy in terms of extent, support and spacing scales between the remotely sensed soil moisture data and ground based data causes the average soil moisture value computed through remote sensing at footprint support scales (also referred to as footprint) to be typically lower than that calculated by averaging limited number of ground based soil moisture measurements across the footprint. The ground based soil moisture averages may match the footprint scale moisture values only if the encompassing variability within the footprint is represented adequately while estimating the averages (which due to logistic reasons is seldom the case). The satellite based soil moisture value thus, cannot be efficiently validated using soil moisture estimates obtained by averaging insufficiently sampled ground based data. Shin and Mohanty (2013) validated their downscaled soil moisture in 3 quarter section (800m x 800m) fields in Oklahoma using soil moisture data collected at 49 points within the fields. Merlin et al. (2012) validated their disaggregated soil moisture 1 km product using intensively collected point scale soil moisture data during the AACES campaign in Australia. The downscaled soil moisture product was underestimated as compared to the ground based data. Piles et al. (2011) also validated their 40, 10 and 1 km soil moisture product using ground based soil moisture data collected in Australia. The highest R^2 achieved in this study when comparing in-situ soil moisture to scaled soil moisture was 0.33. Bircher et al. (2012) designed an intensive soil moisture measurement cluster network based on the within pixel heterogeneity in Skjern River Catchment, Denmark to validate soil moisture over 1 SMOS pixel. Their comparison of retrieved soil moisture and ground based soil moisture led to a better R^2 value of 0.49 but was limited to just 1 SMOS pixel.

Besides the use of intensively collected soil moisture data, more spatially continuous

soil moisture estimates at remote sensing footprint scales have also been generated to represent remotely sensed soil moisture through the use of models. Montzka et al. (2013) retrieved hydraulic parameters from in-situ soil moisture to feed into the Water Flow and Balance Simulation Model (WaSiM-ETH) to generate area wide soil moisture estimates to validate SMOS soil moisture. However, the WaSiM-ETH (Schulla, 1997, and Schulla and Jasper, 2000) and other models used in approaches that involve distributed hydrological models are mostly based on Richard's equation which was not designed to model soil moisture at coarse scales. Also, the use of in-situ Darcy support scale soil moisture used to retrieve hydraulic parameters may not necessarily represent the effective hydraulic parameters at footprint scales wherein the encompassing heterogeneity is much larger than that represented by the small support scale in-situ soil moisture. Hence this technique of generating coarse scale soil moisture products, though useful, may not provide accurate results under all conditions.

An alternative strategy to validating remote sensing footprint soil moisture is to develop guidelines specific to remote sensing footprint scales that coarse scale soil moisture distributions adhere to. There has been extensive work done to evaluate the dependence of soil moisture distribution on geo-physical factors at remote sensing support scales. It has been found that precipitation typically forms the first principal component for explaining the dependence of moisture on geo-physical factors (Joshi and Mohanty, 2010). Besides precipitation, different physical factors like topography of the landscape (Anderson and Burt, 1978, Western et al., 1999, Joshi and Mohanty, 2010), vegetation (Hupet and Vanclooster, 2002), and soil texture and structure (Famiglietti et al., 1998, Gaur and Mohanty, 2013, Jawson and Niemann, 2007, Joshi and Mohanty, 2010, Oldak et al., 2002) have also been described as controlling factors for soil moisture variability at remote sensing support scales. Gaur and Mohanty (2015) described the hierarchy of dependence of soil moisture redistribution on geo-physical factors across a range of remote sensing sup-

port scales in 3 hydro-climates showing that (in general) the effect of soil decreases with coarsening support scale whereas the effect of topography and vegetation increases. They showed that the dominant physical factors controlling soil moisture redistribution depend on the hydro-climate and nature of heterogeneity of the region. Thus, by developing scale specific relationships between soil moisture and geo-physical factors (like precipitation, soil, topography and vegetation) which determine moisture distribution at coarse remote sensing support scales, more accurate validation relationships for soil moisture at remote sensing scales can be developed. In order to develop these scale specific relationships between soil moisture and physical factors, it is foremost required to understand the nature of these relationships which should be viable and reproducible. Soil moisture response to geophysical factors is highly non-linear. Thus, a direct linear relationship cannot be employed. However, the various geo-physical factors on which moisture distribution depends exhibit certain amount of spatial correlations at the footprint scales. For example, vegetation is typically correlated to biomes; soil has characteristic spatial correlation structures depending on its origin and method of formation etc. Precipitation patterns also have large scale embedded correlation structures (Portmann et al., 2009) which can be considered specific to the region of the world under consideration. For example, Indian precipitation dominated by monsoon winds will have a characteristic spatial correlation structure depending on the path the monsoon winds typically adopt to rain over the Indian sub-continent while the storm systems bringing precipitation to different parts of the United States will have different spatial correlation structures. Since soil moisture in the land-surface is redistributed as a result of infiltration in soil, run-off from topography, transpiration from vegetation and precipitation input to land-surface, it should mimic the correlation structures of one dominant or a combination of many dominant geophysical factors. Previously, a few studies have attempted to exploit this spatial dependence albeit in an inverse fashion (i.e. by studying the soil moisture spatial correlations and relating it

to geo-physical factors) to understand the dominant physical controls. Oldak et al. (2000), examined the semi-variograms of airborne soil moisture data to conclude that the dominant geo-physical factors controlling soil moisture distribution were soil (at local scale) and precipitation (at regional scale). Mohanty et al. (2000) also used geostatistics with point scale measurements to describe the effect of microheterogeneity, land covers and mixed vegetation on soil moisture distribution.

Geostatistical analysis or more specifically, semi- variograms of soil moisture are highly sensitive to scale (spacing, support and extent) of the data (Bloschl and Sivapalan, 1995). The first objective of this study was to develop scale based semi-variograms for soil moisture redistribution observed at remote sensing scales (support, spacing and extent) as a function of the scale based dominant physical factors (Gaur and Mohanty, 2015). The semi-variograms generated as a function of the dominant physical factors serve as a validation basis for observed RS footprint scale soil moisture. Such semi-variogram based relationships have two major advantages over the previous validation techniques: 1) They are devoid of assumptions that restrict the application of Richard's equation while being a physical representation of the interdependence of soil moisture on physical factors and, 2) They are scale specific and preserve the spatial structure of soil moisture unlike the isolated point scale measurements. Validation schemes are also typically restricted in terms of transferability because of differences in land-surface heterogeneity in different regions. Thus, the second objective of this study was to functionally relate the soil moisture semi-variogram structures to land-surface heterogeneity and antecedent wetness conditions such that the results can be transferred for different heterogeneity conditions in similar hydro-climates elsewhere.

The study is based on 2 hypotheses. 1) Scale specific soil moisture redistribution (ΔSM) semi-variogram (γ) structures can be generated as a weighted function (weight = α) of the semi-variograms of the most dominant land-surface based physical factor (Figure

4.1). Soil moisture redistribution refers to the change in soil moisture over a fixed time scale (1-2 days in this study).

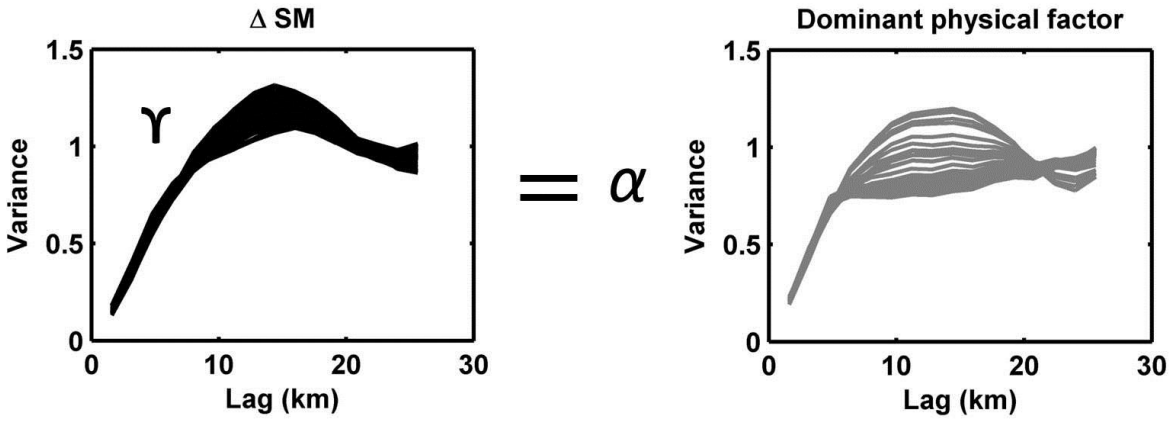

Figure 4.1: γ can be defined as a weighted function of the variograms of the dominant physical factors. (Conceptual diagram)

2) We also hypothesize that these semi-variograms based relationships (parameter α) are specific to the land-surface heterogeneity (soil, vegetation and topography) and antecedent wetness conditions (caused by precipitation), which can be represented by a scale-wetness-heterogeneity (SWHET) cuboid (Figure 4.2).

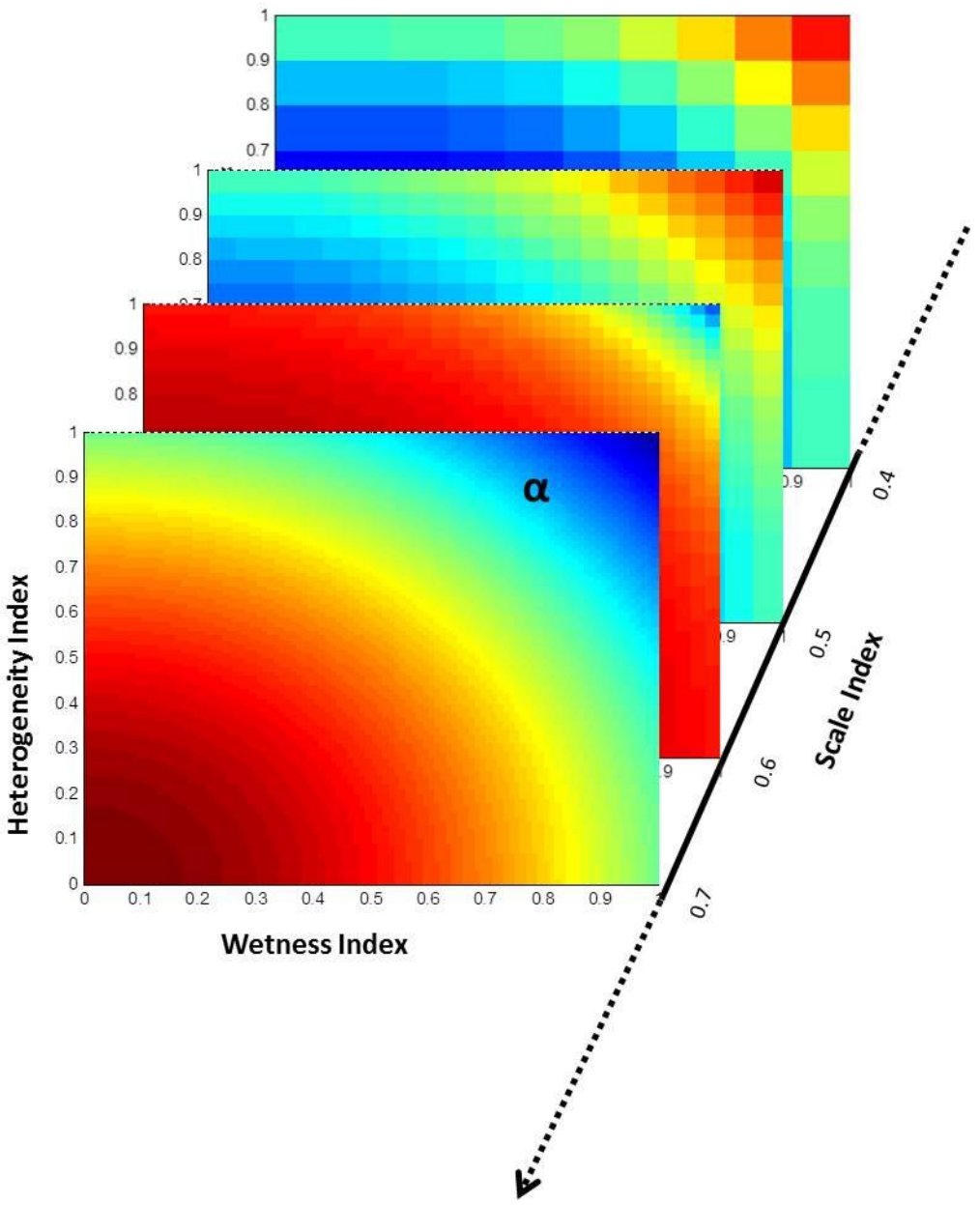

Figure 4.2: Scale-Wetness-Heterogeneity (SWHET) cuboid. Different slices of the cuboid represent values of α defined for specific heterogeneity and wetness conditions at different spatial support scales (Figure represents a conceptualization of the cuboid and not actual data).

4.3 Study Area

Three regions with different land-surface heterogeneity and hydro-climate were selected to develop and evaluate the SWHET cuboid. The first region is characterized by semi-arid hot climate and lies in Arizona. Owing to low yearly rainfalls (30.28 cm average annual rainfall at Tuscon, (http://www.usclimatedata.com/climate/tucson /arizona/united-states/usaz0247, accessed on September 24, 2015), this region is typically characterized as a water limited environment. The second region lies in Iowa and is characterized by moist climate while the third region is classified as sub-tropical climate and lies in Oklahoma. Iowa receives average annual rainfall of 90.60 cm as recorded in Des Moines (http://www.usclimatedata.com/climate/iowa/united-states/3185, accessed on September 24, 2015) and Oklahoma receives average annual rainfall of 92.61 cm as recorded in Oklahoma city (http://www.usclimatedata.com/ climate/oklahoma/united-states/3206, accessed on September 24, 2015). The two regions may be energy or water limited depending on the short term precipitation history in the region. Table 4.1 provides the descriptive statistics of the land-surface based heterogeneity of the study regions.

4.4 Data

The elevation data to generate the necessary topographic parameters, soil and LAI data were obtained from the National Elevation Dataset (Gesch, 2009), Soil Geographic (STATSGO) Data Base for the Conterminous United States (Miller and White, 1998) and 4-day composite MODIS product (NASA Land Processes Distributed Active Archive Center) respectively. ΔSM was generated from airborne soil moisture data collected during Soil Moisture Experiments in 2002 (SMEX02) and 2004 (SMEX04) in Iowa and Arizona respectively using the Polarimetric Scanning Radiometer, PSR (Bindlish et al., 2006, 2008) at 800 m X 800 m spatial resolution. The soil moisture data in Oklahoma was collected during 1997 (Southern Great Plains (SGP) 1997 hydrology experiment) using

Table 4.1: Average and standard deviation (σ) of physical factors representing land surface heterogeneity

Phys. Factor	**Average**	σ
Sand		
Arizona	50	9.5
Iowa	29.92	5.7
Oklahoma	31.51	22.7
Flow Acc.		
Arizona	21.6	85.7
Iowa	4.37	11.3
Oklahoma	10.23	39
LAI		
Arizona	0.46	0.2
Iowa	2.62	0.9
Oklahoma*	0.96	2.6

the Electronically Scanning Radiometer (Jackson, et al. 1999) at 800 m X 800 m spatial resolution.

4.5 Methodology

In order to evaluate the two hypotheses for the study, we 1) evaluated the relationships between the dominant physical factor and soil moisture redistribution and 2) computed the Scale-Wetness- Heterogeneity (SWHET) cuboid. The relationships between soil moisture redistribution and dominant land-surface factor were generated for different scales by computing the semi-variograms of soil moisture redistribution as a linear function (weight = α) of the semi-variograms of the most dominant physical factor (Table 4.2) using data at different support scales. The use of data at different support scales to generate the semi-variogram based relationships eliminates the problems arising as a result of scale discrepancy in validation studies. The use of moisture redistribution semi-variograms as opposed to using soil moisture semi-variograms has added advantages. Firstly, soil mois-

ture redistribution rather than soil moisture is directly affected by the land-surface factors given certain antecedent moisture conditions. Secondly, multiple spatial patterns of soil moisture could result in similar semi-variogram structures. However, when we use soil moisture redistribution structures, we bound the spatial pattern of moisture redistribution between a set antecedent state (moisture value) and present state (moisture value). This restricts the non-uniqueness of the feasible spatial distributions of soil moisture possible for a given semi- variogram structure.

The variability in soil moisture redistribution spatial structure at remote sensing footprints evolves based upon the combination of 1) land-surface factors (soil, vegetation and topography), 2) antecedent wetness conditions and 3) the prevailing meteorological conditions. The SWHET cuboid (Figure 4.2) coalesces the relationships between the land-surface factors, antecedent wetness conditions and soil moisture redistribution for different RS footprint scales. Since the general meteorological conditions for a certain region vary based upon the hydro-climate of the region and the time of the year, the SWHET cuboid (Figure 4.2) has been conceptualized separately for different hydro-climates in this study and represents only the growing season. The computational details are provided below.

Table 4.2: Scale based dominant physical attributes that create ΔSM variability

Region	**Dominant physical attribute**		
	0.8 km	*1.6 km*	*3.2 km*
Arizona	% clay	% clay	% clay
Iowa	% clay	% clay	% clay
Oklahoma	% sand	% sand	% sand

Soil moisture redistribution, ΔSM (eq. 4.1), and the physical attribute parameters (Table 4.2) required for generating semi-variograms (γ) and heterogeneity indices (Table 4.1) were resampled and re-gridded to 0.8 km, 1.6 km and 3.2 km from the original resolution

of 0.8 km by averaging the 0.8 km pixels. Amongst various averaging techniques, a linear averaging scheme was employed since the data was available at a regular and continuous spacing.

$$\Delta SM_t = SM_t - SM_{t-1} \tag{4.1}$$

where,

SM_t = redistributed soil moisture for day, t;

The heterogeneity indices and γ relationships were then defined for fixed extents called sub-regions. It was essential to define a fixed extent since soil moisture variance structures are sensitive to the extent of the region (Bloschl and Sivapalan, 1995). In this study, sub-regions of radius 40 km sampled from the domain by moving the center of a circular window of 40 km radius by one pixel (pixel size = 0.8, 1.6 or 3.2 km) at a time (Figure 4.3) were used as the fixed extent. Moving a window by one pixel at a time resulted in partial overlap of the sub-regions. This was done for increasing number of data and to exhaustively consider the possible conditions that a satellite footprint may encompass. A sub-region size of radius 40 km was chosen keeping in mind the typical resolution of a satellite radiometer based soil moisture product which varies between 30-60 km (depending on the angle of view of the sensor and frequency being used to estimate soil moisture). However the entire analysis presented in this research may be conducted using a different sub-region extent to suit a given study. The number of sub-regions and the number of pixels in each sub-region is provided in Table 4.3. The following section describes the generation of empirical semi-variogram(Figure 4.1) which is followed by the SWHET cuboid (Figure 4.2).

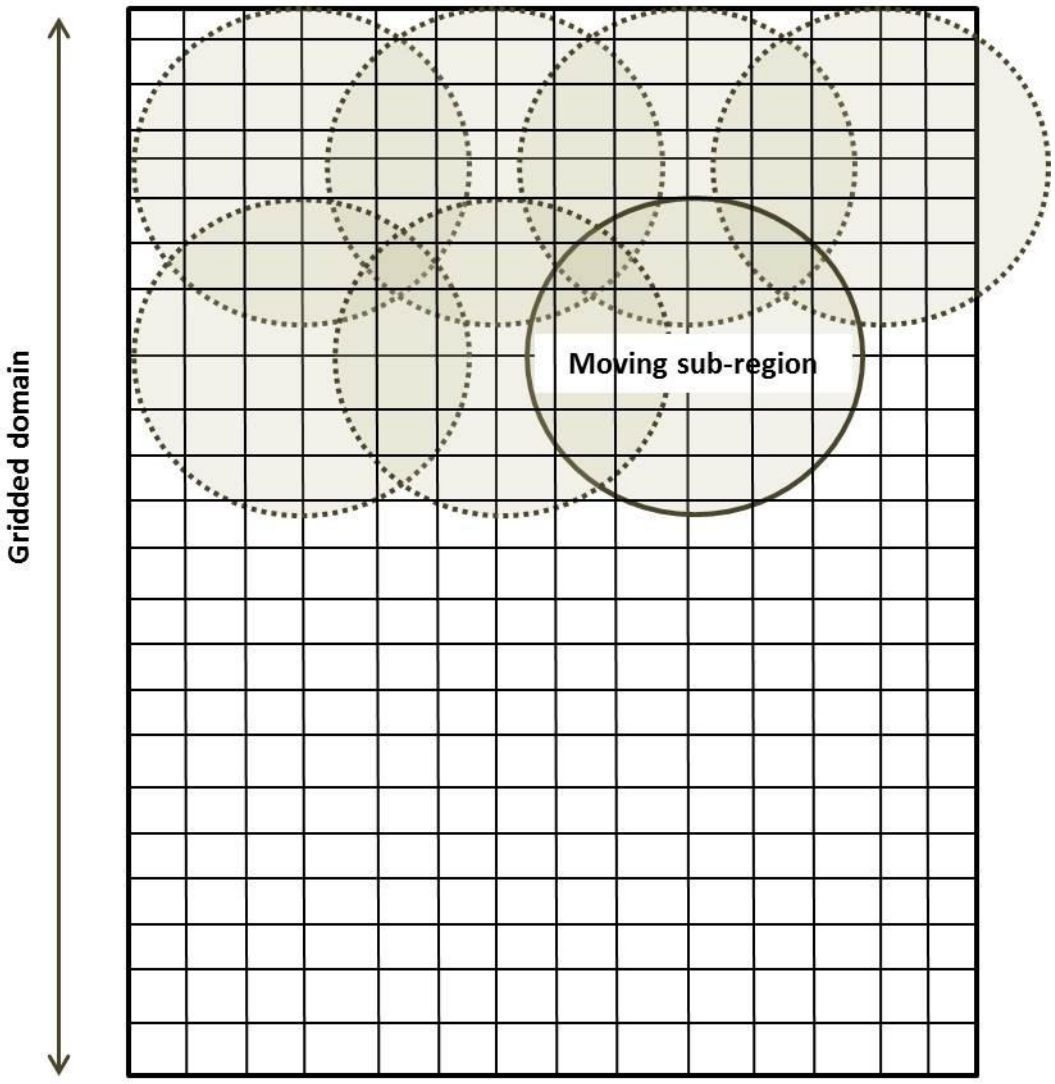

Figure 4.3: Moving window over the gridded domain to define sub-regions (fixed spatial extent scale) for generation of semi-variograms

Table 4.3: Spatial extent of study regions and details of number of pixels used to generate γ

Region (Area, km^2)	**# pixels to generate variograms (# of ~40 km regions)**		
	0.8 km	*1.6 km*	*3.2 km*
Arizona (70 x 62 x0.8^2)	2012-4080 (16320)	516-957 (3828)	135-224 (896)
Iowa (100 x 39 x0.8^2)	1689-3588 (32661)	420-861 (7776)	98-184 (1656)
Oklahoma (111x 40 x0.8^2)	1723-3702 (57988)	420-878 (13608)	98-198 (2912)

4.5.1 Empirical ΔSM Semi-Variogram Structure

A semi-variogram (also referred to as variogram in the manuscript) is used in standard geostatistical analysis (Journel and Huijbregts, 1978, Issaks and Srivastava, 1989, Mohanty et al., 2000, Wackernagel, 2003) for representing spatial relationships within a dataset. The traditional semi-variogram estimator (γ) employed in the study is given in eq. 4.2.

$$\gamma(h_i) = \frac{1}{2N(h_i)} \sum_{i=1}^{N(h_i)} [(\phi(x) - \phi(x+h_i)]^2 \tag{4.2}$$

where ϕ(x) and ϕ(x+h$_i$) represent the values of the variable under consideration separated by a distance hi and N(h$_i$) is the total number of such pairs. In this study, isotropic or non-directional semi-variograms have been considered. Even though this is not strictly correct, reasonable success has been observed while using isotropic semi-variograms in previous remotely sensed soil moisture studies (Joshi and Mohanty, 2010).

We numerically defined the dependence of ΔSM spatial structure on land-surface based heterogeneity at different antecedent conditions by quantifying the relationship between ΔSM semi-variograms (eq. 4.2) and dominant physical factor semi-variograms (eq. 4.2) at

different antecedent wetness conditions. α was obtained by linearly regressing the ΔSM semi-variogram on the dominant physical factor semi-variogram (eq. 4.3). These semi-variograms were constructed using regular spatial intervals (32 intervals at 0.8 km spacing for 0.8 km data, 16 intervals at 1.6 km spacing for 1.6 km data and 8 intervals at 3.2 km spacing for 3.2 km data to go upto a maximum lag of 25.6 km). The dominant physical factors (Table4.2) were selected based on Gaur and Mohanty (2015). The nugget value of the semi-variograms for the dominant physical factor and ΔSM was assumed 0 and hence no intercept was computed for the relationship.

$$\gamma_{\Delta SM} = \alpha \gamma_{df} \tag{4.3}$$

where, $\gamma_{\Delta SM}$ represents the semi-variogram of soil moisture redistribution, and γ_{df} represents the semi-variogram of the dominant physical factor. The semi-variogram based relationship was constructed for each 40 km sub-region for all 3 support scales (0.8, 1.6 and 3.2 km) in all 3 regions . The ΔSM and dominant physical factors were normalized standardized (eq. 4.4) within each sub-region before the semi- variograms were constructed. The standardization was done since the dominant physical factor data and soil moisture redistribution data have a very different range of values which may also change between sub-regions and cause errors while extrapolating the empirical relationships.

$$a_{i,norm} = \frac{a_i - \overline{a}}{\sqrt{\frac{\sum(a_i - \overline{a}^2)}{n-1}}} \tag{4.4}$$

a = variable being normalized (dominant physical factor/ ΔSM)

$\overline{a}$ = mean value of a.

4.5.2 SWHET Cuboid

In order to enable the transferability of the semi- variogram based relationships to regions with varying heterogeneity within the same hydro-climate, the SWHET cuboid was developed. The cuboid describes the relationship between antecedent wetness, heterogeneity and the semi- variogram based physico-empirical relationships across different footprint scales.

In this study, the cuboid has been developed for 3 remote sensing footprint (support) scales and consists of 3 axes representing - scale index, wetness index and heterogeneity index. It defines unique correlation structures for soil moisture redistribution given specific heterogeneity, antecedent wetness and support scale. Each index described below represents a value for the extent of a region representing the resolution of a radiometer soil moisture product (40 km radius sub-region). Using the resampled ΔSM and attribute parameters, the following indices were defined.

Normalized Scale Index, S_{norm}: The scale index (eq. 4.5) is a measure of the degree of averaging that occurs in a domain (sub-region). It represents the support size or pixel resolution as compared to a 40 km domain (extent of the sub-region). A lower scale index implies higher averaging or coarser resolution. A 40 km domain was selected because it describes the scale of the pixel as compared to the extent of the sub-region (described above) which also describes the resolution of most soil moisture products from satellite based radiometers (30-60 km).

$$S_{norm} = \frac{40 - s}{40} \tag{4.5}$$

s = support scale in km

Normalized Wetness Index, SM_{norm}: Antecedent wetness has been described as an important factor controlling soil moisture dynamics (Teuling et. al., 2007 and Ivanov

et. al., in 2010, Gaur and Mohanty, 2015). The static heterogeneity (soil and topography) and dynamic heterogeneity (vegetation) within a domain dynamically redistributes the soil moisture conditioned upon the antecedent wetness conditions in the domain. The wetness index (eq. 4.6) describes the antecedent wetness condition of the 40 km extent sub-region (domain). A lower wetness index implies higher antecedent moisture content.

$$SM_{norm} = \frac{SM_{40,max} - SM_{40}}{SM_{40,max}} \tag{4.6}$$

$SM_{40,max}$ = maximum volumetric water content observed for 40 km support size in the domain

SM_{40} = antecedent soil moisture content of the 40 km sub-region under consideration

Normalized Heterogeneity Index, H_{norm}: The heterogeneity index is a numerical measure of the variability of the land-surface heterogeneity in the 40 km domain. In order for the heterogeneity index to be transferable to other locations it was deemed essential to have a formulation that was general and yet representative enough to describe land-surface heterogeneity in most regions. The heterogeneity index developed in this study represents the variability and co-variability in soil (s), topography (t) and vegetation (v). Since the physical processes that lead to moisture redistribution on the land-surface are dependent on the variability (and co-variability) of these physical factors on the land-surface (given specific wetness and atmospheric conditions), this independent index should quantify and distinguish the hydrologic behavior of land-surface around the globe. The factors chosen to represent soil, topography and vegetation are % sand, flow accumulation and leaf area index (LAI), respectively. These attributes were chosen as % sand determines the infiltration capacity of the soil, flow accumulation is representative of the spatial pattern of the topography of the region (thus, determines overland flow, localized evaporation and infiltration etc.) and LAI is indicative of the leaf area available for transpiration and rainfall

interception.Past studies on controls of soil moisture have also demonstrated the utility of these parameters in defining the near-surface soil moisture distribution dynamics. The soil, vegetation and topography of the region are shown in Figure 4.4

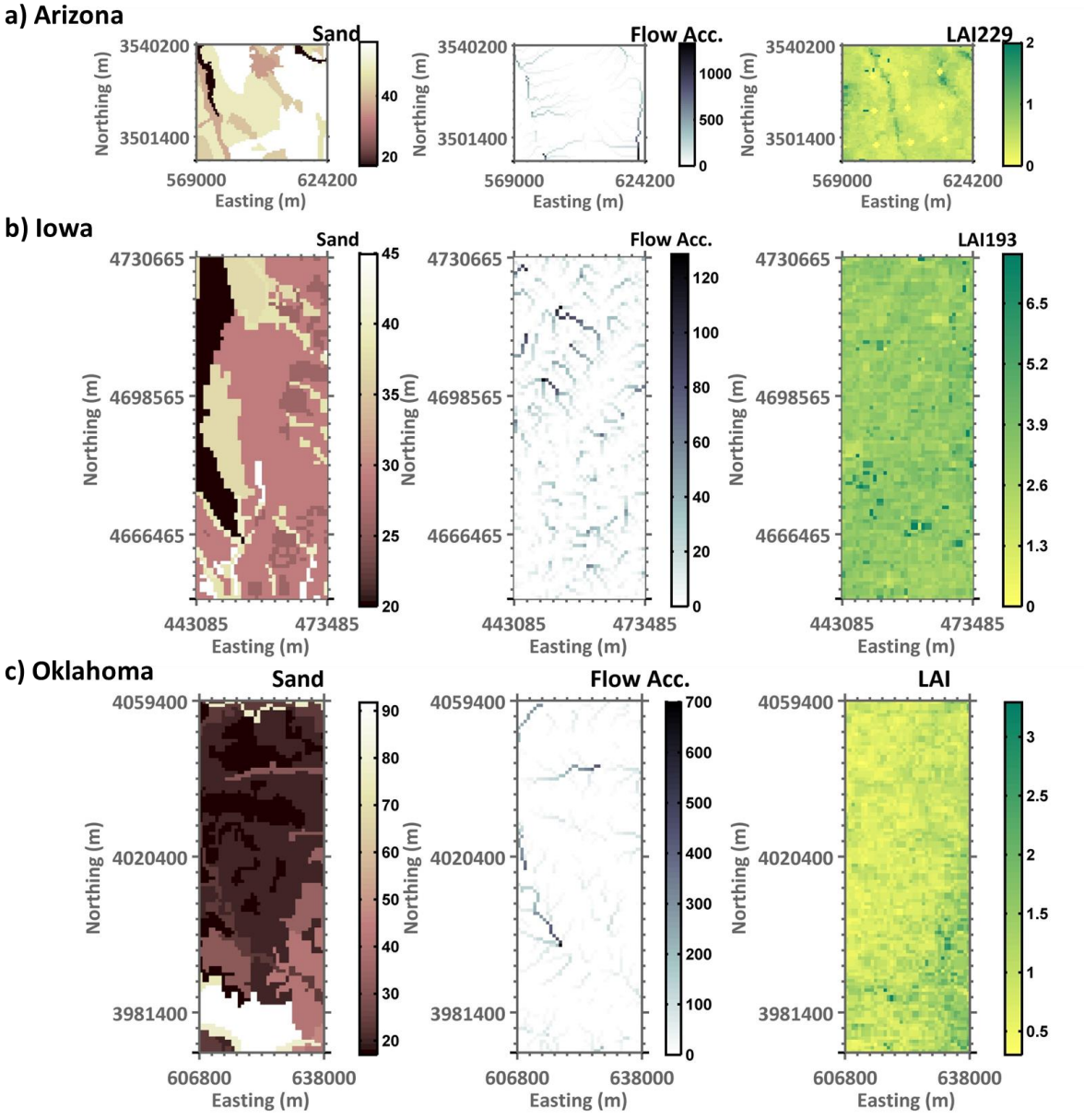

Figure 4.4: Spatial patterns of % sand, flow accumulation and LAI in the study areas.

The heterogeneity in each sub-region was represented by a heterogeneity (**H**) matrix (eq. 4.7).

$$\mathbf{H} = \begin{bmatrix} \sigma_{s,s} & \sigma_{v,s} & \sigma_{t,s} \\ \sigma_{s,v} & \sigma_{v,v} & \sigma_{t,v} \\ \sigma_{s,t} & \sigma_{v,t} & \sigma_{t,t} \end{bmatrix} \tag{4.7}$$

H = heterogeneity matrix

σ = statistical co-variance

s,v,t represent soil (% sand), vegetation (LAI) and topography (flow accumulation) respectively

In order to account for the variable number of fine support pixels within different sampled sub-regions because of the rectangular extent of the entire dataset , the heterogeneity matrix was scaled using the total area of the fine support pixels within the domain (eq. 4.8).

$$\mathbf{H}_a == \frac{\mathbf{H}}{nxA} \tag{4.8}$$

n = number of fine support scale pixels within 40 km sub-region

A = area of fine support scale pixel (km^2)

Eigenvalue decomposition (eq. 4.9) was conducted on each $\mathbf{H}_a$ -matrix to project the land-surface heterogeneity on a de-correlated vector space. In order to account for any statistical bias arising because of a difference in size of dataset or variable area within the sub-region, the H matrix was adjusted by the encompassed area before computing the decomposition as given in eq. 4.8. Owing to the symmetric nature of the covariance matrix, the eigenvectors (u) of the H-matrix are pairwise orthogonal and composed of real values. The eigenvectors together with adjusted eigenvalues can be considered to be

characteristic of and unique to the encompassing heterogeneity.

$$(\mathbf{H}_a - \delta\mathbf{I})\mathbf{U} = 0 \tag{4.9}$$

The highest eigenvalue (δ_{max}) and the corresponding eigenvector (u_{max}) represent the axis along which the maximum variability of the data is oriented. The heterogeneity index, H' (eq. 4.10) is defined as the product of δ_{max} and the unique angle that u_{max} makes with the vector, $\mathbf{i}$. The normalized heterogeneity index (H_{norm}) is defined in eq. 4.11.

$$H' = \delta_{max} cos^{-1}\left(\frac{u_{max}.\mathbf{i}}{||u_{max}||.||\mathbf{i}||}\right) \tag{4.10}$$

$$H_{norm} = \frac{H'_{max} - H}{H'_{max}} \tag{4.11}$$

where $cos^{-1}\left(\frac{u_{max}.\mathbf{i}}{||u_{max}||.||\mathbf{i}||}\right)$ = angle (radians) between dominant eigenvector and a reference vector $\mathbf{i}$ ([1 1 1]). A lower heterogeneity (small δ_{max}) would imply that maximum variability-covariability in heterogeneity cannot be oriented along a single direction in the vector space and hence entail either low variance in the data or more 'divergent' heterogeneity in the sub-region (within a region). Divergent heterogeneity means that most of the variance-covariance structure in the dataset cannot be represented by one single axis. Thus, regions with low variance or less correlated heterogeneity (like in agricultural domains where natural correlations between soil, vegetation and topography have been disturbed) should have a relatively lower heterogeneity index .

Each α value derived using the regression relationships (eq. 4.3) corresponds to a normalized wetness, normalized heterogeneity and normalized scale index. A surface representing the linking parameter α was generated for the entire range of the normalized wetness and heterogeneity indices (Figure 4.2) at different scales by interpolating using a

thin-plate smoothing spline interpolation technique in MATLAB. The surface was generated after removing 10% of the data (random sampling without replacement) for validation. This process of randomly selecting 10% of the data and interpolating with remaining data was repeated 10 times and the resulting rmse were computed. The final generated surface displayed the lowest rmse.

4.6 Results and Discussion

4.6.1 Hydro-climate Based Semi-Variogram Relationships

Scale specific α values for the relationship between moisture redistribution (ΔSM) and dominant land-surface factors were generated for each sub-region within the domain using empirical semi-variograms of normalized ΔSM and the most dominant physical factor (Table 4.2) as above. Plots of the observed ΔSM and dominant physical factor semi- variograms for each scale and all sub-regions are provided in Figure 4.5. A theoretical variogram was not fit to the empirical semi-variograms to retain the inherent spatial correlation structure of ΔSM and dominant physical factors (Figure 4.5). The semi-variograms of ΔSM and dominant physical factor show similarities not only in terms of general trends but also the holes in the semi- variograms. As an example, the slight dip in variance observed in ΔSM semi-variograms in Arizona was also observed in % clay (dominant physical factor) semi-variograms. This feature provides some visual validation of the generation of the ΔSM semi-variogram as a linear function of the dominant physical factor semi-variogram to generate α (Figure 4.1). On computation of these linear relationships, only less than 1% (in Arizona and Iowa) and 2% (in Oklahoma) of the semi- variogram based relationships did not result in statistically significant (p-value<0.05) α values suggesting that the use of a single dominant physical factor to represent the functional relationship is adequate.

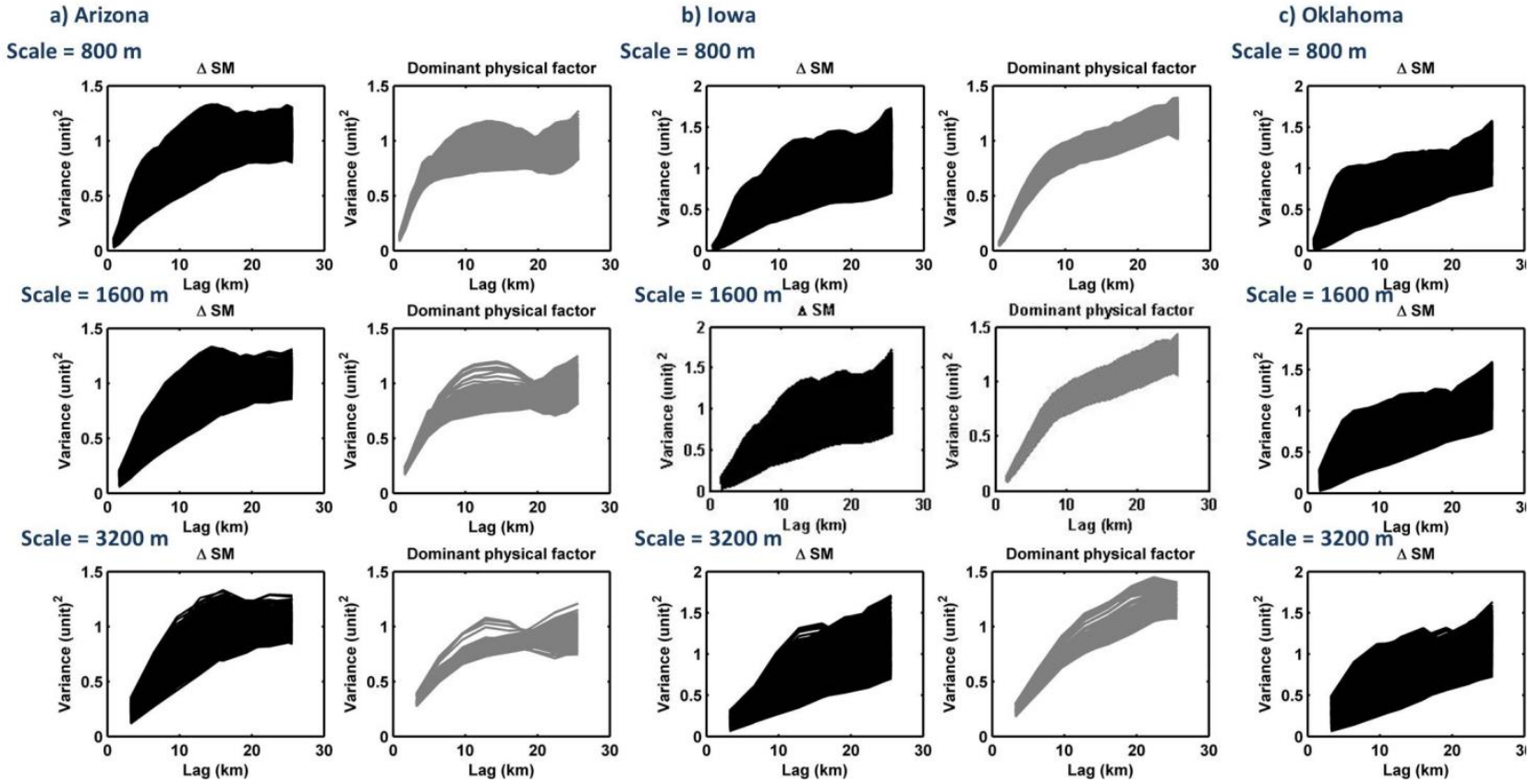

Figure 4.5: Semi-variograms of observed Δ*SM* and dominant physical controls (for all sub-regions) at different scales

The histogram of α values (p-value<0.05) is shown in Figure 4.6. The dominant physical factor used for Arizona as well as Iowa was % clay (Gaur and Mohanty, 2015). However, the distribution of α values at the same scale is significantly different for both the regions. This occurs due to the difference in overall land-surface heterogeneity (co-variability between soil, vegetation and topography). The α values are a function of the variability-co-variability of the land-surface heterogeneous parameters (heterogeneity index) and its interaction with the antecedent wetness conditions (wetness index) which are markedly different in the two regions.

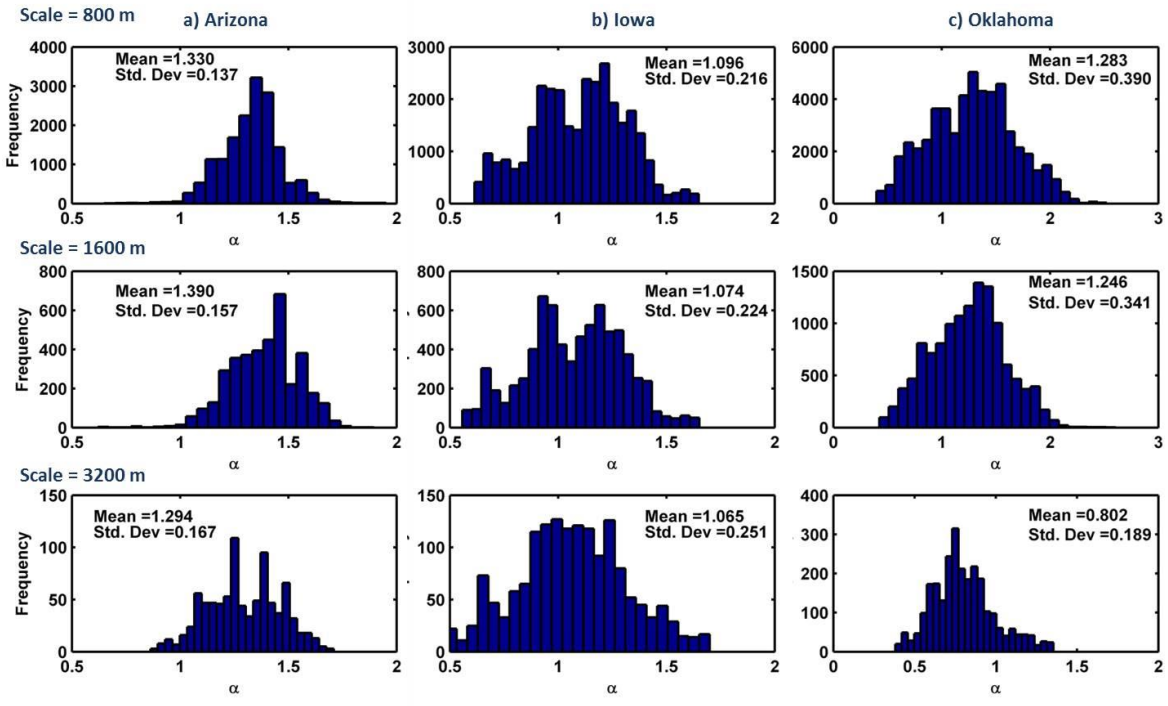

Figure 4.6: Distribution of α values at different scales

Within a region, the number and location of modes of α are similar (though not same) as the scale changes from 800 m to 3200 m, revealing a scale based dependence of the rela-

tionship between the dominant physical factor and moisture redistribution. The mean and standard deviation of α within a hydro-climate are also similar indicating some potential of generating relationships at a particular scale and transporting relationships across scales within a hydro-climate/region. This might also have implications beyond just soil moisture and explain the reasonable success of certain studies like Jana et al. (2008) wherein they used trained neural networks at a coarser scale to estimate fine scale hydraulic parameters. In other words, given the same dominant physical factor at a particular range of scales, transferability of parameters generated at a particular scale to other scales may be feasible. The range of α coefficients (varying around 1) shows that the spatial variance observed in ΔSM may be larger or smaller than the variance of the dominant physical factor. This occurs because of the other less dominant physical factors that control soil moisture redistribution in space. However, the fact that the mean α values across scales for the 3 hydro-climates are close to 1 suggests that the correct dominant physical factor was chosen (Gaur and Mohanty, 2015) to represent the soil moisture redistribution.

The root mean squared error (RMSE) and coefficient of determination (R^2) obtained as a result of linearly regressing the semi-variograms of ΔSM and the dominant physical factors are shown in Figure 4.7. The regression based relationships showed good results with minimum R^2 value of 0.8, 0.92 and 0.88 and maximum rmse of 0.119, 0.097 and 0.086 for Arizona, Iowa and Oklahoma, respectively. This validates our hypothesis of quantifying the spatial structure of ΔSM as a function of the spatial structure of dominant physical factors.

4.6.2 Heterogeneity Index

Soil moisture redistribution at remote sensing footprint scales is a function of the spatial organization of land-surface heterogeneity within a landscape. In the given study, the heterogeneity index was defined to quantify the heterogeneity within a sub-region (fixed

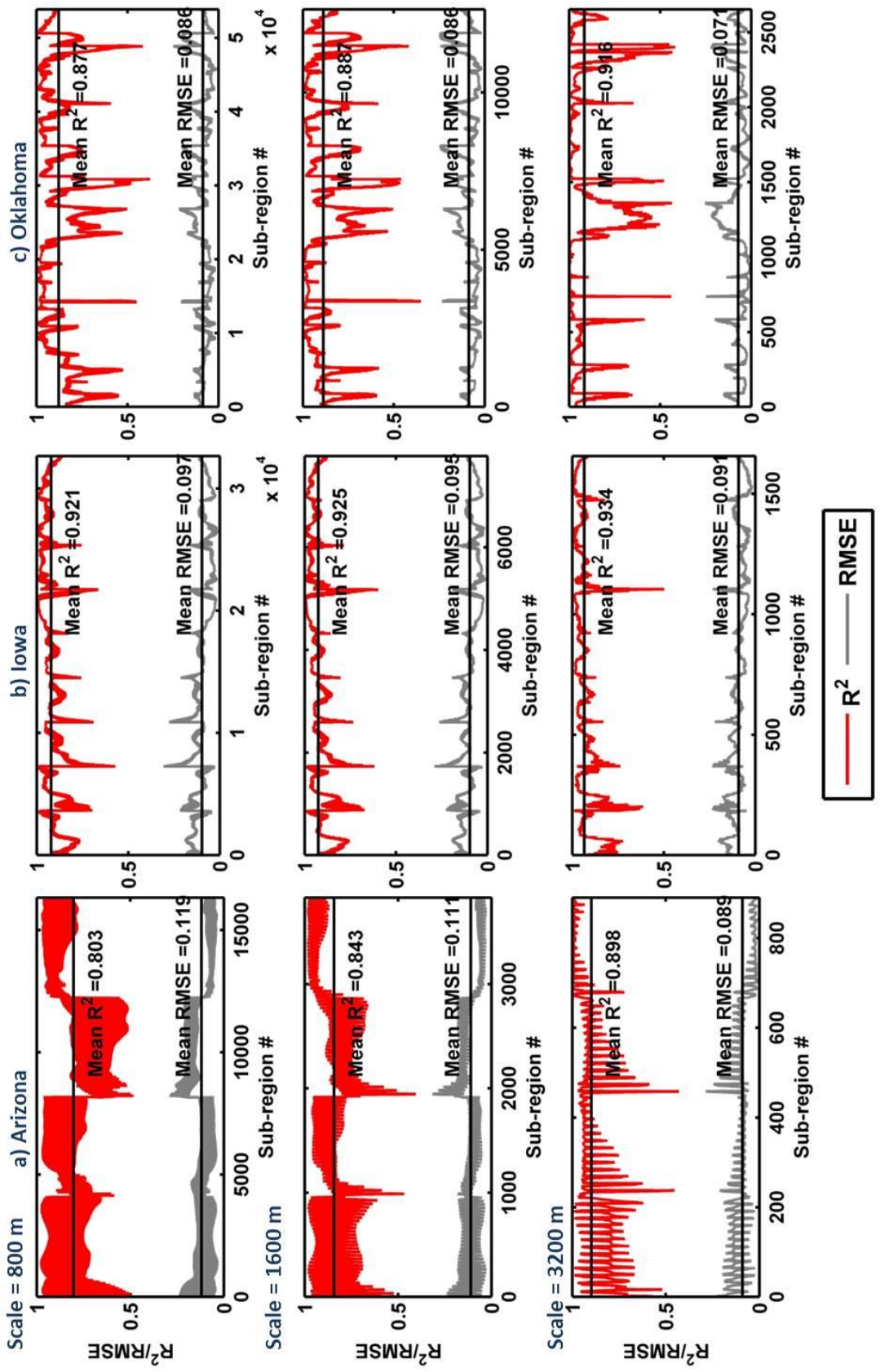

Figure 4.7: R^2 and RMSE values of semi-variograms of soil moisture and physical controls for different regions and scales

extent) using data at different support scales. For any particular support scale, it was defined as a function of the angle (with reference vector [1 1 1]) and eigenvalue of the dominant eigenvector. Large eigenvalues imply that a large amount of variance in the dataset can be explained by projecting the data along the corresponding unit eigenvector. Additionally, large eigenvalue suggest larger correlations within the heterogeneous variables i.e. soil, vegetation and topography or larger variance within the dataset. The eigenangles describe the orientation of the eigenvector or direction of maximum variability and thus will differ based on the inherent correlations between soil, vegetation and topography within a region.

The ranges of the heterogeneity index for three study regions are provided in Table 4.4. In order for the heterogeneity index to singularly quantify the heterogeneity in all physical factors, it was required to be able to represent the complexity of the region in terms of soil, vegetation and topography. Arizona and Oklahoma represent mostly natural domains with some agriculture whereas Iowa is primarily an anthropogenically altered agricultural domain. As such the natural correlations between soil, vegetation and topography can be expected to be larger in Oklahoma and Arizona as opposed to Iowa. The spatial patterns and values of % sand, flow accumulation and LAI (Figure 4.4) along with their respective standard deviations (Table 4.1) reveal that the variations in terms of soil, vegetation and topography are also considerably larger in Oklahoma and Arizona than in Iowa. The standard deviation of the physical factors reflects the diversity within a physical factor observed in the region. It was observed that the heterogeneity index values effectively represent the heterogeneity of the respective regions. At each scale, the index values for Arizona were highest followed by Oklahoma and Iowa. There was some overlap between the heterogeneity index values for Arizona and Oklahoma. This is in agreement with the standard deviation of the physical factors observed in these regions wherein Arizona shows highest standard deviation for vegetation and topography while Oklahoma has higher stan-

dard deviation in terms of % sand. Iowa is a production agricultural region with expected lower correlations between vegetation (i.e., crop type), soil and topography and the same was reflected in the heterogeneity index as well. A scatterplot of adjusted eigenvalues and eigenangles representing the heterogeneity for each hydro-climate is provided in Figure 4.8. The three hydro-climates reveal distinctly different signatures. The scatterplot for Arizona reveals two distinct correlation structures (in terms of eigenangles) between the heterogeneous land-surface factors at each scale. The eigenangle values for Iowa which is completely anthropogenically altered through agriculture and Oklahoma which is a mix of agricultural manipulation and natural landscape shows a wider range of eigenangles and thus correlation structure. The eigenangle ranges do not change much for Arizona and Oklahoma as the scale is coarsened but the ranges become very small in Iowa at 3200 m scale. The eigenvalues are highest for Arizona (with some overlap with Oklahoma) followed by Oklahoma and Iowa. The different distribution of the eigenangles corresponding to the eigenvalues for each domain, characterizes the differences in the correlation between the physical factors within each domain effectively. The formulation of the heterogeneity index can, therefore, effectively distinguish between different heterogeneities within a domain.

Table 4.4: Range of heterogeneity indices

Region	**Min-Max values**		
	0.8 km	*1.6 km*	*3.2 km*
Arizona	0.32-3.21	0.28-3.69	0.14-1.32
Iowa	0.02-0.09	0.01-0.05	0.01-0.04
Oklahoma	0.25-1.31	0.16-1.36	0-1.37

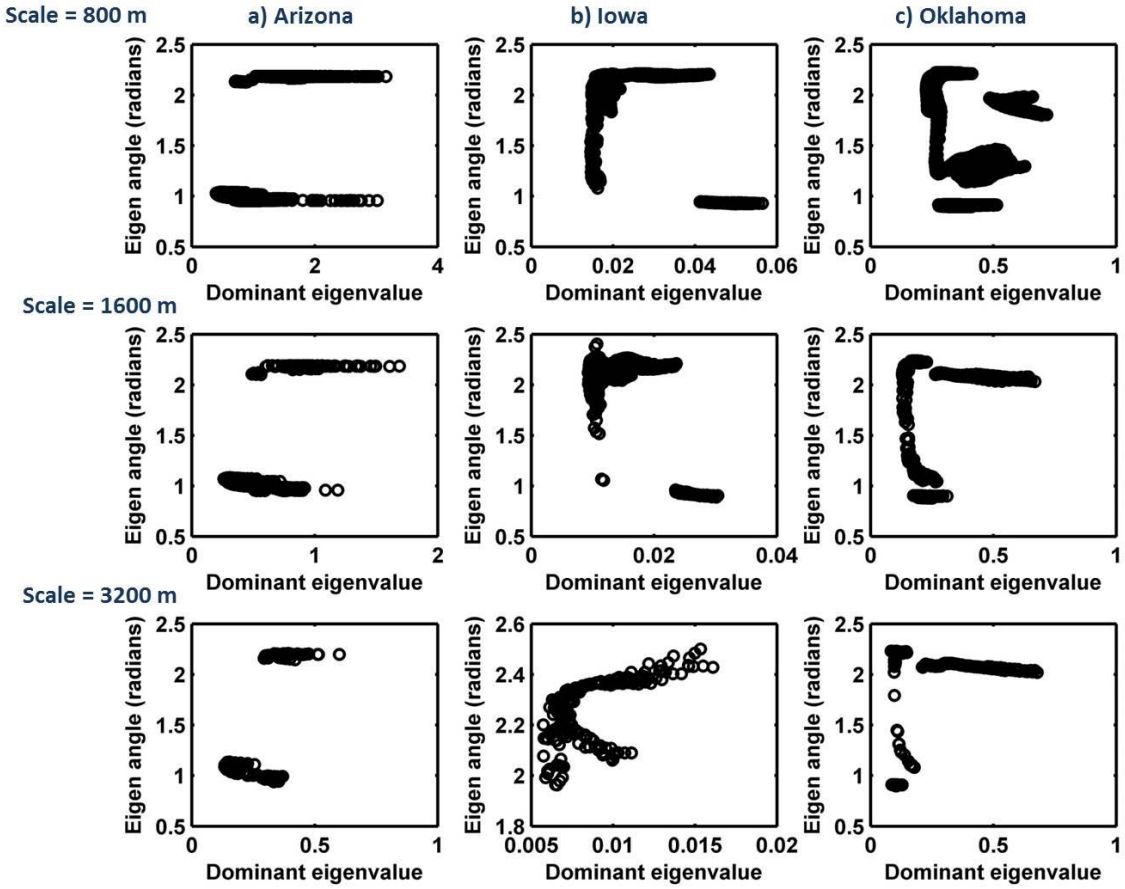

Figure 4.8: Scatter plot for eigenangle vs. eigenvalue of the dominant eigenvector

Within a region, the mean eigenvalue reduces as the support scale is coarsened (Figure 4.8) in Arizona and Iowa. This implies that the variability in data reduces as the support scale is coarsened. This feature is typical of remotely sensed soil moisture data as well wherein subsequent averaging at coarser scales leads to a reduction in the variability of data. Eigenvalue ranges for Oklahoma remain approximately same revealing that this trend in heterogeneity cannot be generalized. Another interesting observation is that the dominant physical factor for Arizona and Iowa (wherein the index values evolved with scale) was % clay for all scales whereas the dominant physical factors changed with scale for Oklahoma. Even though this result cannot be generalized at this stage to imply an association between the two, it is worthwhile to keep in mind while designing/conducting future studies. Figure 4.9 shows the empirical cumulative density plots (cdf) of the normalized heterogeneity index for the regions. The cdf plots represent how the overall apparent heterogeneity in the region varies. It was observed that the heterogeneity in Arizona and Iowa scale up similarly whereas the apparent heterogeneity in Oklahoma varies with scale. This aspect is reflected in the relationship of heterogeneity with soil moisture redistribution as well. Gaur and Mohanty, (2015) found that the soil of the region showed highest dominance on spatial moisture redistribution for Iowa and Arizona. The relative dominance of the physical factors on moisture redistribution also changed proportionally across all scales. However, the dominance (relative as well as absolute) of physical factors in Oklahoma was more dynamic with the relative contribution of each physical factor changing disproportionately with scale (Gaur and Mohanty, 2015). Since soil moisture is a function of land-surface heterogeneity, a change in the apparent heterogeneity of the region would affect a variation in dominance of the physical factors. The same was reflected in the cdf plots where the distribution of the normalized heterogeneity index for Arizona and Iowa remained similar while the distribution for Oklahoma changed markedly with scale.

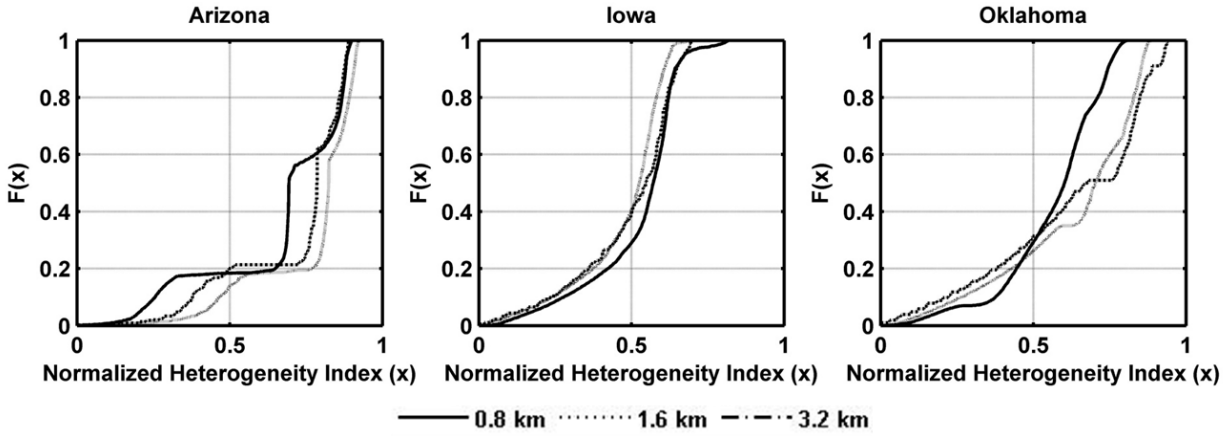

Figure 4.9: Empirical cumulative density plots of normalized heterogeneity index

4.6.3 SWHET Cuboid

The effect of physical controls on soil moisture has been known to vary with wetness conditions (Kim and Barros, 2002, Gaur and Mohanty, 2013) and nature of heterogeneity (Jawson and Niemann, 2007, Joshi and Mohanty, 2010, Gaur and Mohanty, 2013, Ryu and Famiglietti, 2006). Figure 4.10 shows the relationship between wetness, heterogeneity and the coefficient, α. The sub-parts of this figure combined represent the conceptual SWHET cuboid. To put the indices into a physical perspective, a wetness index of 0.5 indicates that the wetness of the 40 km sub-region is half the maximum wetness (SM_{max}) observed for a 40 km sub-region in a particular region. Given the dataset for the growing season, SM_{max} for Arizona, Iowa and Oklahoma was found to be 8.72 x $10^{-}4$, 0.34 and 0.36 v/v respectively.

The SWHET cuboid was conceptualized to estimate the scale based relationships observed between soil moisture redistribution and land-surface factors across scales for heterogeneity conditions not represented by the dataset used to generate the scale based relationships. In order to develop these predictive relationships for α given a certain het-

erogeneity index and wetness index in different hydro-climates, a surface of α values was fitted with respect to the normalized heterogeneity index and wetness index. Given the irregular distribution of dataset, a thin plane spline interpolation technique was employed to generate the surface (Figure 4.10). The surfaces were generated after removing 10% of the α values for validation. This procedure was repeated 10 times for each scale and hydro-climate and the resultant rmse are plotted in Figure 4.11. Each simulation led to a very low rmse value (<0.004) implying that the generated surfaces were robust and the hypothesis holds. The surface with the lowest rmse has been used to represent the final relationship between heterogeneity, wetness and scale.

Building on past research which qualitatively indicates the presence of wetness and heterogeneity based thresholds; Figure 4.10 helps us visualize those thresholds. The pattern of α indirectly represents the pattern of soil moisture distribution dependence on wetness and heterogeneity. The patterns of α in Arizona appear to only have a wetness based threshold (visible boundaries along the wetness axis) whereas Iowa and Oklahoma reveal that the thresholds depend both on heterogeneity and wetness in some structured manner. An interesting observation is that the patterns appear to remain consistent with scale for Arizona and Iowa. This implies that transfer of information from one scale to the other in these regions can be done without much error. The patterns in Oklahoma do not appear to be as scalable since they are inconsistent.

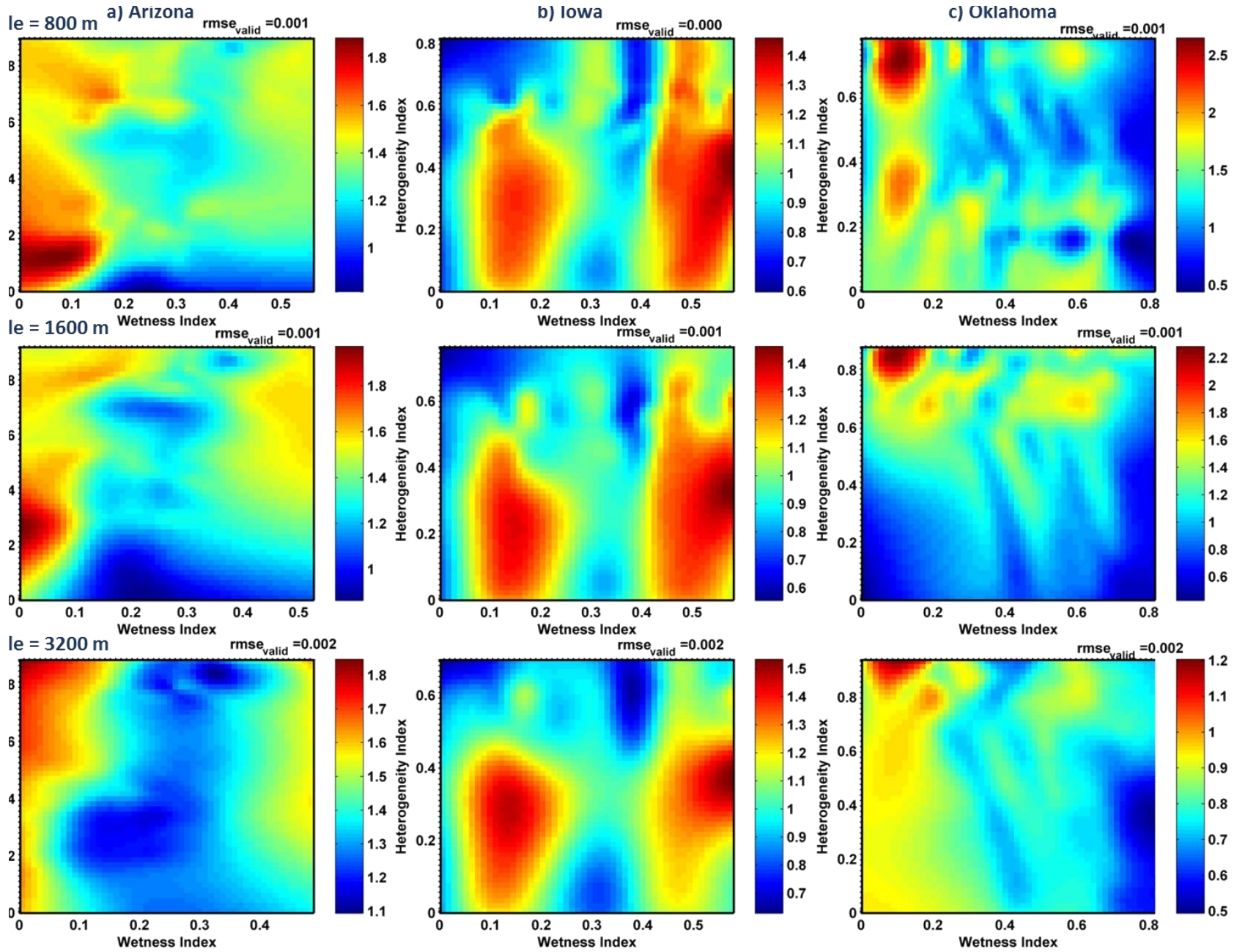

Figure 4.10: Plots of α values interpolated against wetness and heterogeneity index

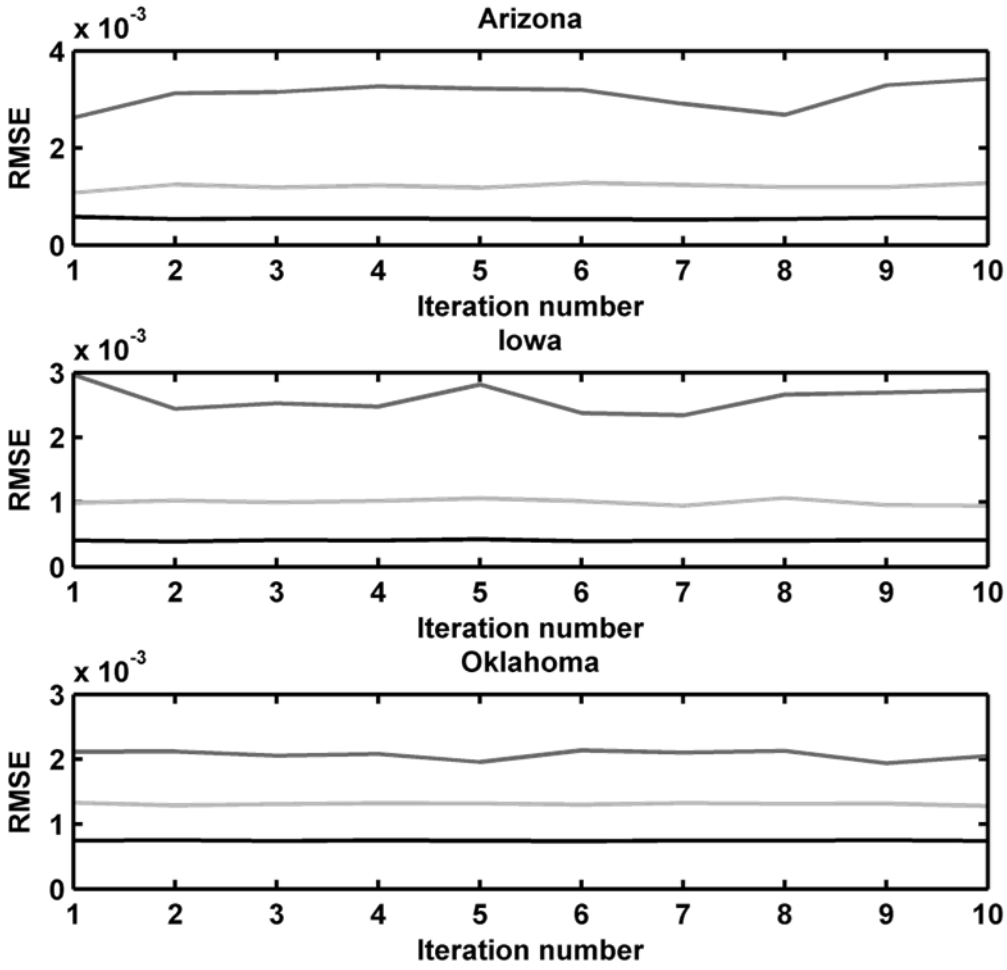

Figure 4.11: RMSE values of the SWHET cuboid surfaces

Our second hypothesis states that scale specific soil moisture redistribution (ΔSM) variogram (γ) structures can be estimated given a specific heterogeneity (soil, vegetation and topography) and antecedent wetness conditions (caused by precipitation), represented by the SWHET cuboid. These conceptual cuboid based results can serve as look-up tables for validating footprint scale soil moisture radar products which promise to have resolutions of 3 km as well as for the validation of downscaled soil moisture. Upon availability of

more data, these results can be extended.

4.7 Conclusions

Accuracy of validation relationships for footprint scale soil moisture is severely restricted because of scale discrepancy of remote sensing support scales and ground based soil moisture measurements. In this study we proposed a scale appropriate physically based technique that can be used to validate footprint scale soil moisture. The results reflect that redistributed soil moisture spatial variance can be modeled as a linear function of the dominant physical factors' spatial variance. We also developed a scale based look-up graph which can potentially be used to generate validation relationships in similar hydroclimates for different land-surface heterogeneity. The results from this study can be highly useful for validating radar based soil moisture products which have spatial resolutions similar to the support scales analyzed in the given study.

The results of this study until validated otherwise should be restricted for use only during growing seasons. This is required since the dominance of physical controls was evaluated only during the growing seasons. However, from an agricultural perspective, when the changes in land-surface heterogeneity are the quickest, the results from this study can prove very valuable as an independent source of validating footprint scale soil moisture data.

5. A SPATIALLY TRANSFERABLE DOWNSCALING SCHEME FOR NEAR-SURFACE SOIL MOISTURE

5.1 Synopsis

The use of remotely sensed soil moisture in hydrological modeling has gained momentum in recent years. However, scale discrepancy between observed and required soil moisture necessitates the use of downscaling algorithms. Even though numerous downscaling algorithms for soil moisture have been defined for different regions of the world, the concern for their spatial and temporal transferability remains. In this study, we have devised a spatially transferable downscaling algorithm for near-surface remotely sensed soil moisture. The algorithm is based on the recently developed Scale-Wetness-Heterogeneity (SWHET) cuboid. The downscaled soil moisture is computed by generating spatially auto-correlated random fields of soil moisture redistribution as a function of the dominant land-surface factor governing soil moisture redistribution and adding to antecedent soil moisture. The functional relationship between the dominant physical factor and soil moisture redistribution was found to be spatially transferable between similar hydro-climates (Iowa, U.S.A. and Manitoba, Canada) under most conditions. The downscaling relationship was evaluated for 3 different coarse scale SMOS pixels which were downscaled to 1500 m under six different heterogeneity conditions. The minimum root mean squared error was 0.06 v/v while the maximum was found to be 0.11 v/v. The study provides a first attempt at proof of concept for devising techniques to generate spatially and potentially temporally transferable downscaling algorithms.

5.2 Introduction

Recent years have seen a surge iαn soil moisture downscaling algorithms owing to the scale discrepancy between footprints of satellite based soil moisture and that required

in numerous hydrological modeling scenarios. The typical footprint of satellite based soil moisture is between 25-60 km. Spatial transferability of downscaling schemes for near-surface soil moisture for such large footprints (also referred to as pixels) becomes challenging for 2 reasons- 1) variable land-surface factors based heterogeneity within the pixel, and 2) differential wetting within the pixel as a result of isolated rainfall events.

Land-surface factors i.e. soil, vegetation and topography, jointly yet variably control the distribution of soil moisture at different scales. Past studies (Gaur and Mohanty, 2015; Gaur and Mohanty, 2013; Ryu and Famiglietti, 2006; Jawson and Nieman, 2007; Joshi and Mohanty, 2010; Joshi and Mohanty, 2011; Oldak et al., 2002) have shown that even though a single dominant heterogeneous factor controlling soil moisture distribution may be defined, it can differ with scale and the variability-co-variability of the land-surface factors. Thus, downscaling schemes based on the relationship between a particular land-surface factor and soil moisture in a certain region may not be spatially transferable to another region with different land-surface heterogeneity. Kim and Barros (2002) who used linear combinations of a single land-surface factor (topography) data for a region in Oklahoma to downscale soil moisture using a modified fractal interpolation method also suggested the limitation of spatial transferability of their scheme to regions with varying heterogeneity. Other popular downscaling methods such as the 'universal triangle' method (Carlson et al., 1994; Carlson et al., 1995; Gillies et al., 1997) and UCLA method (Kim and Hogue, 2012) are based on the relationship between vegetation based heterogeneity, temperature and soil wetness. The universal triangle method exploits the triangular or trapezoidal nature of the relationship between vegetation or more specifically normalized difference vegetation index (NDVI) and surface temperature given different wetness conditions. However, the technique becomes limited in regions where the within pixel data is not sufficient to map the universal triangle/trapezoid completely or where the soil moisture-temperature variability is related to parameters besides vegetation which is often the case in soil type based

or topographically heterogeneous locations. Numerous studies (Chauhan et al., 2003; Piles et al., 2011 etc.) have employed this technique to get downscaled soil moisture with varying success. The UCLA method utilizes a soil wetness relationship developed by Jiang and Islam (2003) to determine soil wetness based on its relationship with the enhanced vegetation index and soil temperature and is thus, similarly limited. The other factor which affects transferability of downscaling relationships is the variable antecedent wetness conditions within the pixel caused by variable rainfall. Precipitation is the most dominant factor controlling soil moisture distribution (Joshi and Mohanty, 2010). Other studies (Teuling et. al., 2007; Ivanov et. al., 2010, Gaur and Mohanty, 2015) have also shown that the relationship between soil moisture and land-surface heterogeneity is heavily dependent on antecedent wetness conditions. Thus, the uncertainty in downscaling methods based on the relationships between land-surface heterogeneity and soil moisture can become much higher under scenarios of differential wetting within the pixel. A major limitation of the downscaling relationships based on vegetation based heterogeneity also arises because of the differences in sensitivity of soil wetness to temperature and vegetation based on the antecedent wetness conditions. The land-surface temperature is more sensitive to wetness under relatively wet conditions whereas vegetation is more sensitive only during relatively drier conditions (Kim and Hogue, 2012). Therefore, variable wetting within the pixel may lead to high uncertainty in the downscaled soil moisture generated through these techniques and consequently affect their spatial transferability.

The objective of this study is to design a soil moisture downscaling algorithm that is spatially transferable under various land-surface heterogeneity and antecedent wetness conditions.

The downscaling scheme developed in this study is based on the Scale-Wetness Heterogeneity (SWHET) Cuboid (Gaur and Mohanty, 2015). The SWHET cuboid describes the scale and hydro-climate specific relationships between soil moisture redistribution and

dominant land-surface factors through a parameter, α. The parameter α, is unique to a specific normalized wetness index and normalized heterogeneity index. The wetness index describes the antecedent wetness conditions and the heterogeneity index honors the within pixel variability and co-variability of land-surface based heterogeneity i.e. soil, vegetation and topography. Thus, enabling the results to be spatially transferable.

5.3 Study Area

The generated downscaling scheme was assessed in the Red river watershed in southern Manitoba, Canada. The soil texture varies in an east to west gradient from heavy clays to loamy fine sands. The topography in the region is flat (< 2% slope) while the primary land-use is agricultural. The climate of the region is classified as moist climate with severe winter. The % sand, leaf area index (LAI) and flow accumulation values from the region are provided in Figure 5.1. A more detailed description of the region can be found in McNairn et al., 2015.

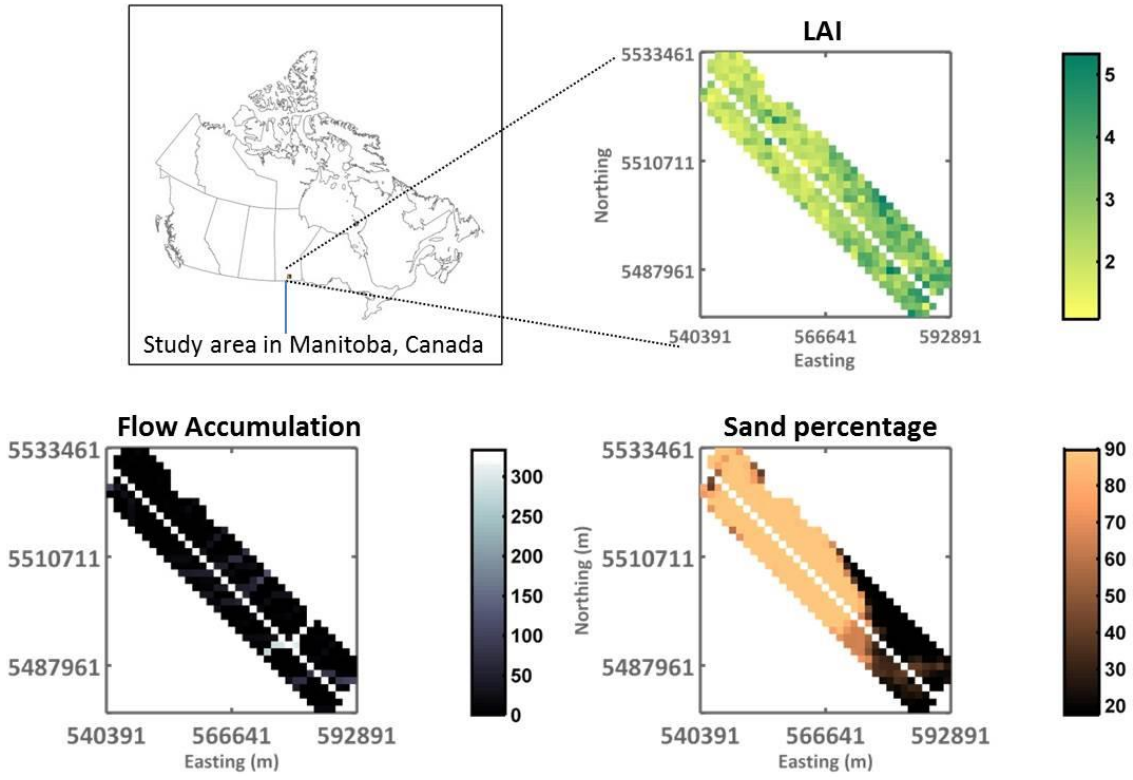

Figure 5.1: Study area and the prevailing heterogeneity in terms of vegetation, topography and soil.

5.4 Data

The coarse scale soil moisture to be downscaled was obtained from the Soil Moisture Ocean Salinity (SMOS) satellite. A Level 2 soil moisture data product, MIR_SMUDP2, was used for the study (Figure 5.2). This dataset is provided by the European Space Agency on the Icosahedral Snyder Equal Area (ISEA) projection (Carr et al., 1997). The multiple pixels in the dataset that appear to form a hexagonal cell correspond to one set of latitude and longitude defined at the center of the hexagonal cell. The actual average product spatial resolution is 43 km but the data are oversampled and the coordinates are equispaced at 15 km. More details about this soil moisture product can be obtained in Sanchez et al., 2012.

The airborne soil moisture data, % sand, elevation and leaf area index data were obtained from Dr. Andreas Colliander through personal communication. Figure 5.2 also shows the centers of the airborne pixels of soil moisture data that was collected using the passive active L-band (PALS) sensor during the SMAPVEX12 field campaign in Manitoba, Canada. The spatial support of the airborne and ancillary data is 1500 m.

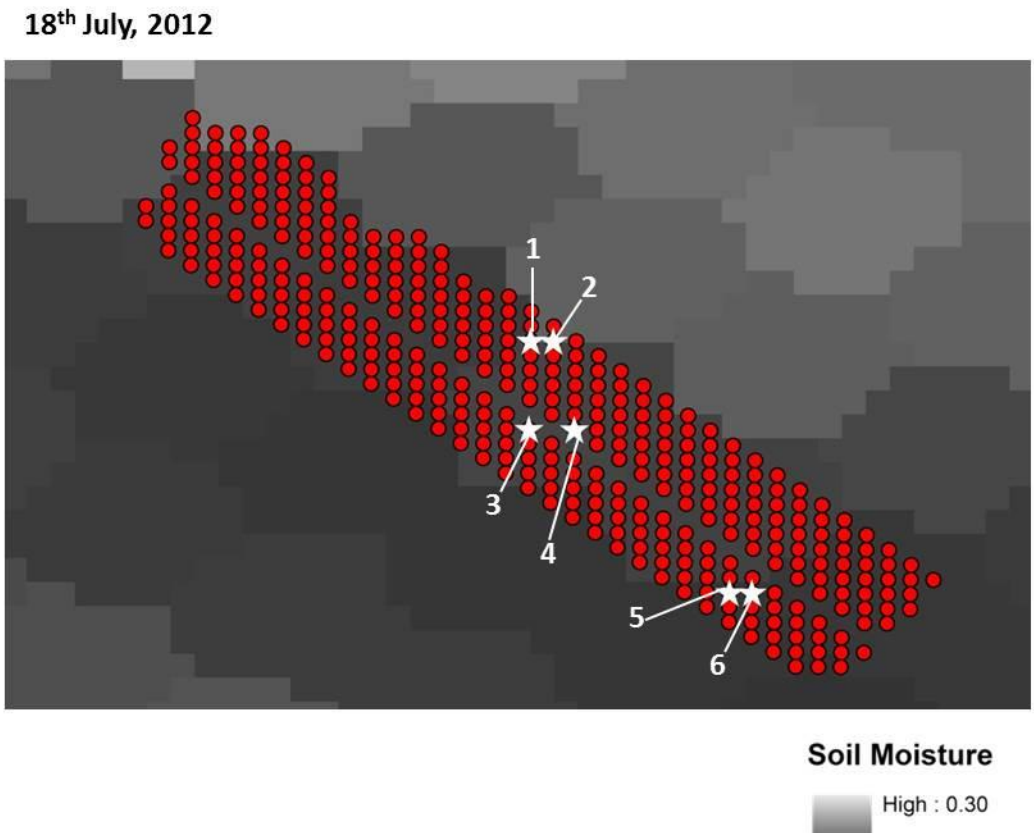

Figure 5.2: SMOS based soil moisture data and pixel centers of the soil moisture data collected using PALS sensor. Pixels 1-6 represent the center of the downscaled pixels.

5.5 Methodology

Our study region in Manitoba, Canada may be considered to have a hydro-climate similar to Iowa. Thus, we chose the results from the SWHET cuboid for Iowa to assess the spatial transferability of the downscaling scheme in Manitoba, Canada. In this study, fine scale refers to the scale being downscaled to (i.e 1500 m) while coarse scale refers to the satellite pixel scale (43 km).

5.5.1 Overview of Downscaling Scheme

The downscaled soil moisture was generated as shown in the downscaling algorithm schematic (Figure 5.3). A normalized wetness index and heterogeneity index were computed using the coarse support scale SMOS data and fine support scale ancillary data respectively. The heterogeneity index acts as a bridge between the fine and coarse scale since it is computed at the coarse scale but composed of land-surface factors defined at the fine support scale. Based on the two indices, an α parameter was computed from the SWHET cuboid. The α parameter in conjunction with the semi-variograms of a previously determined dominant land-surface factor was used to generate the empirical semi-variograms of soil moisture redistribution at the fine support scale. Soil moisture redistribution (ΔSM) refers to changes in soil moisture over a specific time period (1-2 days in this study). Random fields specific to the derived semi-variograms of were generated to provide spatial distribution of ΔSM. The ΔSM values were added to the antecedent soil moisture at the fine support scale to generate downscaled soil moisture. Each of these steps is described in detail below.

5.5.2 Generation of Indices

Normalized Wetness Index: The normalized wetness index, SM_{norm} describes the relative antecedent wetness conditions of the coarse scale. Antecedent wetness conditions

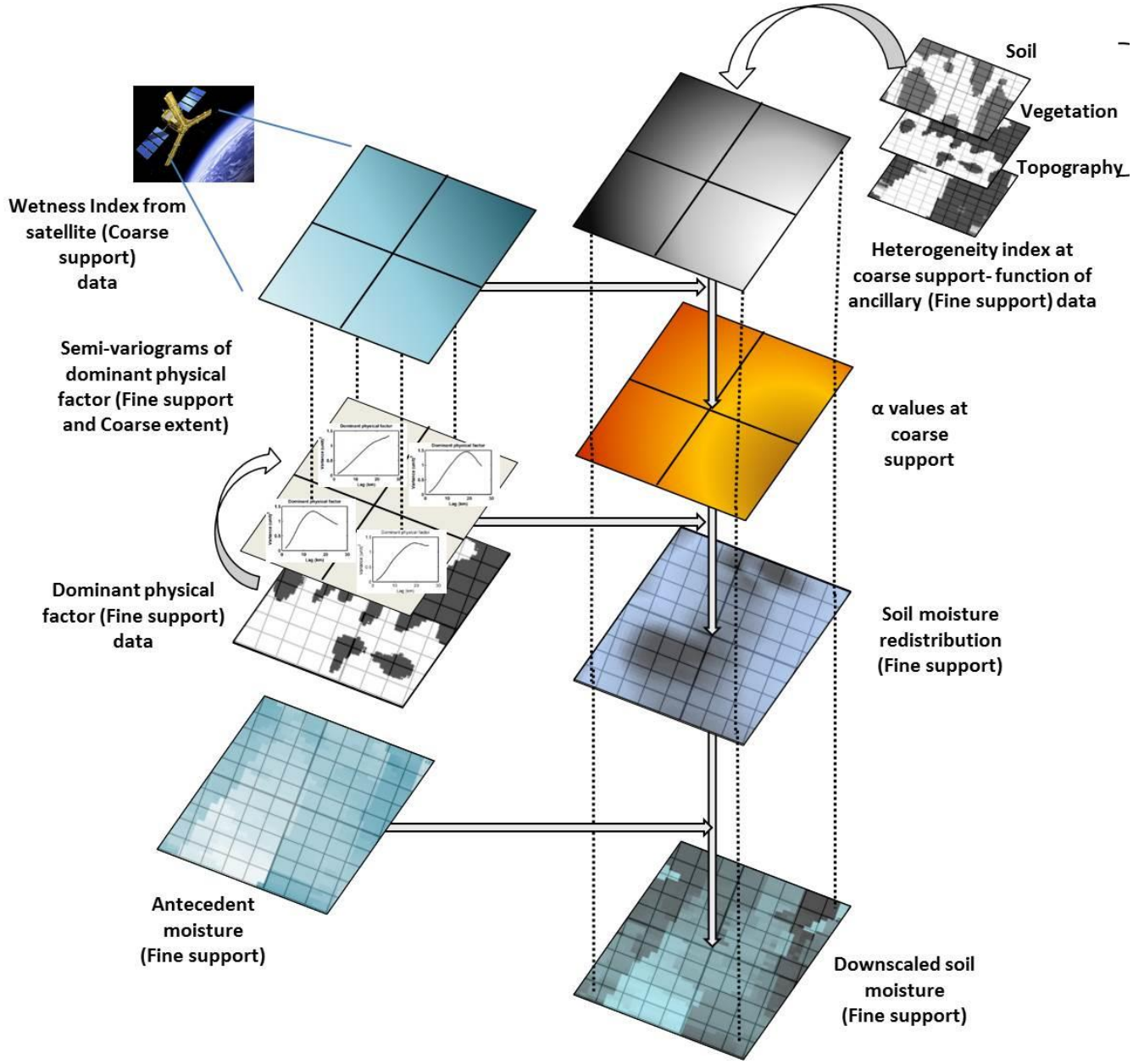

Figure 5.3: Schematic of the downscaling algorithm

determine the nature of relationship between soil moisture redistribution and land-surface factors. The index was defined using the SMOS data as given in eq. 5.1.

$$SM_{norm} = \frac{SM_{SMOS,max} - SM_{SMOS}}{SM_{SMOS,max}} \tag{5.1}$$

$SM_{SMOS,max}$ = maximum volumetric water content observed for SMOS pixels

SM_{SMOS} = antecedent volumetric water content of the SMOS pixel under consideration

Normalized Heterogeneity Index: The heterogeneity index describes the variability-co-variability between the factors creating land-surface heterogeneity. A heterogeneity index value was generated for each coarse pixel using ancillary data (%sand, flow accumulation and LAI) at 1500 m as described below. Such a formulation of the index at both scales acts as a bridge between the two scales. In order to generate the index, the first step is the creation of a covariance matrix of heterogeneity (eq. 5.2). The covariance matrix is defined using the fine support scale ancillary data for the extent of a SMOS pixel.

$$\mathbf{H} = \begin{bmatrix} \sigma_{s,s} & \sigma_{v,s} & \sigma_{t,s} \\ \sigma_{s,v} & \sigma_{v,v} & \sigma_{t,v} \\ \sigma_{s,t} & \sigma_{v,t} & \sigma_{t,t} \end{bmatrix} \tag{5.2}$$

H = heterogeneity matrix

σ = statistical co-variance

s,v,t represent soil (% sand), vegetation (LAI) and topography (flow accumulation) respectively

In order to account for the variable number of fine support pixels within different SMOS pixels, the heterogeneity matrix was normalized using the total area of the fine support pixels within the domain (eq. 5.3).

$$\mathbf{H}_a == \frac{\mathbf{H}}{nxA} \tag{5.3}$$

n = number of fine support scale pixels within SMOS pixel extent

A = area of fine support scale pixel = 1.5 x 1.5 km^2

An eigenvalue decomposition was then computed on $\mathbf{H}_a$ (eq. 45.4) to generate the heterogeneity index *H'* (eq. 5.5).

$$(\mathbf{H}_a - \delta\mathbf{I})\mathbf{U} = 0 \tag{5.4}$$

I = identity matrix **U** = eigenvector matrix δ= eigenvalue (scalar)

$$H' = \delta_{max} cos^{-1}(\frac{u_{max}.\mathbf{i}}{||u_{max}||.||\mathbf{i}||}) \tag{5.5}$$

The heterogeneity index was normalized (eq. 5.6) based on the maximum value of the index calculated for the region.

$$H_{norm} = \frac{H'_{SMOS,max} - H}{H'_{SMOS,max}} \tag{5.6}$$

where $cos^{-1}(\frac{u_{max}.\mathbf{i}}{||u_{max}||.||\mathbf{i}||})$ = angle (radians) between dominant eigenvector and a reference vector **i** ([1 1 1]).

α values based on the normalized wetness and heterogeneity index were obtained from the SWHET cuboid for Iowa at 1600 m (Gaur and Mohanty, 2015).

5.5.3 Generation of Fine Scale Soil Moisture Redistribution

5.5.3.1 Semi-variogram Based Relationships

As found previously for a similar hydro-climate in Iowa, % clay was selected as the dominant physical factor controlling soil moisture redistribution. The % clay values were

normalized within each coarse extent using eq. 5.7.

$$c_{i,norm} = \frac{c_i - \overline{c}}{\sqrt{\frac{\sum(c_i - \overline{c}^2)}{n-1}}} \tag{5.7}$$

Empirical semi-variograms (eq. 5.8) for the % clay data, γ_c were generated for the approximate extent of a SMOS pixel by using data representing a support and spacing of 1500 m.

$$\gamma_c(h_i) = \frac{1}{2N(h_i)} \sum_{i=1}^{N(h_i)} [(c(x) - c(x+h_i)]^2 \tag{5.8}$$

Where $\gamma_c(h_i)$ is the semi-variogram estimator and $c(x)$ and $c(x+h_i)$ represent the values of the dominant physical factor, i.e. % clay separated by a distance h_i and $N(h_i)$ is the total number of such pairs. Estimates of empirical semi-variograms, $\gamma_{\Delta SM}$ for soil moisture redistribution values at the fine scale were estimated using the α values and semi-variogram of the dominant physical factor as show in eq. 5.9 (assuming a 0 nugget value and hence 0 intercept)

$$\gamma_{\Delta SM} = \alpha\gamma_c \tag{5.9}$$

5.5.3.2 Theoretical Semi-Variogram Fitting and Random Field Generation

A theoretical semi-variogram was fit to $\gamma_{\Delta SM}$ in MATLAB using a variogram fitting function, variogramfit (Schwanghart, 2010). Based on the theoretical variogram, 50 random fields of soil moisture redistribution, ΔSM_{norm} were generated for a fine scale grid of size n (as defined in eq. 5.3) using the R package gstat (Pebesma, 2004, Pebesma and Wesseling, 1998). A large number of random fields were generated to account for non-uniqueness of the random fields. These values were then de-normalized using eq. 5.10 to obtain actual soil moisture redistribution values.

$$\Delta SM_i = \Delta SM_{i,norm}\sqrt{\frac{\Sigma(\Delta SM_i - \overline{\Delta SM})^2}{n-1}} + \overline{\Delta SM} \tag{5.10}$$

The standard deviation, $\Delta SM_{i,norm}\sqrt{\frac{\Sigma(\Delta SM_i - \overline{\Delta SM})^2}{n-1}}$ and mean, $\overline{\Delta SM}$ of the soil moisture redistribution values was computed from the actual observed data (at 1500 m resolution) in the study. However, there are numerous studies which give estimates of standard deviation, variance etc. based on past field experiments (for example, Famiglietti et al., 2008) from where these values may be extracted.

5.5.4 Generation of Downscaled Soil Moisture

Downscaled soil moisture was generated by adding the mean of the generated soil moisture redistribution (50 realizations) to the antecedent soil moisture data (eq. 5.11). Such data may be obtained from soil moisture modeling at finer scales where the applicability of Richard's equation has been proven or from well distributed in-situ datasets. In this study, we used the available soil moisture data at the fine scale.

$$SM_i = SM_{i-1} + \Delta SM_i \tag{5.11}$$

5.6 Results and Discussion

5.6.1 Heterogeneity Index

The heterogeneity index of Manitoba, Canada was compared to that of Iowa from where the inter-relationships between heterogeneity, wetness and fine scale soil moisture were being assessed for transferability. Figure 5.4 shows the empirical cumulative distribution (cdf) function plots of the normalized heterogeneity for the Iowa (Gaur and Mohanty, 2015) and Manitoba, Canada region. A Kolmogorov-Smirnov test to assess whether the two distributions comprise of a single continuous distribution shows that the two cdf plots do not match (p-value >0.05). This implies the heterogeneity in Iowa and Canada is

different from each other in terms of variability and co-variability of the land-surface factors. Even though the two regions have similar land-use, this inequality may be expected. The crop types grown in Iowa were mostly soybean and corn whereas the crops grown in Canada were more diverse comprising of canola, winter wheat, soybean, corn and wheat. On average, the % sand content in Canada is also much higher that Iowa as is its distribution within the region. This could lead to differences in the values and distribution of the heterogeneity index.

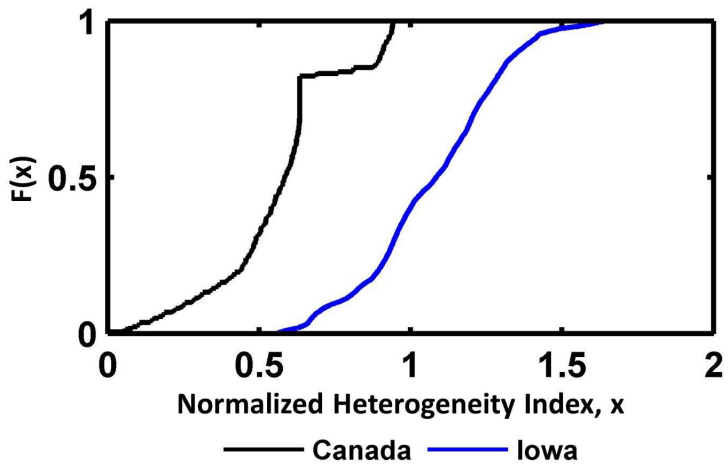

Figure 5.4: Cumulative distribution function plots of the normalized heterogeneity index for Iowa and Canada.

5.6.2 Soil Moisture Downscaling

A typical SMOS satellite overpass does not repeat itself for 2-3 days. This implies that the radiation values used to derive a typical daily SMOS soil moisture product over a fixed grid does not comprise of the radiations from the exact same region. This leads to each overpass potentially representing slightly different land-surface heterogeneity be-

tween days. In order to assess our downscaling scheme for insulation against such effects, we selected two adjacent heterogeneity combinations to represent a SMOS pixel. The starred locations (Pixel 1-6) in Figure 5.2 represent that centers of the pixels around which a 40 km radius area was chosen to represent a SMOS pixel. These locations were chosen in the center of the domain as well as at the edges to assess different combinations. Pixel 1-4 are located in higher sand content and less diverse LAI conditions than pixel 5-6 where there is more heterogeneity in terms of crops and LAI (Figure 5.1). Each pair of pixels (1-2;3-4;5-6) represents the two adjacent heterogeneity combinations for one SMOS pixel. The wetness conditions for each pair is also different from each other. (Table 5.1).

Table 5.1: SWHET cuboid values to generate the empirical semi-variograms of soil moisture redistribution

Pixel	**SWHET cuboid values**		
	Normalized Heterogeneity Index	*Normalized Wetness Index*	α
1	0.6349	0.2702	0.9655
2	0.6349	0.2702	0.9655
3	0.6349	0.3493	0.7281
4	0.6331	0.3493	0.7244
5	0.3655	0.4771	1.2806
6	0.3425	0.4771	1.2895

The normalized heterogeneity index and wetness index values along with the corresponding α values are provided in Table 5.1. The α values were obtained from the SWHET cuboid for Iowa. It was observed that shifting the center of the SMOS pixel by 1500 m (or one fine scale pixel) resulted in slightly different heterogeneity index values which combined with the wetness index generated unique α values. Lower normalized heterogeneity index (or higher heterogeneity index) may represent either high variability in the region or higher correlations within the land-surface factors. Since Manitoba, Canada

is an agricultural area, natural correlations between different land-surface factors can be assumed to minimal. Thus, a lower normalized heterogeneity index can be attributed to higher variability in the land-surface factors in that location. The region represented by pixel 5-6 had the lowest normalized heterogeneity index and was therefore most heterogeneous (or variable) whereas region represented by pixel 1-4 had lower heterogeneity. This can also be visually observed from Figure 5.1. Pixel 5-6 represent a more heterogeneously cropped area with varying sand content while pixels 1-4 encompass the almost uniformly sandy area as well.

The computed α values were multiplied with the empirical semi-variograms of % clay (eq. 5.9) to estimate the empirical semi-variograms of the soil moisture redistribution. Most appropriate theoretical semi-variograms were then fitted to the empirical variograms. The parameters for the fitted semi-variograms are provided in Table 5.2. It was seen that the sill and range values for the semi-variograms for % clay using pixels with adjacent centers are similar and not necessarily same.

Table 5.2: Details of the fitted theoretical semi-variograms

Pixel	**Fitted semi-variogram parameters**		
	Type	*Sill*	*Range (m)*
1	Spherical	1.1051	35271
2	Spherical	1.1051	35271
3	Spherical	0.8334	35271
4	Spherical	0.8286	35305
5	Spherical	1.9237	37548
6	Spherical	1.9842	37528

The downscaled soil moisture was then computed as shown above. The observed soil moisture and the downscaled soil moisture for the various pixels is shown in Figure 5.5-5.7. The downscaled region for pixels 1-4 is same. The downscaling region with these 4

pixels as centers falls within 2 adjacent SMOS pixels. It was observed that the downscaled results for the pixels whose centers correspond to pixels 1-2 showed relatively better results than pixel 3-4 where the downscaled soil moisture was overestimated. The root mean squared error (rmse) of the same is provided in Table 5.3. The minimum rmse for these pixels was 0.07 v/v while the maximum was 0.11 v/v (Table 5.3). The normalized wetness index for pixel 1-2 was slightly lower than that for pixel 3-4 implying that the coarse pixel represented by 3-4 was slightly drier (lower wetness) as compared to pixel 1-2. The overestimated downscaled soil moisture for pixel 3-4 implies that at lower wetness, the computed redistribution values were lower than the actual redistribution values. This may be attributed to the higher sand content in the region than Iowa. Since the relationships derived in Iowa (Gaur and Mohanty, 2015) do not account for such high estimates of % sand, the relationship between heterogeneity and soil moisture redistribution may be inadequately represented. The region downscaled using pixel centers 5-6 lies slightly south of the first downscaled region. The rmse values for this region were relatively lower (0.06 v/v). Akin to pixel 3-4, this region is also relatively dry (high wetness index) but lies in relatively lower sand content. The downscaled soil moisture values match well under these conditions.

Table 5.3: Root mean squared error for the downscaled pixels

Pixel	**Downscaled rmse (v/v)**
1	0.0790
2	0.0721
3	0.1168
4	0.1082
5	0.0664
6	0.0656

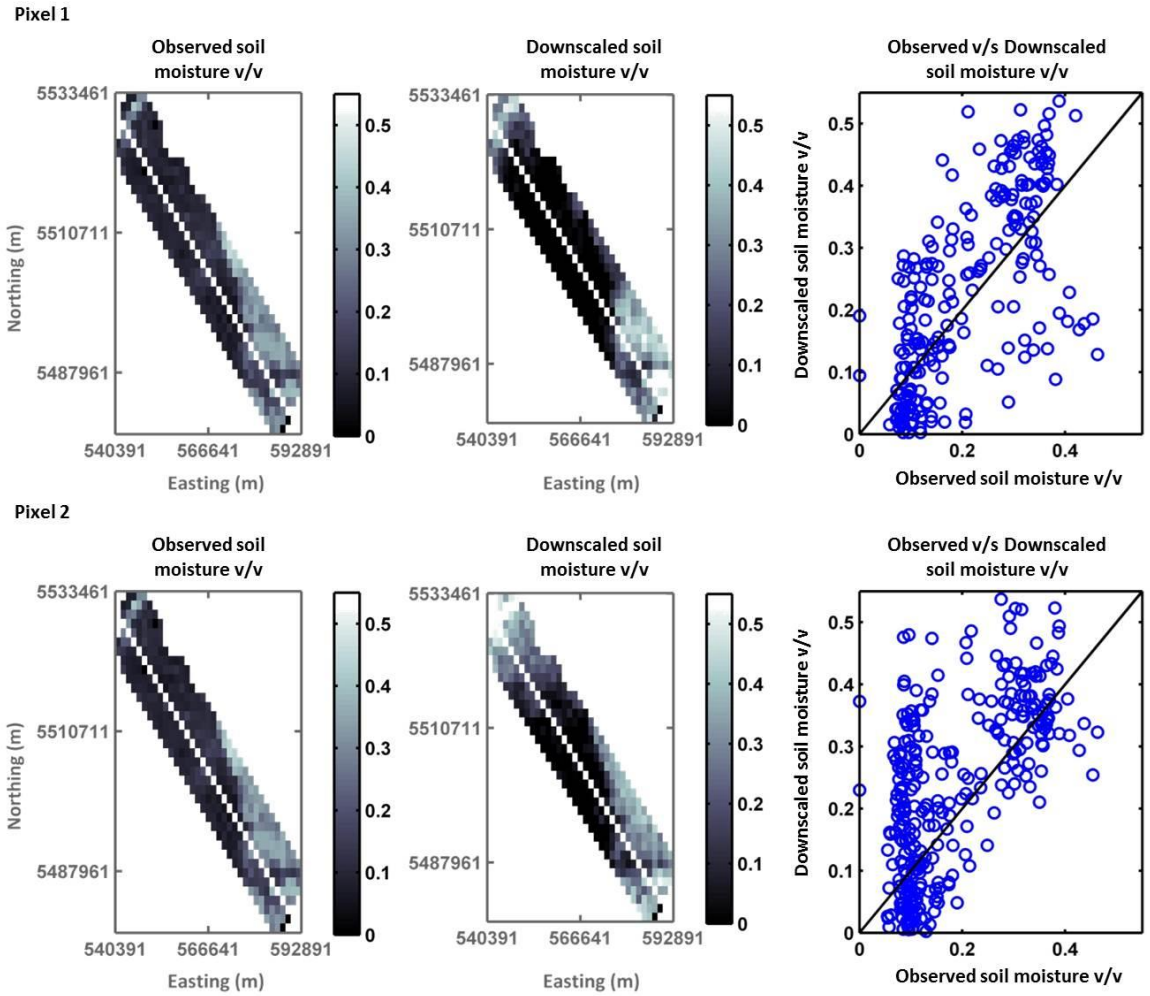

Figure 5.5: Downscaled soil moisture results for the region representing low heterogeneity and relatively high soil moisture conditions.

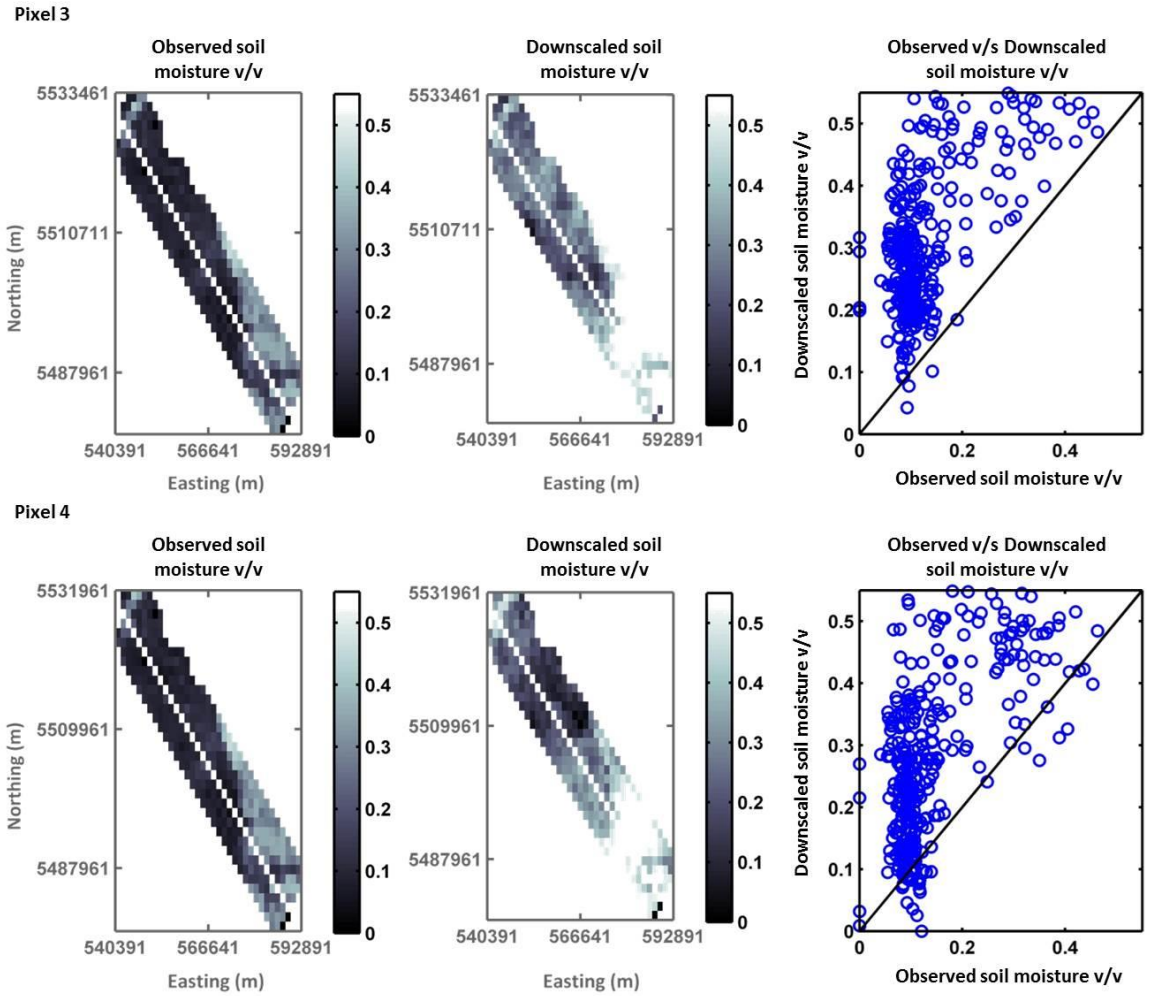

Figure 5.6: Downscaled soil moisture results for the region representing low heterogeneity and relatively dry soil moisture conditions.

Despite different rmse values, the trend of relative wetness across the domain is represented by all the downscaled regions using different antecedent wetness conditions. This may also be attributed to the fine scale antecedent wetness conditions that were added to the soil moisture redistribution. Since precipitation forms the first principal component in explaining soil moisture variability over a domain, the general good trend could also be attributed to the good antecedent soil moisture data at the fine scale. However, the results are encouraging considering the transferability of results from Iowa to Canada which has similar hydro-climate but different heterogeneity conditions.

5.7 Conclusions

In the given study a spatially transferable soil moisture downscaling scheme was defined. The scheme was based on the Soil-Wetness-Heterogeneity (SHWET) Cuboid. The most important finding of this study is the possibility of spatial transferability of downscaling schemes given similar hydro-climates if the within pixel heterogeneity and antecedent wetness conditions are properly accounted for. The scheme designed in this study performed well (maximum rmse 0.07) for regions with heterogeneity comparable to the regions where SWHET was defined but did not perform as well (maximum rmse 0.11) under extremely different heterogeneity conditions. A limitation of this scheme is the potential temporal propagation of error since antecedent soil moisture conditions form an important component of the downscaling scheme.

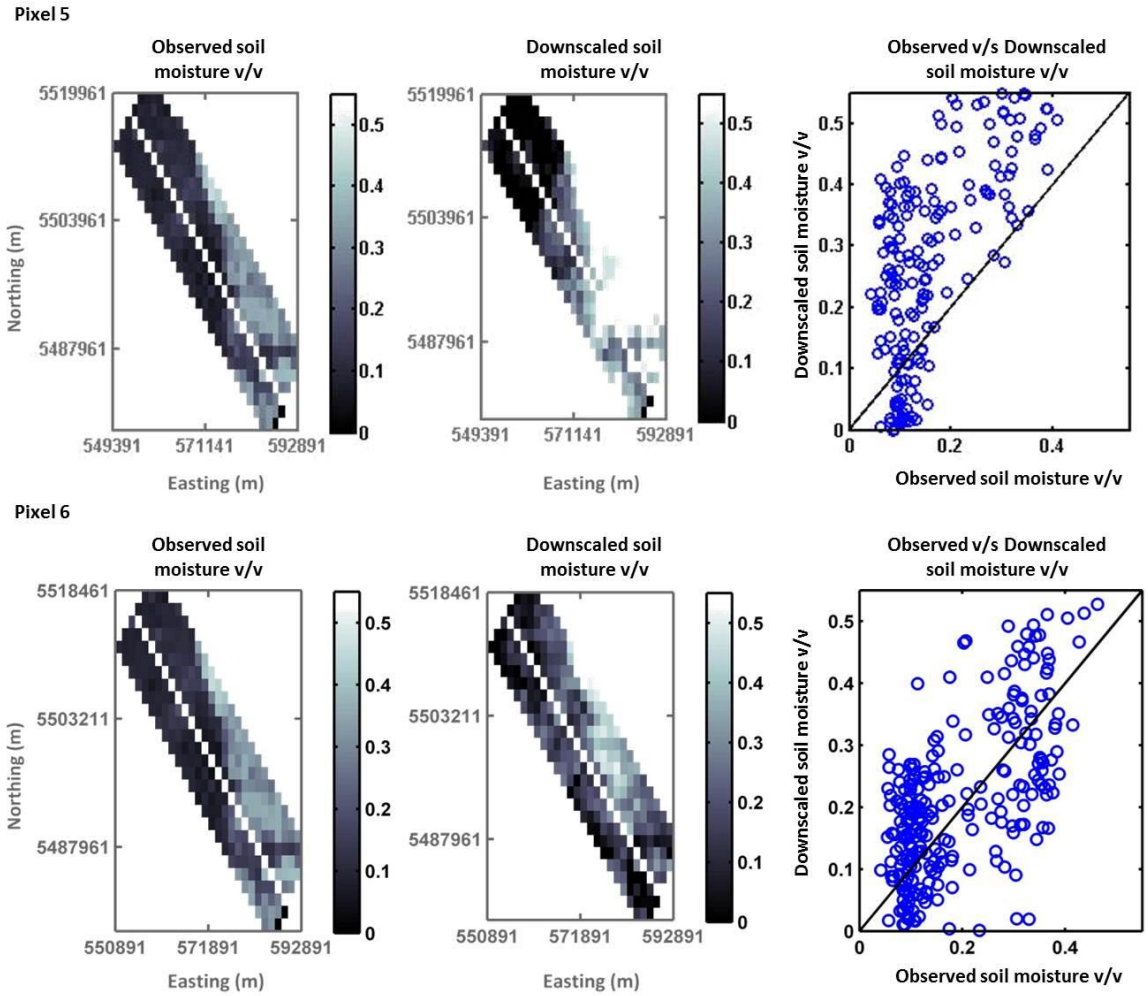

Figure 5.7: Downscaled soil moisture results for the region representing high heterogeneity and relatively dry soil moisture conditions

6. EFFECT OF OBSERVATION SCALE ON REMOTE SENSING BASED ESTIMATES OF EVAPOTRANSPIRATION IN A SEMI-ARID ORCHARD ENVIRONMENT

6.1 Synopsis

Partially vegetated fields like fruit orchards wherein different trees are subject to different kinds of fertilizer/irrigation treatments, require spatially distributed estimates of evapotranspiration (ET) to monitor water use. Estimating spatially distributed evapotranspiration for these environments can be achieved by using remote sensing. However, the computation of ET under such conditions is complicated because of the complex parameterizations required to derive ET for the mixed orchard pixels comprising bare soil and well watered plants. Also, the parameterization of processes is not scale invariant, owing to change in the nature of mixed pixels across remote sensing observation scales. In this study, our main objectives were 1) to isolate and evaluate the effect of varying spatial scales (comparable to canopy sizes and larger) of the remote sensing data on ET estimates; and 2) provide a user-friendly method for estimating remote sensing based ET for orchard conditions. ET was computed using an empirical technique (Simplified- Surface Energy Balance Index Algorithm) for almond and pistachio orchards from remote sensing imagery collected at 5.8/7.2 m and 120 m using the MASTER and Landsat sensors, respectively. In order to account for the effect of mixed pixels, an NDVI based correction factor was applied to the derived ET values and the results were validated with Penman-Monteith based ET estimates. It was found that the corrected mean ET estimates were in agreement with the Penman-Monteith based ET estimates at 120m (RMSEaverage = 0.12 mm/hr) whereas they were underestimated at the finer resolutions. The results indicated that a remote sensing pixel resolution comparable to the row spacing and smaller or comparable to

the canopy size overestimated the land surface temperature and consequently, underestimates ET. The results reflect that good spatial estimates of crop ET can be made for crops growing in orchards using simple ET models that require minimal data and freely available Landsat imagery. These findings are very encouraging for the regular monitoring of crop health and effective management of irrigation water in highly water stressed agricultural orchards.

6.2 Introduction

The Central Valley region in California is one of the most productive agricultural regions of the United States. Over 250 different crops are grown in the region with an estimated value of $ 17 billion per year (Faunt, 2009). The summer agriculture in the valley depends solely on irrigation (Zhong et al., 2009), which makes water management in this water-stressed period a crucial task. In order to effectively manage water resources without jeopardizing the agrarian economy of the region, the use of irrigation water needs to be optimized by minimizing water losses. Evapotranspiration (ET) accounts for up to 80 % of the water losses in such semi-arid regions (Chehbouni et al., 2008). An accurate estimation of ET can thus, lead to better determination of the water losses by the plants and thus enable effective management of irrigation planning.

The most extensively and successfully applied method for estimating crop ET (ETc) for irrigation systems planning is the two-step crop coefficient (Kc) x reference ET (ETref) method (Allen and Pereira, 2009, Pruitt and Doorenbos, 1977, Allen et al., 1998). This method of ET estimation provides numerically accurate ET estimates in basin wide studies but no spatial representation of ET. Also, the estimation of Kc becomes complicated when the percent crop cover, irrigation techniques and routines vary across the region (Allen and Pereira, 2009). In the irrigated fruit orchards of the Central Valley, where the fertilizer treatments, irrigation techniques and age of various trees within the orchard (and conse-

quently water demands) are often variable, a numerically accurate spatial representation of ET is highly desirable. This can be achieved through properly validated ET estimates from remote sensing, which provides spatial representation of ET while preserving the numerical accuracy of the crop coefficient based methodology (Price 1990; Kustas et al. 1994; Bastiaanssen et al. 1998, Roerink et al. 2000; McCabe and Wood 2006).

Remote sensing data is available at multiple spatial scales which determine the amount of detail that can be extracted from the dataset. Under full crop cover conditions, there is loss in spatial information as the scale coarsens (Mauser and Schadlich 1998, McCabe and Wood 2006, Kustas et al. 2004). However, the orchards in Central Valley consist of evenly spaced trees, such that a large amount of bare soil is exposed between the trees. Higher discrepancies in ET estimates based on remote sensing data at different scales have been observed under such conditions owing to complex parameterization of the energy balance processes (Chang and Hong, 2012, Moran et al., 1997).

The objective of the study was to assess the scaling behavior of ET by comparing spatially distributed ET derived from high resolution (5.8-7.2 m) and relatively coarser (120 m) remote sensing imagery with MODIS based (1km) and Penman-Monteith (fetch scale) based ET estimates under orchard conditions. It was hypothesized that in orchard (partially vegetated) conditions, finer resolution imagery may not necessarily imply better ET estimates from the dataset. The land surface temperature estimates from smaller mixed pixels (pixel resolution comparable to canopy size) may be higher on average than that obtained from a coarser mixed pixel where the pixel resolution is much larger than the canopy size. This would occur since a pixel resolution comparable to the canopy size will lead to presence of higher amount of bare soil in most pixels (pistachio canopy in Figure 6.1 a) and thus lead to higher land surface temperature estimates (and consequently, lower ET estimates) as opposed to a coarser pixel (Figure 6.1 b). Thus, the size of the pixel or observation scale would affect the ET value estimated from a remote sensing dataset. Since

land-surface temperature is a major input in all ET estimating algorithms, this variability due to scale can impact ET estimates irrespective of the algorithm used.

To verify this hypothesis, the Simplified- Surface Energy Balance Index (S-SEBI) algorithm (Roerink et al., 2000) was used to estimate ET. S-SEBI is an empirical approach and consequently removes scope of error due to incorrect parameterization of processes in such complex settings. In this study, ET from two different crops (pistachios and almonds) with different canopy sizes and percent ground cover was calculated using S-SEBI. A correction factor that explicitly reduces the discrepancy between measured, ground based ET and ET derived from remote sensing imagery under row orchard conditions was also introduced to improve ET estimates under orchard conditions.

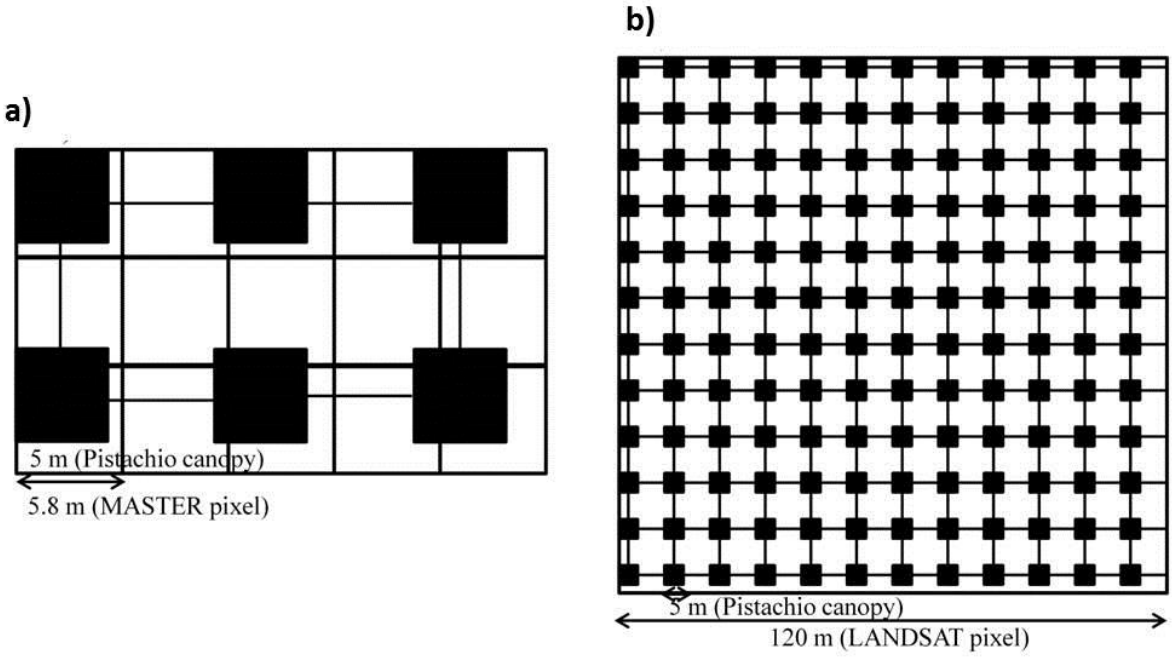

Figure 6.1: Conceptual diagram representing relative size of canopies and remote sensing pixels

6.3 Study Area

The study was conducted in almond and pistachio orchards in Lost Hills, Kern county, California (Figure 6.2). The climate of the region is semi-arid. The summer months in this area are extremely hot and dry with virtually no precipitation, with most of the crop water demands fulfilled by irrigation. The ET from these areas is thus directly dependent on irrigation. The study was conducted on four adjacent orchards (Figure 6.2) planted in rows and irrigated through fanjet and drip irrigation. The pistachio orchards were planted in the year 2000 and the rows are spaced 5.8 m apart. The two almond orchards were planted one year apart (1999 and 2000) with a row spacing of 7.5 m. The almond trees were 2.5-7.0 m high whereas the pistachio trees were shorter with tree heights varying between 1.5-3.0 m. (Cheng et al. 2013).

6.4 Materials and Methods

6.4.1 Remote Sensing Platforms

The study uses imagery from two different remote sensing platforms: an airborne sensor, MASTER, and a space borne sensor, Landsat 5. The MASTER imagery was collected on July 24th, 2009 (7.2 m resolution, time of overpass 2 P.M. local time) and June 29th, 2010 (5.8 m resolution, time of overpass 10:30 A.M. local time) as part of the Student Airborne Research Program (SARP) campaign organized by NASA in collaboration with the National Sub-Orbital Education and Research Center, whereas the Landsat (120 m thermal band resolution, time of overpass 10:30 A.M. local time) imagery was collected on July 28th, 2009 and June 29th, 2010. The necessary calibration data for the remote sensing imagery was collected at the field site as part of the SARP campaign.

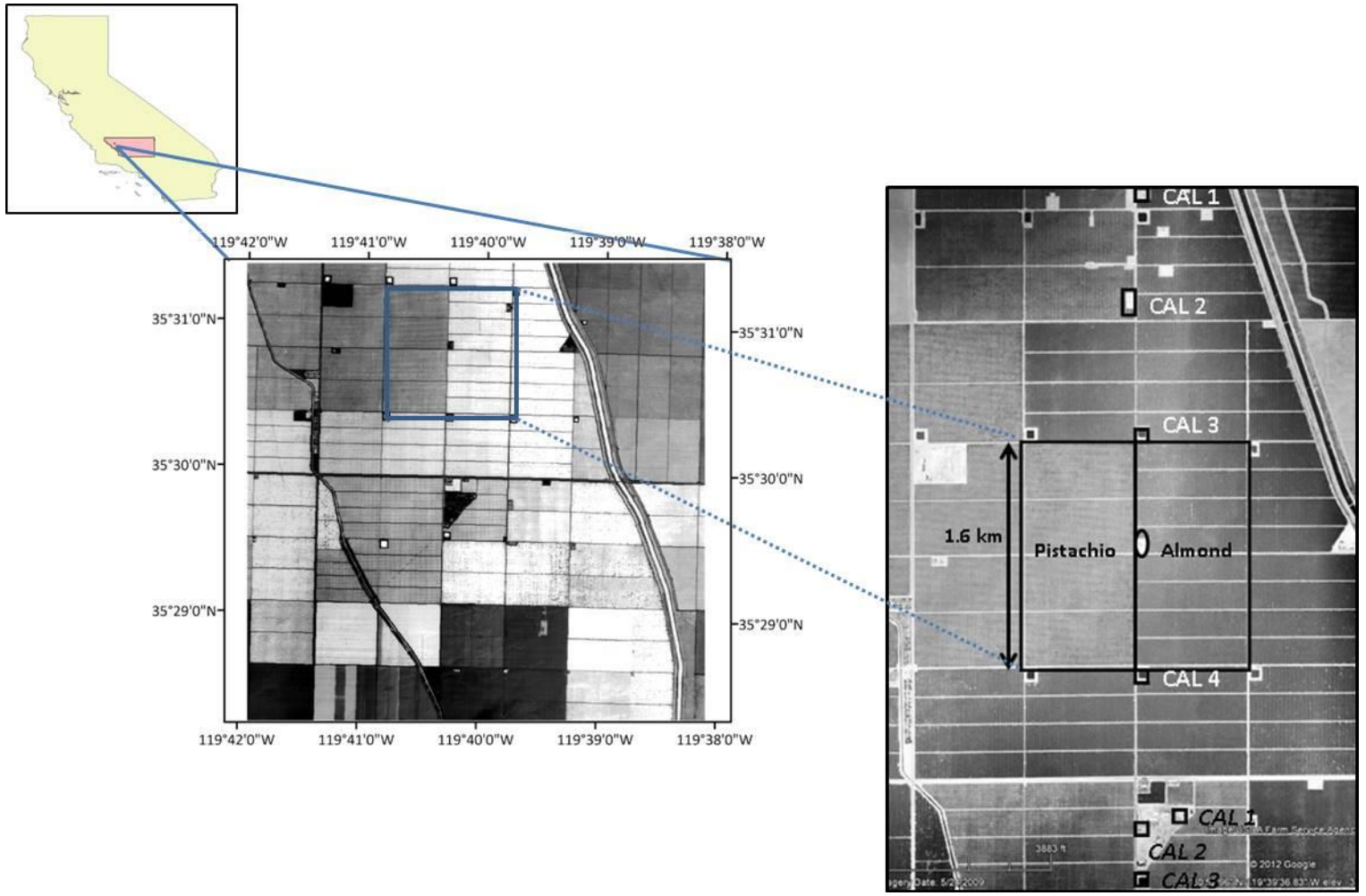

Figure 6.2: Location and imagery of the study orchards in California. The calibration sites marked in white represent calibration sites for 2009 while those marked in black represent calibration sites for 2010. The encircled area is a bare dry patch in the almond field.

6.4.1.1 Landsat

Landsat 5 imagery (path 42, row 35) was used in this study. A basic atmospheric correction was applied to the terrain corrected imagery using Fast Line-of-Sight Atmospheric Analysis of Spectral Hypercubes (FLAASH) module provided by ENVI version 4.3 (Exelis Visual Information Solutions, Boulder, Colorado). The necessary parameters for the correction were obtained from the metadata file. Band 6 was used for temperature extraction from the imagery. The procedure used to extract at-satellite temperature values from Landsat was adopted from Landsat 7- Science Data User's Handbook, NASA.

Land surface temperature was derived from at-satellite temperature by accounting for surface emissivity of the respective pixels depending on the land cover. Per-pixel emissivity was determined based on the red (R) and near infra-red (NIR) bands using the technique developed by Valor and Caselles (1996). The various assumed emissivity components used in the calculation were obtained from those developed for fruit trees.

$$\varepsilon_0 = \varepsilon_v P_v + \varepsilon_g (1 - P_v) + 4(d\varepsilon) P_v (1 - P_v) \tag{6.1}$$

$$P_v = \frac{1 - \frac{NDVI}{NDVI_g}}{(1 - \frac{NDVI}{NDVI_g}) - k(1 - \frac{NDVI}{NDVI_v})} \tag{6.2}$$

$$k = \frac{\rho_{2v} - \rho_{1v}}{\rho_{2g} - \rho_{1g}} \tag{6.3}$$

ε: Dimensionless emissivity of the pixel

$d\varepsilon$: Cavity effect of a rough surface (Caselles and Sobrino 1989) 0.04

P_v : Vegetation fraction cover

ρ_2 : Reflectance in NIR band

ρ_1 : Reflectance in R band

$NDVI = \frac{\rho_2 - \rho_1}{\rho_2 + \rho_1}$: Normalized difference vegetation index (Tucker, 1979)

The sub-scripts 0, g and v refer to the pixel under consideration, a bare ground pixel and a fully vegetated pixel respectively. The values of emissivity for a bare ground pixel and fully vegetated pixel were assumed to be 0.95 and 0.99.

The uncalibrated land surface temperature was obtained by correcting the satellite (radiative) surface temperature for emissivity effects of the surface.

$$T_0 = \sqrt[4]{\frac{T_{sat}^4}{\varepsilon_0}} \tag{6.4}$$

T_0 = Uncalibrated land surface temperature

T_{sat} = At-satellite temperature

The remote sensing based land surface temperature was calibrated using with the temperature data collected on the ground using empirical line correction (ELC). Ground truth data (as described in section below) for the same was collected on July 22nd 2009 and June 29th, 2010. The equations developed to calibrate the derived temperature estimates to the actual land surface temperature are given below in eq. 6.5 and 6.6 for 2009 and 2010, respectively ($R^2 > 0.9$).

$$T_{act} = 3.7156.T_0 - 96.093 \tag{6.5}$$

$$T_{act} = 2.2632.T_0 - 46.918 \tag{6.6}$$

T_0 = Uncalibrated derived land surface temperature, °C

T_{act} = Calibrated derived land surface temperature, °C

6.4.1.2 MODIS/ASTER Airborne Simulator (MASTER)

The MASTER sensor collects information over 50 optical and thermal wavelengths. The temperature estimates for the MASTER sensor were obtained from band 42. Atmospheric correction using MODTRAN 4 and the In-Scene Atmospheric Compensation (ISAC) algorithm for 2009 and 2010 respectively, were applied to the thermal imagery prior to ELC and temperature estimation. A standard MODTRAN 4 and FLAASH correction for optical bands was applied for 2009 and 2010, respectively.

6.4.2 Field Data Collection

In order to calibrate the remote sensing derived temperature data, calibrated thermal infra-red (TIR) guns were used to measure the temperature of the ground. In 2009, 4 locations (2 bare soil and 2 water bodies) in the field were chosen to calibrate the imagery (Figure 6.2). Each location was divided in a 3 by 3 grid and the temperature of all 9 grid points was estimated using the TIR gun. This was done twice through the afternoon. Since each location was sampled twice, a linear relationship between temperature and time of temperature collection was assumed (Figure 6.3(a)). The temperature of the ground at the time of over pass of the sensor was estimated from this curve. Three such targets (light, dark and water), each divided into a 2 by 2 grid were chosen to calibrate the imagery in 2010 (Figure 6.2). This was done 8 times through the afternoon. The temperature of each location at the time of overpass was estimated using the fitted polynomial curve as shown in Figure 6.3(b).

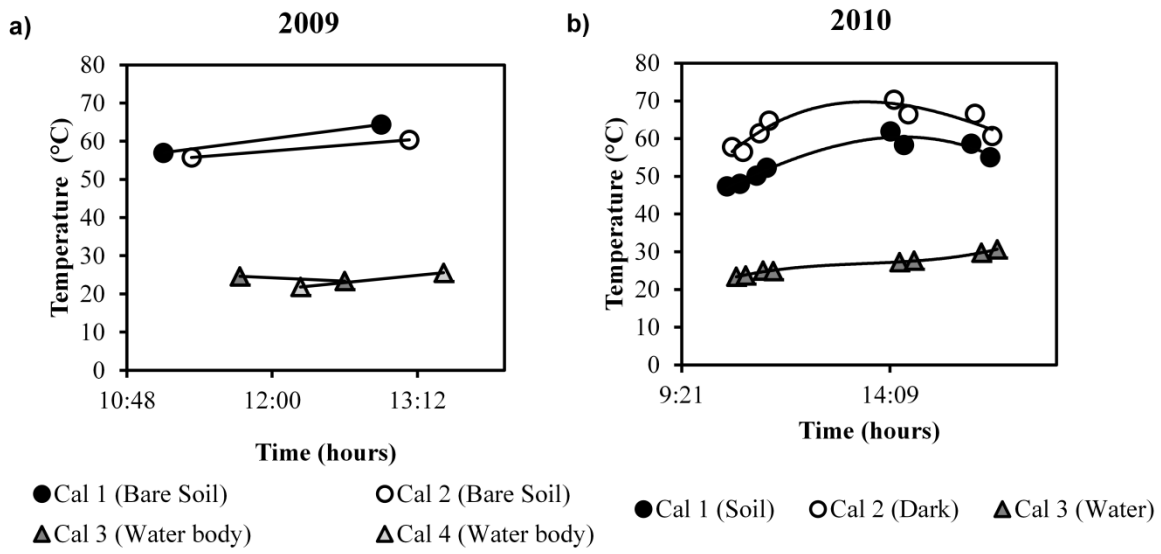

Figure 6.3: Calibration curves for estimation of ground temperature at the time of satellite and airborne sensor overpass.

The value of hourly incoming solar radiation (Table 6.1) and reference ET estimates were obtained from weather station No. 146 (Belridge) managed by CIMIS. The station is located 800 m west of the pistachio orchards. CIMIS generates ET estimates for the state of California and calculates reference ET over a standard grass or alfalfa land cover using the modified Penman equation (Pruitt and Doorenbos 1977). The necessary crop coefficients required to compute ET estimates specific to the crop are also calculated by CIMIS based on the technique developed by Allen et al. (1998).

Table 6.1: Incoming solar radiation (CIMIS, Belridge station)

Date	Solar Rad (W m-2)
July 24th, 2009	835.1
July 28th, 2009	834.2
June 29th, 2010	858.9

6.4.3 Estimating ET

6.4.3.1 Energy Balance Method: S-SEBI

The ET for the region was estimated using the S-SEBI algorithm. The algorithm requires minimal data inputs and assumptions to estimate ET. It is compatible with multiple sensors and works well for various land covers. S-SEBI was used successfully by Sobrino et al. (2007), Verstraeten, Veroustraete and Feyen (2005) over diverse landscapes using imagery from AVHRR. Roerink, Su and Mementi (2000) used this algorithm using imagery from Landsat. More recently, S-SEBI was deemed most useful in a semi-arid irrigated environment in Mexico (Chirouze et al. 2014). A brief description of S-SEBI, with minor variations in computation of albedo, is provided below for completeness. However, readers are referred to (Roerink, Su and Mementi 2000) for details of the algorithm.

$$R_n = G + H + LE \tag{6.7}$$

R_n = Net radiation, $\frac{W}{m^2}$

H = Sensible heat flux, $\frac{W}{m^2}$

LE = Latent heat flux, $\frac{W}{m^2}$

G = Soil heat flux, $\frac{W}{m^2}$

Incoming solar radiation, RS was measured close to the field site at weather station No. 146 managed by CIMIS. Rn was estimated using the relationship given below

$$R_n = R_S(1-\alpha) + R_{ld} - R_{lu} \tag{6.8}$$

α = Dimensionless albedo

R_{ld} = Long-wave downwards radiation $\frac{W}{m^2}$

$$R_{ld} = \varepsilon_a \sigma T_a^4 \frac{W}{m^2} \tag{6.9}$$

T_a = air temperature (K)

ε_a = Dimensionless atmospheric emissivity

$$\varepsilon_a = 1.24(\frac{e_a}{T_a})^{\frac{1}{7}} \tag{6.10}$$

e_a = Vapor Pressure (mBar)

R_{lu} = Long-wave upwards radiation

$$R_{lu} = \varepsilon_s \sigma T_s^4 \frac{W}{m^2} \tag{6.11}$$

ε_s = Land Surface emissivity (calculated in equation 6.1)

σ = Stefan-Boltzman Constant ($\frac{W}{m^2 K^4}$)

T_s = Land surface temperature (K)

Soil heat flux, G, was estimated as a function of NDVI using the model developed by Daughtry et al (1990) and assuming that the same relationship held good for our field site. The use of a vegetation based relationship for calculating soil heat flux was justifiable since the area under consideration was an agricultural region.

$$G = (0.325 - 0.208NDVI)R_n \tag{6.12}$$

H and LE were lumped into one factor called the evaporative fraction, defined as the ratio between latent heat and the sum of latent and sensible heat fluxes. The advantage of using the evaporative fraction to estimate latent and sensible heat fluxes, as certain studies suggest, is that the evaporative fraction remains constant throughout the day (Shuttleworth et al. 1989; Brutsaert and Chen 1996; Crago 1996,). The evaporative fraction (Λ) as per

the S-SEBI model is calculated as given below.

$$\Lambda = \frac{LE}{R_n - G} \tag{6.13}$$

$$\Lambda = \frac{T_H - T_0}{T_H - T_{\lambda E}} \tag{6.14}$$

$$T_H = a_H + b_H r_0 \tag{6.15}$$

$$T_{\lambda E} = a_{\lambda E} + b_{\lambda E} r_0 \tag{6.16}$$

Λ = Evaporative fraction corresponding to pixel albedo, r_0

T_H = Theoretical land surface temperature for an albedo value when all available energy gets converted to sensible heat

$T_{\lambda E}$ = Theoretical temperature for a land-surface albedo value when all available energy gets converted to latent heat

a_H ,b_H, $a_{\lambda E}$, $b_{\lambda E}$ = fitting parameters

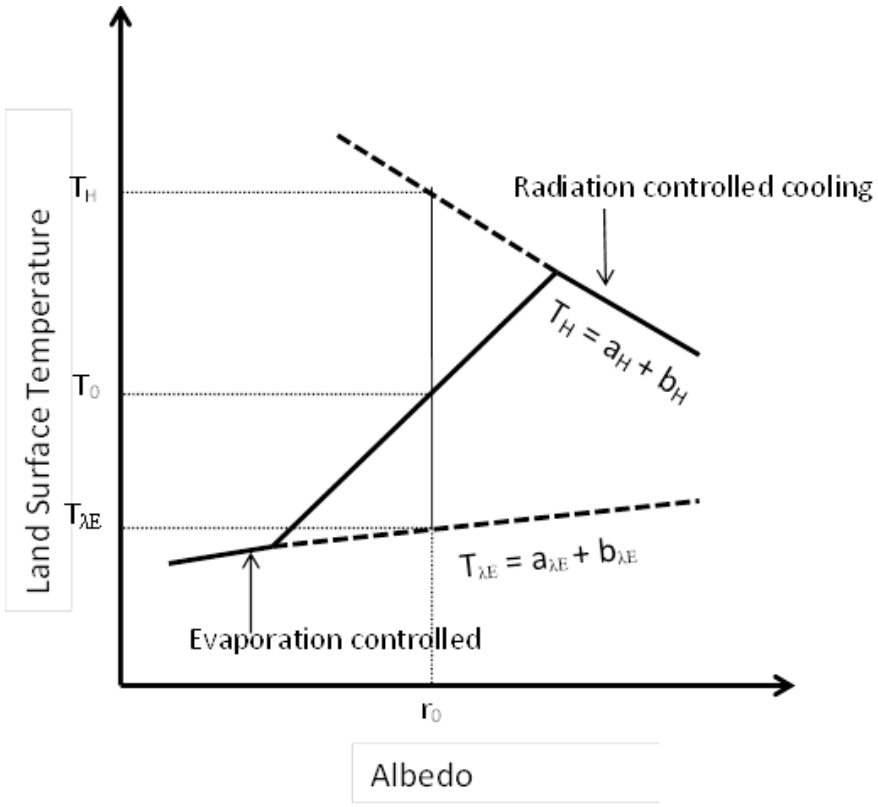

Figure 6.4: Relationship between albedo and land surface temperature (adapted from Roerink et al, 2000).

These fitting parameters were obtained by bounding the albedo versus temperature graphs as shown for the MASTER and Landsat sensors (Figure 6.5). The accuracy of the bounding lines is subject to the nature of the heterogeneity present in the area (i.e. presence of light and dark pixels). Ideally, the light pixels should correspond to bare soil that is completely devoid of moisture whereas the dark pixels should correspond to pure water pixels. The bounding lines approximate the theoretical evaporation and radiation controlled cooling lines shown in Figure 6.4. Albedo, r0, was estimated using Brest and Goward (1987) model using the Red (R) and Near Infrared bands (NIR).

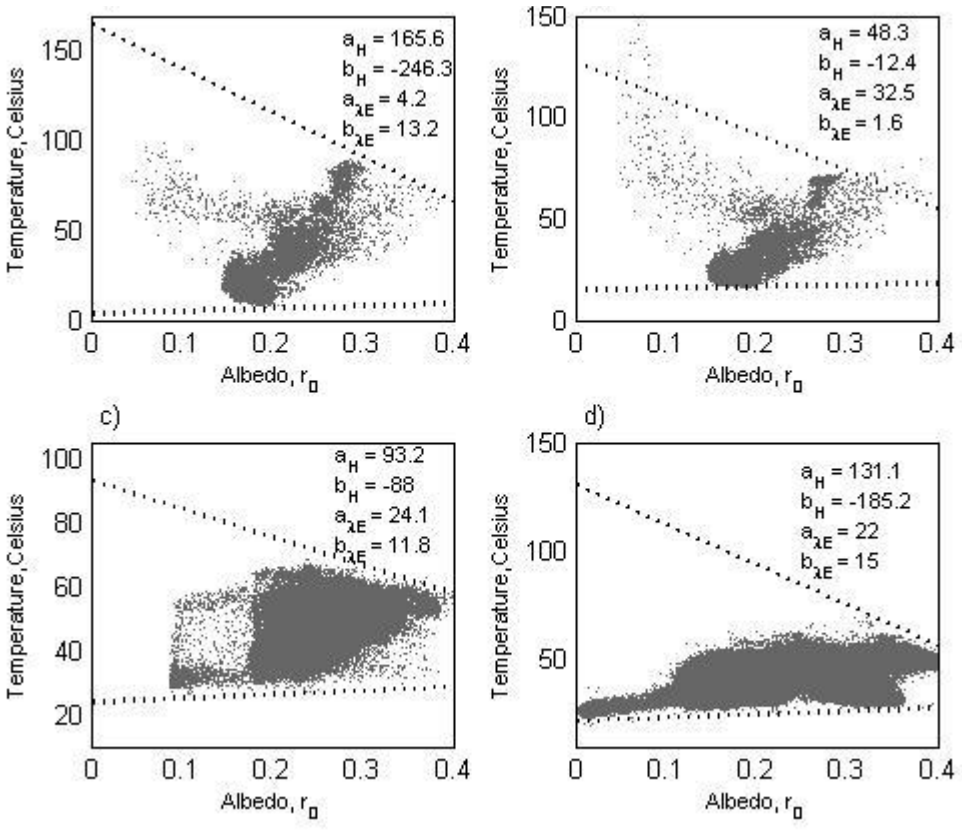

Figure 6.5: Albedo v/s land surface temperature for a) Landsat sensor, 2009, b) Landsat sensor, 2010, c) MASTER sensor, 2009, and d) MASTER sensor, 2010

$$r_0 = 0.512R + 0.418NIR \tag{6.17}$$

NIR = Band 4 (Landsat) or Band 9 (MASTER)

R = Band 3 (Landsat) or Band 5 (MASTER)

The latent heat, (LE) was then estimated as

$$LE = \Lambda(r_n - G) \tag{6.18}$$

The latent heat flux was converted to ET estimates (mm/hr) using eq. 6.19.

$$ET_{S-SEBI} = LE\frac{3600}{L} \tag{6.19}$$

$$L = 2.5e^6 - 2.386e^3(T - 273.15) \tag{6.20}$$

6.4.3.2 Correction Factor for S-SEBI Based ET

Penman-Monteith based ET estimates provide an accurate estimate of the potential water loss from a crop with complete ground cover (unless a variation of percent ground cover is accounted for in the computation of Kc). On the other hand, ET obtained from S-SEBI is based on the relationship between land surface temperature and albedo data derived at pixel resolution of the remote sensor and as such gives an estimate of the water loss per pixel (which may be fully or partially vegetated). This relationship, however, holds good only for homogeneous pixels whose albedo changes proportionally to the temperature (also water content) of the entire pixel. In the given study, the bare soil around the canopy and within the rows was parched dry and as a result each pixel was comprised of the well watered trees and soil at vastly different temperatures. The resultant

albedo/temperature of the mixed (partially vegetated) pixel would not change in proportion with the water content of the pixel. A well-watered plant in such conditions may appear to be water stressed because of the high temperature of the mixed pixel due to the presence of bare soil in it. Thus, as a result of averaging over the mixed pixel, the ET values in the pixel will be underestimated. In order to correct for the averaging effect, the ET values estimated using S-SEBI were adjusted based on the percent vegetation cover (eq. 6.21).

$$ET = \frac{ET_{S-SEBI}}{\frac{NDVI}{NDVI_{max}}} \tag{6.21}$$

$\frac{NDVI}{NDVI_{max}}$ = percent vegetation cover

NDVI = NDVI of the pixel under consideration

$NDVI_{max}$ = NDVI of a completely vegetated pixel or maximum NDVI of the region (with similar leaf area index as the crop under consideration)

ET_{S-SEBI} = modeled ET estimates (mm/hr)

Such a correction was based on the assumption that the ET increases in proportion to the NDVI of the pixel and was intended to increase the estimated ET value to match a fully vegetated pixel. Such a correction will enable the user to compare and validate the estimated ET with the more accurate Penman-Monteith based ET values while retaining the spatial variability in ET estimates as available from remote sensing.

6.5 Results and Discussion

6.5.1 Effect of Correction Factor on ET Estimates

Figures 6.6 (a) and 6.6 (b) show the ET derived using S-SEBI from the Landsat and MASTER sensor in 2010. On average, ET losses from the almond fields were higher as compared to the pistachio fields. However, since S-SEBI is an empirical technique and based on a relationship between land surface temperature and albedo, the derived ET

values were underestimated as a result of the bare soil in the pixel. By scaling the ET as given in eq. 21, corrected ET from the plants was calculated (Figures 6.6 (c) and 6.6 (d)) which was higher than the averaged ET across the pixel. The increase in ET values was larger for the pistachio orchards as compared to almond orchards (Figure 6.6) since pistachios had a smaller canopy and consequently consisted of more bare soil compared to almond pixels.

The field averages and standard deviation for ET (Figures 6.7 (a) and 6.7 (b)) and corrected ET (Figures 6.7 (c) and 6.7 (d)) are plotted against Penman-Monteith based ETc (Kc x ETref) estimates (Table 6.2). The calculation of ETref that represents the ET from a reference crop (either clipped, well watered grass or a taller full-cover alfalfa crop) has been standardized by Food and Agriculture Organization (FAO), (Allen et al. 1998, 2006) and the American Society of Civil Engineers (ASCE-EWRI 2005). Kc is the crop specific coefficient representing ratio of the crop's potential ET (ETc) and ETref. This formulation does not account for agricultural practices like planting in rows that result in partial ground cover. The orchards in our study area were not under water stress and the trees were expected to be transpiring nearly at the potential (Penman-Monteith) rate; however, S-SEBI generated ET (uncorrected) estimates were lower than the Penman-Monteith based estimates (Figures 6.7 (a) and 6.7 (b)). ET from pistachio orchards which comprise of trees with smaller canopies was underestimated more than that from the almond trees with larger canopies. After applying the correction for percent crop cover, the ET estimates became comparable with the Penman-Monteith based estimates (Figures 6.7 (c) and 6.7 (d)). The observed root mean square error (RMSE) for pistachios changed from 0.65 mm/hr to 0.08 mm/hr and 0.76 mm/hr to 0.62 mm/hr for Landsat and MASTER, respectively. The difference in RMSE for almonds was lower. It can be inferred that accounting for percent vegetation cover improves estimates of remote sensing derived ET in orchard conditions. This finding is very encouraging for remote sensing based ET estimation over agricultural

orchards in California that solely depend on irrigation, since spatial estimates of ET can be obtained with the use of simple models like S-SEBI and routinely available Landsat data. This can also be used to design targeted irrigation schemes.

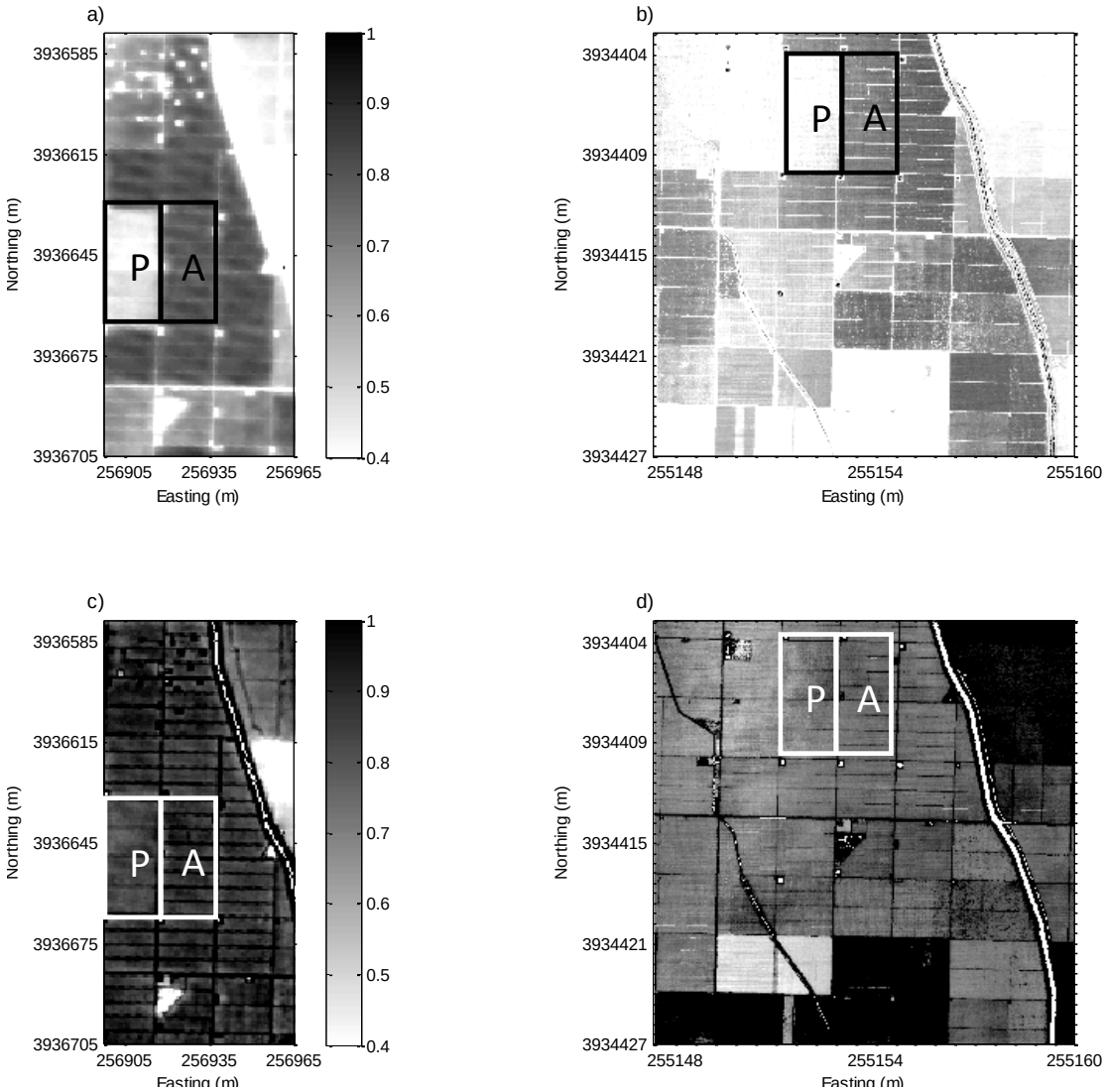

Figure 6.6: ET (S-SEBI estimated) distribuition in 2010 as estimated from a) Landsat and b)MASTER sensor and Corrected ET distribution in 2010 c) Landsat and d)MASTER sensor. (P-pistachio and A-almonds)

Table 6.2: CIMIS (Belridge station) based ET estimates

Date	Crop	ET0 (mm/hr)**	Crop Coefficient, Kc*	ET Kc x ET0 (mm/hr)
July 24th, 2009	Almonds	0.762	1.08	0.823
July 28th, 2009	Almonds	0.762	1.08	0.823
June 29th, 2010	Almonds	0.762	1.06	0.808
July 24th, 2009	Pistachio	0.762	1.19	0.907
July 28th, 2009	Pistachio	0.762	1.19	0.907
June 29th, 2010	Pistachio	0.762	1.19	0.907

* Crop coefficients were chosen based on time of year and have been provided by CIMIS for mature almond crops
** Provided by CIMIS

6.5.2 Effect of Varying Scale on ET Estimates

In order to compare the Landsat and MASTER based ET, the violin plots of corrected ET as obtained from both sensors in 2009 (Figure 6.8 (a)) and 2010 (Figure 6.8 (b)) were plotted. The ET from crops was typically normally distributed except for Landsat based ET in almond orchards which was right skewed. This implies that the apparent ET distribution changes across the two scales under certain crop cover conditions and a general conclusion for all heterogeneous orchard environments cannot be drawn. ET estimates as obtained from MASTER were lower than those obtained from Landsat. The higher contrast between the two in 2009 could be because of differences in irrigation amounts on the two days when imagery was collected. Table 6.3 provides the mean and variance for the distribution of the MASTER-based S-SEBI calculated ET values. The MASTER sensor provided lower mean ET estimates than Landsat during both the years. In 2010, when the imagery from MASTER and Landsat was collected almost simultaneously, the differences between the two ET estimates were smaller. The variance values for the pistachio fields were almost the same at both resolutions implying that the variance captured at 5.8/7.2 m and 120 m

resolution was nearly similar in the orchards. . The variance value for the almond fields was slightly higher in Landsat because of the dry patch in the almond field (Figure 6.2), which was averaged into the Landsat pixels.

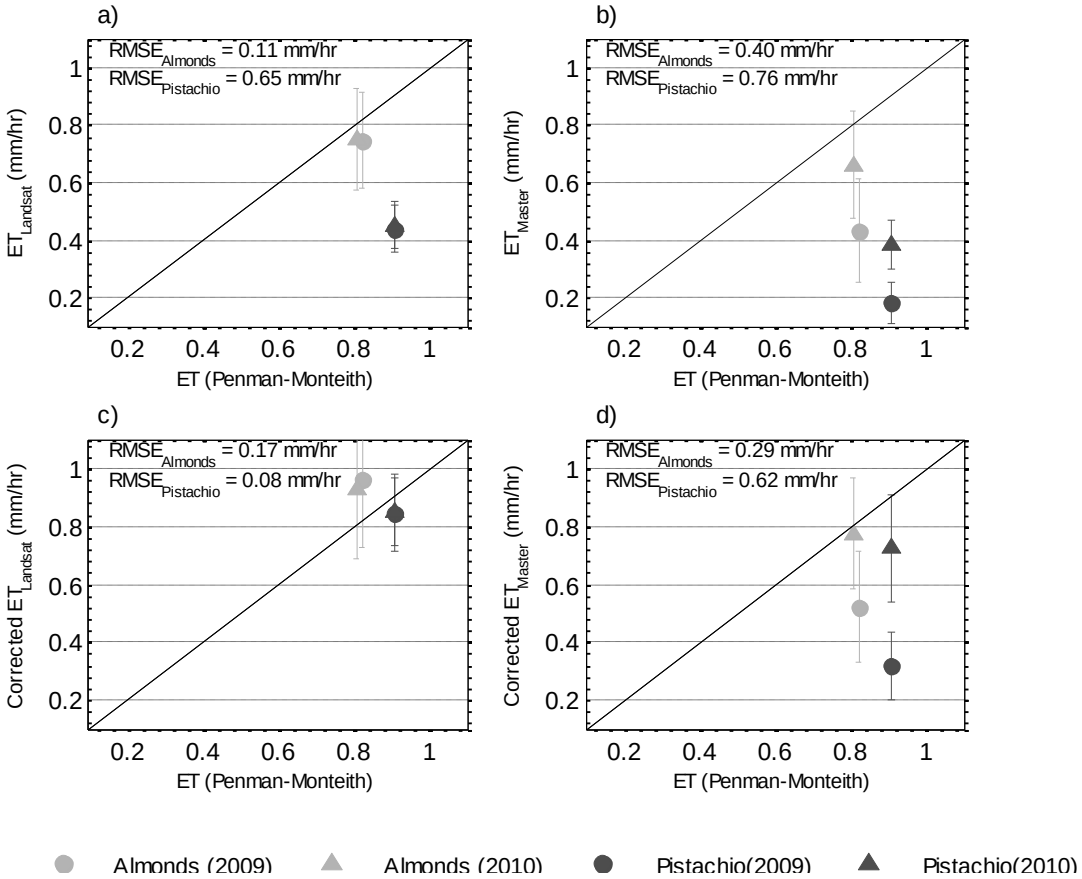

Figure 6.7: Average ET values in 2009 and 2010 before correcting for partial vegetation cover for a) Landsat and b) MASTER and after correcting for partial vegetation cover for c) Landsat and d) MASTER

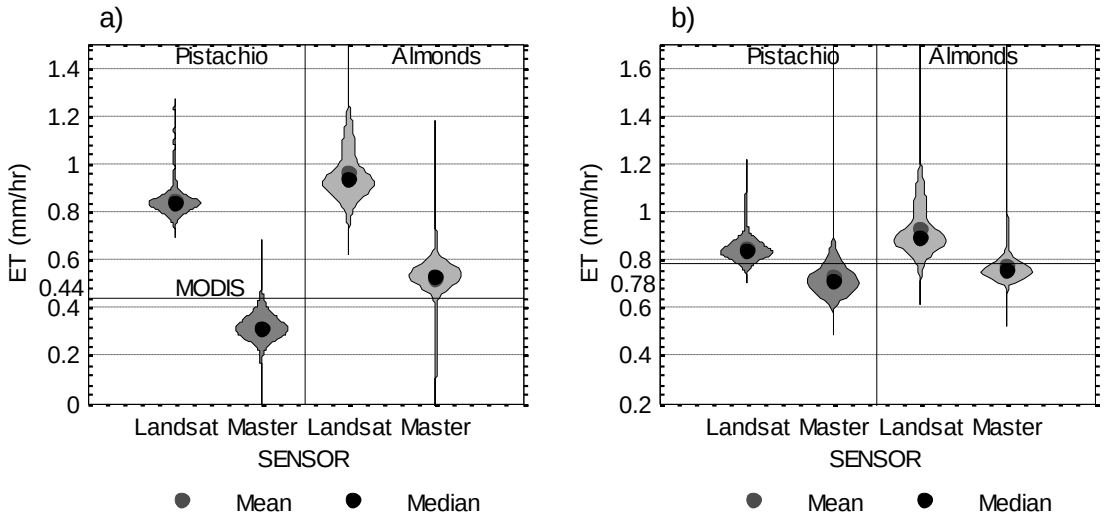

Figure 6.8: Violin plots representing distrbution of ET in the year a) 2009 and b) 2010. Red line depicts MODIS based average ET.

The underestimation of mean ET by MASTER can be attributed to the pixel resolution of the sensors (Landsat, 120 m thermal; MASTER, 5.8 m). The Landsat pixel was large enough to comprise of multiple trees and the ET that was generated from it was an average of the trees and bare soil (Figure 6.1 (a)). On the other hand, the small pixel resolution of the MASTER sensor at most allowed one tree per pixel (Figure 6.1 (b)). Most pixels for the MASTER sensor consisted of either a portion of a tree and bare soil or in some cases bare soil itself. This led to higher pixel temperatures in the MASTER sensor and consequently S-SEBI generated lower ET estimates observed from the MASTER sensor. This also indicates that remote sensing derived ET at a finer scale may not match remote sensing derived ET at coarser scale and an adequate scaling scheme will need to be applied. The results indicate that akin to the typical loss of information on upscaling there may be loss of information in selecting resolutions that are comparable to canopy sizes under row

Table 6.3: Mean (Variance) of corrected ET estimates obtained for almonds and pistachio from Landsat and MASTER

Year: 2009		
Crop	Landsat	MASTER
Almonds	0.96 (0.013)	0.52 (0.009)
Pistachio	0.84 (0.004)	0.32 (0.003)
Year: 2010		
Crop	Landsat	MASTER
Almonds	0.93 (0.014)	0.77 (0.009)
Pistachio	0.85 (0.003)	0.72 (0.009)

orchard conditions. A comparison of variance within the sensors across the years shows that the variance values are almost similar. This indicates that the sensor behavior was consistent for both the years. The MODIS based ET values were typically lower than Landsat and higher than MASTER sensor derived ET. The MODIS pixel has a resolution of 1 km and, under the given agricultural settings, comprises various crops that differ in terms of growth stage, irrigation patterns and types. Thus, at the scale of a MODIS pixel, the representativeness of an agricultural field is lost.

The above analysis indicates that specifically for partially vegetated or orchard conditions, the spatial resolution of remote sensing can lead to under/over estimation ET. It is also not necessary that finer resolution of remote sensing will enable better estimation of ET.

6.6 Conclusions

In the given study, we evaluated the effect of varying spatial resolutions on ET estimates for two different crop orchards in California. ET was estimated over almond and pistachio orchards using S-SEBI algorithm. The data used was obtained from the MASTER sensor at a resolution of 5.8 m and 7.2 m and from the Landsat sensor at 120 m resolution across two years. We found that Landsat provided more accurate estimates of

ET than MASTER, which tended to underestimate the ET from the plants. An NDVI based rescaling technique was also applied to correct for the mixed pixel effects in the orchard conditions which improved ET estimates with respect to the crop coefficient method. A comparison of the derived ET estimates with MODIS based ET estimates revealed that MODIS based ET estimates do not compare well with the ET estimates from individual crop types because of its coarse pixel size. The results of the study are very encouraging toward the incorporation of remote sensing data in estimating evapotranspiration in the region for use toward precision agriculture. The freely available Landsat data can be used in conjunction with a simple ET model with minimal data requirements to provide ET and related crop health maps to farmers regularly.

7. CONCLUSIONS

The key to accurate and reliable hydrologic modeling is to incorporate soil moisture data that honors the spatial and temporal scale of the processes simulated in the models. An understanding of the spatio-temporal distribution of soil moisture across different support, spacing and extent scales spanning beyond the observed is central for the success of this effort. This study describes a data based framework for understanding and predicting the variability in soil moisture dynamics during the growing season across spatial scales that are atypical for soil moisture data collection but useful in modeling scenarios.

The dominant land-surface factors controlling near-surface soil moisture spatial distribution were found to evolve with hydro-climates, antecedent moisture conditions and scale specific land-surface heterogeneity. In chapter II, a technique based on Shannon entropy was developed to evaluate the dominant physical controls of soil moisture at Darcy and airborne footprint (0.8 km) scale in a humid (Iowa) and sub-humid (Oklahoma) hydro-climate. The data available for this analysis comprised soil moisture data from the growing season for a normal and wet year for the humid hydro-climate and dry and wet year for the sub-humid hydro-climate. It was found that soil texture was the dominant physical factor controlling soil moisture distribution at the Darcy support scale for all conditions except for the wet year in the sub-humid hydro-climate where topography was found to be dominant. At the airborne footprint scale, soil texture showed an effective partitioning of soil moisture variability for both the hydro-climates. In chapter III, this analysis was extended using non-decimated wavelet transform to evaluate the land-surface controls of soil moisture redistribution across support scales varying from 1.6-25.6 km for three hydro-climates- humid (Iowa), sub-humid (Oklahoma) and semi-arid (Arizona). It was found that the dominance of soil on soil moisture dynamics typically decreased as we

went from 1.6 km to 25.6 km support scales whereas the influence of topography and vegetation increased with increasing support scale for all three hydro-climates. The distinct effect of hydro-climate was identifiable in the soil attributes dominating the soil moisture dynamics where clay content (effective limiting parameter for evaporation) and sand content (effective limiting parameter for drainage) showed more dominance in the semi-arid (Arizona) and sub- humid (Oklahoma) hydro-climate respectively. A hierarchy of dominance of different land-surface factors on soil moisture redistribution at remote sensing footprint scales during the growing season in the three hydro-climates was also developed.

In chapter IV, the dominant physical attributes found in the previous chapters were incorporated to generate relationships between soil moisture redistribution and dominant physical factors for the growing season in the same three hydro-climates. The scale based dependence of these relationships on land-surface heterogeneity and antecedent wetness was exploited to develop a Scale-Wetness-Heterogeneity (SWHET) cuboid to enable spatial transferability of these relationships. In Chapter V, the spatial transferability of the SWHET cuboid in a similar hydro-climate with different land-surface heterogeneity was assessed. The scheme based on the SWHET cuboid performed well for regions representing highly correlated land-surface heterogeneity and relatively dry soil moisture conditions, low correlated land-surface heterogeneity and relatively high soil moisture conditions but not for regions representing low correlated land-surface heterogeneity and relatively dry soil moisture conditions.

In chapter VI, the effect of varying spatial support scales on evapotranspiration estimates for two different crop orchards in a semi-arid region in California was evaluated. The data used for estimating evapotranspiration was obtained from the MASTER sensor at a resolution of 5.8 m and 7.2 m and from the Landsat sensor at 120 m resolution across two years. It was found that Landsat provided more accurate estimates of evapotranspiration than MASTER, which tended to underestimate the ET from the trees.

The results from this research pave the way to evaluate various impactful concepts in soil moisture literature like time stability (Grayson and Western, 1998, Mohanty and Skaggs, 2001, Martinez-Fernandez and Ceballos, 2003, Cosh et al., 2004, Jacobs et al., 2004, Joshi and Mohanty, 2011 etc.) at different extent and support scales which enables scientists to determine watershed averages using a single monitoring site or pixel. The existence of time stable pixels is conditioned upon some appropriate combination of land-surface based heterogeneity as outlined in the previous studies. The understanding of the dominance or hierarchy of dominance of physical factors provided through this study can assist in predicting the location of time stable pixels for different extent scales (field, watershed, region etc.) in some of the unmapped areas of the world and thus, enable the scientists to accurately select installation sites for long term soil moisture monitoring using sensors that measure soil moisture at different support scales (hand-held sensors, COSMOS etc.). The key is to select monitoring sites that represent the dominant physical factor for a given extent scale and at a particular support. For example, at the extent of the field or a watershed (based on results from chapter II) and using point support scale sensors, a soil texture based installation scheme must be incorporated to capture soil moisture dynamics in most cases. On the other hand, if the intent is to capture soil moisture dynamics at the regional extent scale (based on results from chapter III) using sensors that give coarser support scale soil moisture estimates, an installation scheme that honors the dominant physical factor for a given hydro-climate and support scale must be selected. Ideally located soil moisture monitoring stations can aid in upscaling soil moisture and consequently enhance the predictive capabilities of hydrological models operating at scales that span beyond the Darcy scale.

Soil moisture variability varies with spatial and temporal scale. While the focus of this research spans a range of spatial support and extent scales, the finding from this research are limited in their temporal extent. Since the relationships and findings of this research

are data driven, it is imperative that the findings are not generalized while implementing in other studies. Further research also needs to be done in evaluating the downscaling scheme with regards to propagation of error in time and its applicability over a larger domain. However, this research lays the foundation for developing a promising method of analyzing and incorporating spatial soil moisture data at varying support, spacing and extent scales into hydrologic modeling at coarse remote sensing footprints where the science pertaining to hydrology is yet limited.

REFERENCES

Ackerman, E. A. (1941), The Koppen classification of climates in North America, Geographical Review 31, no. 1 (1941): 105-111.

Albertson, J. D. and N. Montaldo (2003), Temporal dynamics of soil moisture variability: 1. Theoretical basis, Water Resources Research 39(10): 1274. doi: 10.1029/2002WR0--01616

Allen R.G., L.S. Pereira, D. Raes and M. Smith (1998), Crop evapotranspiration-Guidelines for computing crop water requirements-FAO Irrigation and drainage paper 56. FAO, Rome 300: 6541.

Allen, R. G., and L. S. Pereira (2009), Estimating crop coefficients from fraction of ground cover and height. Irrigation Science, 28(1), 17-34. doi:10.1007/s00271-009-0182-z

Anderson, M.G., and T.P. Burt (1978), Role of topography in controlling throughfall generation, Earth Surface Processes Landforms,3,331-344

Asner, G. P. (1998) ,Biophysical and biochemical sources of variability in canopy reflectance. Remote Sensing of Environment 64(3): 234-253. doi: 10.1016/S0034-4257(98)00014-5

Aubert, D., C. Loumagne, and L. Oudin (2003), Sequential assimilation of soil moisture and streamflow data in a conceptual rainfall-runoff model, Journal of Hydrology., 280(14), 145-161, doi:10.1016/S0022-1694(03)00229-4

Baldocchi, D. D., B. B. Hincks and T.P.Meyers (1988), Measuring biosphere-atmosphere exchanges of biologically related gases with micrometeorological methods. Ecology 69(5): 1331-1340.

Bastiaanssen, W., M. Menenti, R. A. Feddes and A.A.M Holtslag (1998), A remote sensing surface energy balance algorithm for land (SEBAL). 1. Formulation. Journal of

Hydrology 212: 198-212. doi:10.1016/S0022-1694(98)00253-4

Bindlish, R., T. J. Jackson, A. Gasiewski, B. Stankov, M. Klein, M. H. Cosh, I. Mladenova, C. Watts, E. Vivoni, V. Lakshmi, J. Bolten and T. Keefer (2008), Aircraft based soil moisture retrievals under mixed vegetation and topographic conditions, Remote sensing of environment 112, no. 2: 375-390. doi:10.1016/j.rse.2007.01.024

Bindlish, R., T. J. Jackson, A.J. Gasiewski, M. Klein and E.G. Njoku (2006), Soil moisture mapping and AMSR-E validation using the PSR in SMEX02, Remote Sens. of Environ. 103(2): 127-139. doi:10.1016/j.rse.2005.02.003

Bircher, S., N. Skou, K. H. Jensen, J. P. Walker,and L. Rasmussen (2012), A soil moisture and temperature network for SMOS validation in Western Denmark, Hydrology and Earth System Science, 16, 1445-1463, doi:10.5194/hess-16-1445-2012.

Bloschl, G. and M. Sivapalan (1995), Scale issues in hydrological modelling: a review, Hydrological processes 9(3-4): 251-290.

Bolten, J. D., V. Lakshmi, and E. G. Njoku (2003), Soil moisture retrieval using the passive/active L-and S-band radar/radiometer., IEEE Transactions on Geoscience and Remote Sensing, 41(12), 2792-2801. doi:10.1109/TGRS.2003.815401

Brest, C. and S. Goward (1987), Deriving surface albedo measurements from narrow band satellite data. International Journal of Remote Sensing 8(3): 351-367. doi: 10.1080/01431168708948646

Brutsaert, W. and D. Chen (1996), Diurnal variation of surface fluxes during thorough drying (or severe drought) of natural prairie. Water Resources Research 32(7): 2013-2019. doi: 10.1029/96WR00995

Burt, T. P., and D. P. Butcher (1985), Topographic controls of soil moisture distributions. Journal of Soil Science 36, no. 3: 469-486.

Carlson T., R. Gillies, and E. Perry (1994), A method to make use of thermal infrared temperature and NDVI measurements to infer surface soil water content and fractional

vegetation cover, Remote Sensing Review, vol. 9, no. 1/2, pp. 161-173, Mar. 1994.

Carlson T., W. Capehart, and R. Gillies (1995), A new look at the simplified method for remote sensing of daily evapotranspiration, Remote Sensing of Environment, vol. 54, no. 2, pp. 161-167.

Carr D. B., R. Kahn, K. Sahr, and T. Olsen (1997), ISEA discrete global grids, Statist. Comput. Statistical Computing & and Graphics Newsletter, vol. 8, no. 2/3, pp. 31-39

Caselles, V. and J. E. A. Sobrino (1989), Determination of frosts in orange groves from NOAA-9 AVHRR data. Remote Sensing of Environment 29(2): 135-146. doi: 10.1016/0034-4257(89)90022-9

Chang, N. B., and Y. Hong (2012), Multiscale hydrologic remote sensing: perspectives and applications. CRC Press Inc.

Chauhan N., S. Miller, and P. Ardanuy (2003), Spaceborne soil moisture estimation at high resolution: A microwave-optical/IR synergistic approach, International Journal of Remote Sensing, vol. 24, no. 22, pp. 4599-4622. doi:10.1080/ 0143116031000156837

Chehbouni, A, R. Escadafal, B. Duchemin, G. Boulet, V. Simonneaux, G. Dedieu, B. Mougenot, S. Khabba, H. Kharrou, P. Maisongrande, O. Merlin, A. Chaponniere, J. Ezzahar, S. Er-Raki, J. Hoedjes, R. Hadria, A. Abourida, A. Cheggour, F. Raibi, A. Boudhar, I. Benhadj, L. Hanich, A. Benkaddour, N. Guemouria, A. H. Chehbouni, A. Lahrouni, A. Olioso, F. Jacob, D. G. Williams and J. A. Sobrino (2008), An integrated modelling and remote sensing approach for hydrological study in arid and semi-arid regions: the SUDMED Programme, International Journal of Remote Sensing 29, no. 17-18 2008: 5161-5181. doi: 10.1080/01431160802036417

Cheng, T., D. Riano, A. Koltunov, M. L. Whiting, S. L. Ustin, and J. Rodriguez (2013), Detection of diurnal variation in orchard canopy water content using MODIS/ASTER airborne simulator (MASTER) data, Remote Sensing of Environment, 132, 1-12. doi:10.1016/--j.rse.2012.12.024

Chirouze, J., G. Boulet, L. Jarlan, R. Fieuzal, J. C. Rodriguez, J. Ezzahar, S. Er-Raki, G. Bigeard, O. Merlin, J. Garatuza-Payan, C. Watts, and G. Chehbouni (2014), Intercomparison of four remote-sensing-based energy balance methods to retrieve surface evapotranspiration and water stress of irrigated fields in semi-arid climate, Hydrology and Earth System Science, 18, 1165-1188, doi:10.5194/hess-18-1165-2014.

Coleman, M. L., and J. D. Niemann (2013), Controls on topographic dependence and temporal instability in catchment-scale soil moisture patterns, Water Resour. Res., 49, 1625-1642, doi:10.1002/wrcr.20159.

Cosh, M. H. and W. Brutsaert (1999), Aspects of soil moisture variability in the Washita'92 study region, Journal of Geophysical Research 104(D16), 19751-19719,19757.

Cosh, M. H., T. J. Jackson, R. Bindlish, and J. H. Prueger (2004), Watershed scale temporal and spatial stability of soil moisture and its role in validating satellite estimates, Remote Sens. Environ., 92(4), 427-435.

Crago, R. (1996), Conservation and variability of the evaporative fraction during the daytime. Journal of Hydrology 180(1-4): 173-194. doi:10.1016/0022-1694(95) 02903-6

Crow, W. T., E. F.Wood, and R.Dubayah (2000), Potential for downscaling soil moisture maps derived from space borne imaging radar data, Journal of Geophysical Research, 105, 2203-2212. doi: 10.1029/1999JD901010

Das, N. N., and B.P. Mohanty (2008), Temporal dynamics of PSR-based soil moisture across spatial scales in an agricultural landscape during SMEX02: A wavelet approach, Remote Sensing of Environment, 112(2), 522-534, doi:10.1016/j.rse.2007.05.007

Daughtry, C.S.T, W. P. Kustas, M.S. Moran, P.J. Pinter Jr., R.D. Jackson, P.W. Brown, W.D. Nichols and L.W. Gay (1990), Spectral estimates of net radiation and soil heat flux. Remote Sensing of Environment 32(2-3): 111-124. doi: 10.1016/0034-4257(90)90012-B

Entin, J. K., A. Robock, K. Y. Vinnikov, S. E. Hollinger, S. X. Liu, and A. Namkhai (2000), Temporal and spatial scales of observed soil moisture variations in the extratropics,

Journal of Geophysical Research, 105(D9), 11865-11877.

Famiglietti, J. S., D. Ryu, A. A. Berg, M. Rodell, and T. J. Jackson (2008), Field observations of soil moisture variability across scales, Water Resoures Research, 44, W01423. doi:10.1029/2006WR005804.

Famiglietti, J., J. Devereaux, C.A. Laymon, T. Tsegaye, P.R. Houser, T.J. Jackson, S.T. Graham, M. Rodell, P.J. van Oevelen (1999), Ground-based investigation of soil moisture variability within remote sensing footprints during the Southern Great Plains 1997(SGP 97) Hydrology Experiment, Water Resources Research 35(6): 1839-1851.

Famiglietti, J.S., J.W. Rudnicki, and M. Rodell (1998), Variability in surface moisture content along a hillslope transect: Rattlesnake Hill, Texas, Journal of Hydrology, 210, 259-281.

Faunt, C.C., ed., 2009, Groundwater Availability of the Central Valley Aquifer, California: U.S. Geological Survey Professional Paper 1766, 225 p.

Feddes, R. A., P.I. Kowalik, H. Zarachy (1978), Simulation of field water use and crop yield, Centre for Agricultural Publishing and Documentation.

Gaur, N., and B.P. Mohanty (2013), Evolution of physical controls for soil moisture in humid and subhumid watersheds, Water Resour. Res., 1244-1258, doi: 10.1002/wrcr.20069.

Gaur, N., and B.P. Mohanty (2015) Land-Surface Controls on Near-Surface Soil Moisture Dynamics: Traversing Remote Sensing Footprints, submitted to Water Resoures Research,2015WR018095

Geli, H.M.E. (2012), Modeling spatial surface energy fluxes of agricultural and riparian vegetation using remote sensing. Ph.D. thesis, Utah State University, 68 pp

Gesch, D., G. Evans, J. Mauck, J. Hutchinson, W.J. Carswell Jr. (2009), The National Map-Elevation: U.S. Geological Survey Fact Sheet 2009-3053, 4 p.

Gillies R., T. Carlson, J. Cui, W. Kustas, and K. Humes (1997), A verification of the 'triangle' method for obtaining surface soil water content and energy fluxes from remote

measurements of the normalized difference vegetation index (ndvi) and surface radiant temperature, Int. J. Remote Sens., vol. 18, no. 15, pp. 3145-3166, Oct. 1997.

Goulden, M. L., R. G. Anderson, R. C. Bales, A. E. Kelly, M. Meadows, and G. C. Winston (2012), Evapotranspiration along an elevation gradient in California's Sierra Nevada, Journal of Geophysical Research, 117, G03028. doi:10.1029/2012JG002027

Grayson, R. B., and A. W. Western (1998), Towards areal estimation of soil water content from point measurements: Time and space stability of mean response, Journal of Hydrology, 207, 68-82.

Hatfield, J., D. Jaynes, M. Burkart, C. Cambardella, T. Moorman, J. Prueger (1999), Water Quality in Walnut Creek Watershed: Setting and Farming Practices, Journal of Environmental Quality 28(1): 11.

Henderson-Sellers, B. (1984), A new formula for latent heat of vaporization of water as a function of temperature. Quarterly Journal of the Royal Meteorological Society 110(466): 1186-1190. doi: 10.1002/qj.49711046626

Hupet, F. and M. Vanclooster (2002), Intraseasonal dynamics of soil moisture variability within a small agricultural maize cropped field, Journal of Hydrology, 261, 86-101. doi:10.1016/S0022-1694(02)00016-1

Irish, R. R., Landsat 7 science data users handbook. National Aeronautics and Space Administration, Report (2000): 430-15.

Ivanov, V. Y., S. Fatichi, G. D. Jenerette, J. F. Espeleta, P. A. Troch, and T. E. Huxman (2010), Hysteresis of soil moisture spatial heterogeneity and the 'homogenizing' effect of vegetation, Water Resources Research, 46, W09521, doi:10.1029/2009WR008611

Jackson, T. J., D. M. Le Vine, A. Y. Hsu, A. Oldak, P. J. Starks, C. T. Swift, J. D. Isham, and M. Haken (1999), Soil moisture mapping at regional scales using microwave radiometry: The Southern Great Plains Hydrology Experiment, IEEE Transactions on Geoscience and Remote Sensing, 37, no. 5 (1999): 2136-2151.

Jacobs, J. M., B. P. Mohanty, En-Ching Hsu, Douglas Miller (2004), SMEX02: Field scale variability, time stability and similarity of soil moisture, Remote Sensing of Environment 92(4): 436-446. doi:10.1016/j.rse.2004.02.017

Jana, R. B., B. P. Mohanty, and E. P. Springer (2008), Multiscale Bayesian neural networks for soil water content estimation, Water Resources Research, 44, W08408, oi:10.1029/2008WR006879.

Jawson, S. D., and J. D. Niemann (2007), Spatial patterns from EOF analysis of soil moisture at a large scale and their dependence on soil, land-use, and topographic properties, Advances in Water Resources, 30(3), 366-381., doi:10.1016/ j.advwatres.2006.05.006

Joshi, C., and B. P. Mohanty (2010), Physical controls of near-surface soil moisture across varying spatial scales in an agricultural landscape during SMEX02, Water Resources Research, 46, W12503, doi:10.1029/2010WR009152.

Joshi, C., B. P. Mohanty, J. M. Jacobs, and A. V. M. Ines (2011), Spatiotemporal analyses of soil moisture from point to footprint scale in two different hydroclimatic regions, Water Resources Research, 47, W01508, doi:10.1029/2009WR009002.

Kim J. and T. S. Hogue (2012), Improving Spatial Soil Moisture Representation Through Integration of AMSR-E and MODIS Products, in IEEE Transactions on Geoscience and Remote Sensing, vol.50, no.2, pp.446-460, Feb. 2012, doi: 10.1109/TGRS.2011.2161318

Kim, G. and A. P. Barros (2002), Space-time characterization of soil moisture from passive microwave remotely sensed imagery and ancillary data, Remote Sensing of Environment 81(2-3): 393-403. doi:10.1016/S0034-4257(02)00014-7

Kim, G. and Barros, A. P. (2002). Downscaling of remotely sensed soil moisture with a modified fractal interpolation method using contraction mapping and ancillary data. Remote Sensing of Environment, 83(3), 400-413, doi:10.1016/S0034-4257(02)00044-5

Kumar, P., and E. Foufoula-Georgiou (1993), A multicomponent decomposition of spatial rainfall fields: 1. Segregation of large- and small-scale features using wavelet

transforms, Water Resources Research., 29(8), 2515-2532, doi:10.1029/93WR00548.

Kumar, P., and E. Foufoula-Georgiou (1997), Wavelet analysis for geophysical applications, Reviews of Geophysics 35, no. 4 (1997): 385-412.

Kustas, W., E. Perry, P.C. Doraiswamy and M.S. Moran. (1994), Using satellite remote sensing to extrapolate ET estimates in time and space over a semiarid rangeland basin. Remote Sensing of Environment 49(3): 275-286. doi: 10.1016/0034-4257(94)90022-1

Kustas, W., F. Li, T.J. Jackson, J.H. Prueger, J.I. MacPherson and M. Wolde. (2004), Effects of remote sensing pixel resolution on modeled energy flux variability of croplands in Iowa. Remote Sensing of Environment 92(4): 535-547. doi: 10.1016/j.rse.2004.02.020

L. Jiang and S. Islam (2003), An intercomparison of regional latent heat flux estimation using remote sensing data, International Journal of Remote Sensing, vol. 24, no. 11, pp. 2221-2236.doi:10.1080/01431160210154821

Liew, M. W. and J. Garbrecht (2003), Hydrologic simulation of the little washita river experimental watershed using SWAT1, Journal of the American Water Resources Association 39(2): 413-426.doi: 10.1111/j.1752-1688.2003.tb04395.x

Martinez-Fernandez, J., and A. Ceballos (2003), Temporal stability of soil moisture in a large-field experiment in Spain, Soil Science Society of America Journal, 67, 1647-1656.

Mauser, W. and S. Schadlich (1998), Modelling the spatial distribution of ET on different scales using remote sensing data. Journal of Hydrology 212: 250-267. doi: 10.1016/S0022-1694(98)00228-5

McCabe, M. F. and E. F. Wood (2006), Scale influences on the remote estimation of ET using multiple satellite sensors. Remote Sensing of Environment 105(4): 271-285. doi: 10.1016/j.rse.2006.07.006

McNairn, H., T. J. Jackson, G. Wiseman, S. Belair, A. Berg, P. Bullock, A. Colliander, M. H. Cosh, K. Seung-Bum, R. Magagi, M. Moghaddam, E. G. Njoku, J. R. Adams, S. Homayouni, E. Ojo, T. Rowlandson, J. Shang, K. Goita and M. Hosseini (2015), The Soil

Moisture Active Passive Validation Experiment 2012 (SMAPVEX12): Prelaunch Calibration and Validation of the SMAP Soil Moisture Algorithms, in IEEE Transactions on Geoscience and Remote Sensing, vol.53, no.5, pp.2784-2801, doi: 10.1109/TGRS.2014.236491--3

Merlin O., M. J. Escorihuela, M. A. Mayoral, O. Hagolle, A. Al Bitar, et al. (2012), Self-calibrated evaporation-based disaggregation of SMOS soil moisture: An evaluation study at 3 km and 100 m resolution in Catalunya, Spain. Remote Sensing of Environment, Elsevier, 2012, pp.10.1016/j.rse.2012.11.008

Merlin, O., C.Rudiger, A.Al Bitar, J. P.Walker, and Y. H.Kerr (2012), Disaggregation of SMOS soil moisture in southeastern Australia, IEEE Transactions on Geoscience Remote Sensing., 50(5), 1556-1571. doi: 10.1109/TGRS.2011.2175000

Merlin, O., J.Walker, A.Chehbouni, and Y.Kerr (2008), Towards deterministic downscaling of SMOS soil moisture using MODIS derived soil evaporative efficiency, Remote Sensing of Environment, 112, 3935-3946, doi:10.1016/j.rse.2008.06.012.

Miller, D.A. and R.A. White (1998), A Conterminous United States Multi-Layer Soil Characteristics Data Set for Regional Climate and Hydrology Modeling, Earth Interactions, 2. (Available on-line at http://EarthInteractions.org)

Mishra, A. K., M. Ozger and V.P. Singh (2009), An entropy-based investigation into the variability of precipitation, Journal of Hydrology 370(1-4): 139-154.

Moellering, H. and W. Tobler (1972), Geographical variances. Geographical Analysis 4(1): 34-50.

Mogheir, Y., J. De Lima, V.P. Singh (2004), Characterizing the spatial variability of groundwater quality using the entropy theory: I. Synthetic data, Hydrological processes 18(11): 2165-2179.

Mohanty B.P. and J. Zhu, (2007): Effective Hydraulic Parameters in Horizontally and Vertically Heterogeneous Soils for Steady-State Land-Atmosphere Interaction, Journal of

Hydrometeorology, 8, 715-729, doi: http://dx.doi.org/10.1175/JHM606.1

Mohanty, B. P., and T. H. Skaggs (2001), Spatio-temporal evolution and time-stable characteristics of soil moisture within remote sensing footprints with varying soil, slope, and vegetation. Advances in Water Resources 24.9 (2001): 1051-1067, doi:10.1016/S0309-1708(01)00034-3

Mohanty, B. P., J. S. Famiglietti, and T. H. Skaggs (2000b), Evolution of soil moisture spatial structure in a mixed vegetation pixel during the Southern Great Plains 1997 (SGP97) Hydrology Experiment, Water Resources Research, 36(12), 3675-3686, doi:10.10--29/2000WR900258.

Mohanty, B. P., T. H. Skaggs, and J. S. Famiglietti (2000a), Analysis and mapping of field-scale soil moisture variability using high-resolution, ground-based data during the Southern Great Plains 1997 (SGP97) Hydrology Experiment, Water Resources Research, 36(4), 1023-1031, doi:10.1029/1999WR900360

Mohseni, O., Hanratty, M.P. and Stefan, H.G, Uncertainties in Projecting Streamflows in Two Watersheds Under 2xCO_2 Climate Conditions, Project Report No. 416, St. Anthony Falls Laboratory, University of Minnesota, March 1998, 24 pp.

Montzka, C., H. Moradkhani, L. Weihermuller, H.-J. H. Franssen, M. Canty, and H. Vereecken (2011), Hydraulic parameter estimation by remotely-sensed top soil moisture observations with the particle filter, J. Hydrol., 399(34), 410-421, doi:10.1016/j.jhydrol.20--11.01.020

Montzka, C., H. R. Bogena, L. Weihermuller, F. Jonard, C. Bouzinac, J. Kainulainen, J. E. Balling, A. Loew, J. T. dall'Amico, E. Rouhe, J. Vanderborght and H. Vereecken (2013), Brightness Temperature and Soil Moisture Validation at Different Scales During the SMOS Validation Campaign in the Rur and Erft Catchments, Germany, IEEE Transactions on Geoscience and Remote Sensing, vol.51, no.3, pp.1728,1743, March 2013 doi: 10.1109/TGRS.2012.2206031

Moran, S. M., K. S. Humes, and P. J. Pinter Jr. (1997), The scaling characteristics of remotely-sensed variables for sparsely-vegetated heterogeneous landscapes. Journal of Hydrology 190, no. 3: 337-362. doi: 10.1016/S0022-1694(96)03133-2

Nachshon, U., N. Weisbrod, M. I. Dragila, and A. Grader (2011), Combined evaporation and salt precipitation in homogeneous and heterogeneous porous media, Water Resources Research, 47, W03513, doi:10.1029/2010WR009677.

Narayan, U., V. Lakshmi, and E. G. Njoku (2004), Retrieval of soil moisture from passive and active L/S band sensor (PALS) observations during the Soil Moisture Experiment in 2002 (SMEX02). Remote Sensing of Environment, 92(4), 483-496. doi:10.1016/j.rse.2--004.05.018

NASA Land Processes Distributed Active Archive Center (LP DAAC) MODIS (LAI/FP--AR- 4 day composite) - USGS/Earth Resources Observation and Science (EROS) Center, Sioux Falls, South Dakota. 2001

Njoku, E. G., W. J. Wilson, H. Y. Simon, S. J. Dinardo, K. L. Fuk, T. J. Jackson, V. Lakshmi and J. Bolten (2002), Observations of soil moisture using a passive and active low frequency microwave airborne sensor during SGP99, IEEE Transactions on Geoscience and Remote Sensing, 40(12), 2659-2673.

NOAA Technical Report NWS 33 (1982), Evaporation Atlas for the Contiguous 48 United States.

Oldak A, T. J. Jackson and Y. Pachepsky (2002), Using GIS in passive microwave soil moisture mapping and geostatistical analysis, International Journal of Geographical Information Science, 16:7, 681-698, doi: 10.1080/13658810210149407

Pebesma, E.J. and C.G. Wesseling (1998), Gstat, a program for geostatistical modelling, prediction and simulation. Computers and Geosciences 24 (1), 17-31.

Pebesma, E.J. (2004), Multivariable geostatistics in S: the gstat package. Computers and Geosciences 30 (7), 683-691

Percival, D. B., and A. T. Walden, (2000), Wavelet Methods for Time Series Analysis (Cambridge Series in Statistical and Probabilistic Mathematics.

Percival, D. B., S. M. Lennox, Y.-G. Wang, and R. E. Darnell (2011), Wavelet-based multiresolution analysis of Wivenhoe Dam water temperatures, Water Resources Research, 47, W05552, doi:10.1029/2010WR009657

Phillips, J. D. (2001), Divergent evolution and the spatial structure of soil landscape variability, Catena 43(2): 101-113. doi:10.1016/S0341-8162(00)00122-3

Piles, M., A.Camps, M.Vall-llossera, I.Corbella, R.Panciera, C.Rudiger, Y. H.Kerr, and J.Walker (2011), Downscaling SMOS-derived soil moisture using MODIS visible/infrared data, IEEE Transactions on Geoscience and Remote Sensing, 49(9), 3156-3166. doi: 10.1109/TGRS.2011.2120615

Pohl, C. and J. Van Genderen (1998), Review article Multisensor image fusion in remote sensing: concepts, methods and applications. International Journal of Remote Sensing 19(5): 823-854. doi:10.1080/014311698215748

Portmann, R. W., S. Solomon, and G. c. Hegerl (2009), Spatial and seasonal patterns in climate change, temperatures, and precipitation across the United States. Proceedings of the National Academy of Sciences, 106(18), 7324-7329. doi: 10.1073/ pnas.0808533106

Preisendorfer, R. W. and C. D. Mobley (1988), Principal Component Analysis in Meteorology and Oceanography, New York: 1-455.

Price, J. C. (1990), Using spatial context in satellite data to infer regional scale evapotranspiratoin., IEEE Transactions on Geoscience and Remote Sensing 28(5): 940-948. doi: 10.1109/36.58983

Pruitt and Doorenbos (1977) Proceeding of the International Round Table Conference on "Evapotranspiration", Budapest, Hungary.

R Core Team (2013), R: A language and environment for statistical computing. R Foundation for Statistical Computing, Vienna, Austria. URL http://www.R-project.org/.

Richards, Lorenzo Adolph (1931), Capillary conduction of liquids through porous mediums Physics 1, no. 5 : 318-333.

Rodriguez-Iturbe, I. (2000), Ecohydrology: A hydrologic perspective of climate-soil-vegetation dynamics, Water Resources Research 36(1): 3-9. doi:10.1029/ 1999WR900210

Roerink, G., Z. Su and M.Mementi (2000), S-SEBI: A simple remote sensing algorithm to estimate the surface energy balance. Physics and Chemistry of the Earth, Part B: Hydrology, Oceans and Atmosphere 25(2): 147-157. doi: 10.1016/S1464-1909(99)00128-8

Ryu, D. and J. S. Famiglietti (2006), Multi-scale spatial correlation and scaling behavior of surface soil moisture, Geophysical Research Letters 33(8): L08404.

Sanchez, N., J. Martinez-Fernandez, A. Scaini, C. and Perez-Gutierrez, (2012), Validation of the SMOS L2 soil moisture data in the REMEDHUS network (Spain)., IEEE Transactions on Geoscience and Remote Sensing, 50(5), 1602-1611. doi: 10.1109/TGRS-.2012.2186971

Santanello, J., C. D. Peters-Lidard, M. E. Garcia, D. M. Mocko, M. A. Tischler, M. S. Moran, and D. Thoma (2007), Using remotely-sensed estimates of soil moisture to infer soil texture and hydraulic properties across a semi-arid watershed, Remote Sens. Environ., 110(1), 79-97, doi:10.1016/j.rse.2007.02.007.

Schulla, J. (1997) Hydrologische Modellierung von Flussgebieten zur Abschatzung der Folgen von Klimaanderungen. Zurcher Geographische Schriften, Heft 69, ETH Zurich, pp. 187.

Schulla, J., Jasper, K., (2000), Model Description WaSiM-ETH. IAC ETH Zurich, pp. 166.

Schwanghart, W. (2010), Surface Fitting using gridfit (http://www.mathworks.com /matlabcentral/fileexchange/25948-variogramfit), MATLAB Central File Exchange. Retrieved August , 2015.

Scott, D. W. (1979), On optimal and data-based histograms, Biometrika 66(3): 605.

Shannon, C. E. (1948), A mathematical theory of communication, Bell System Technical Journal 27:623-56.

Shannon, C. E. (2001), A mathematical theory of communication, ACM SIGMOBILE Mobile Computing and Communications Review 5(1): 3-55.

Shin, Y., and B. P. Mohanty (2013), Development of a deterministic downscaling algorithm for remote sensing soil moisture footprint using soil and vegetation classifications, Water Resources Research, 49, 6208-6228, doi:10.1002/wrcr.20495.

Shuttleworth, W. J., R. J. Gurney, A. Y. Hsu, and J. P. Ormsby (1989), FIFE: the variation in energy partition at surface flux sites. IAHS Publication 186 67-74.

Si, B. C. (2008), Spatial scaling analyses of soil physical properties: A review of spectral and wavelet methods, Vadose Zone Journal, 7(2), 547-562, doi: 10.2136/vzj2007.0040

Si, B. C., and T. B. Zeleke (2005), Wavelet coherency analysis to relate saturated hydraulic properties to soil physical properties, Water Resources Research, 41, W11424, doi:10.1029/2005WR004118.

Sobrino, J. A., M. Gomez, J. C. Jimenez-Munoz, and A. Olioso (2007), Application of a simple algorithm to estimate daily evapotranspiration from NOAA-AVHRR images for the Iberian Peninsula. Remote Sensing of Environment 110, no. 2: 139-148. doi: 10.1016/j.rse.2007.02.017

Stagakis, S., Gonzalez-Dugo, V., Cid, P., Guillen-Climent, M. L., and Zarco-Tejada, P. J. (2012), Monitoring water stress and fruit quality in an orange orchard under regulated deficit irrigation using narrow-band structural and physiological remote sensing indices. ISPRS Journal of Photogrammetry and Remote Sensing, 71, 47-61. doi:10.1016/j.isprsjpr--s.2012.05.003

Strand, E. K., Smith, A. M., Bunting, S. C., Vierling, L. A., Hann, D. B., and Gessler, P.

E. (2006), Wavelet estimation of plant spatial patterns in multitemporal aerial photography. International Journal of Remote Sensing, 27(10), doi: 10.1080/01431160500447642049-2054

Su, Z (2002), The Surface Energy Balance System (SEBS) for estimation of turbulent heat fluxes. Hydrology and Earth System Sciences Discussions 6.1: 85-100. doi:10.5194/he--ss-6-85-2002

Sutanudjaja, E. H., L. P. H. van Beek, S. M. de Jong, F. C. van Geer, and M. F. P. Bierkens (2014), Calibrating a large-extent high-resolution coupled groundwater-land surface model using soil moisture and discharge data, Water Resources Research, 50, doi:10.1002/2013WR013807.

Taylor, C M., R. A. de Jeu, F. Guichard, P.P. Harris and W.A. Dorigo , Taylor, C. M., de Jeu, R. A., Guichard, F., Harris, P. P., and Dorigo, W. A. (2012). Afternoon rain more likely over drier soils. Nature, 489(7416), 423-426. doi:10.1038/nature11377

Teuling, A. J. and P. A. Troch (2005), Improved understanding of soil moisture variability dynamics, Geophysical Research Letters 32(5). doi: 10.1029/2004GL021935

Teuling, A. J., F. Hupet, et al. (2007), Climate variability effects on spatial soil moisture dynamics, Geophysical Research Letters 34(6): L06406.doi: 10.1029/ 2006GL029080

Teuling, A. J., F. Hupet, R. Uijlenhoet, and P. A. Troch (2007), Climate variability effects on spatial soil moisture dynamics, Geophysical Research Letters, 34, L06406, doi:10.1029/2006GL029080.

Tucker, C. J. (1979),Red and photographic infrared linear combinations for monitoring vegetation. Remote Sensing of Environment 8(2): 127-150 doi: 10.1016/ 0034-4257(79)90013-0

Valor, E. and V. Caselles (1996), Mapping land surface emissivity from NDVI: Application to European, African, and South American areas. Remote Sensing of Environment 57(3): 167-184. doi: 10.1016/0034-4257(96)00039-9

Verstraeten, W., F. Veroustraete and J. Feyen (2005), Estimating evapotranspiration of European forests from NOAA-imagery at satellite overpass time: Towards an operational processing chain for integrated optical and thermal sensor data products. Remote Sensing of Environment 96(2):256-276. doi: 10.1016/j.rse.2005.03.004

Wanders, N., M. F. P. Bierkens, S. M. Jong, A. Roo, and D. Karssenberg (2014), The benefits of using remotely sensed soil moisture in parameter identification of large-scale hydrological models, Water Resour. Res., 50, 6874-6891, doi:10.1002/2013WR014639.

Western, A W., R. B. Grayson, G. Bloschl, G. R. Willgoose, and T. A. McMahon (1999), Observed spatial organization of soil moisture and its relation to terrain indices, Water Resources Research 35, no. 3 (1999), 797-810.

Western, A. W. and R. B. Grayson (1998), The Tarrawarra data set: Soil moisture patterns, soil characteristics, and hydrological flux measurements, Water Resources Research 34(10), 2765-2768.

Western, A. W., G. Bloschl, and R.B. Grayson (1998), Geostatistical characterisation of soil moisture patterns in the Tarrawarra catchment. Journal of Hydrology, 205(1), 20-37.

Western, A. W., R. B. Grayson, G. Bloschl (2002), Scaling of soil moisture: a hydrologic perspective, Annual Review of Earth and Planetary Sciences 30(1): 149-180.

Whitcher, B. (2012). waveslim: Basic wavelet routines for one-, two- and three-dimensional signal processing. R package version 1.7.1. http://CRAN.R- project.org /package=waveslim

Zhiqiang, P., L. Gaohuan and Z. Chenghu (2003), Dynamic analysis of evapotranspiration based on remote sensing in Yellow River Delta. Journal of Geographical Sciences 13(4): 408-415. doi: 10.1007/BF02837878

Zhong, L, P. Gong, and G. S. Biging (2012), Phenology-based crop classification algorithm and its implications on agricultural water use assessments in California's Cen-

tral Valley, Photogrammetric Engineering and Remote Sensing 78, no. 8: 799-813. doi: 10.14358/PERS.78.8.799

Zhu, J, and B.P. Mohanty (2002), Spatial averaging of van Genuchten hydraulic parameters for steady-state flow in heterogeneous soils. Vadose Zone Journal 1.2 (2002): 261-272. doi:10.2113/1.2.261

APPENDIX A

The results for the Scale-Wetness-Heterogeneity Cuboid for the 6.4 km support scale are provided below. The semi-variograms for the ΔSM and dominant physical factor (Table A.1) were evaluated by extending the maximum lag to 51.2 km. 49.7%, 55.4%, 28.6% of the α values obtained for the semi-variogram based relationships in Arizona, Iowa and Oklahoma respectively were found to be statistically not significant ($p>0.05$). This can be explained based on Figure 3.9 wherein the dominance of multiple factors becomes comparable at the 6.4 km scale.The comparable dominance of different physical factors is much higher in Arizona and Iowa and not as much for Oklahoma which is also reflected in the relatively less statistically insignificant α values obtained for Oklahoma. These results imply that when a clear dominant factor cannot be outlined, it is essential to incorporate the effect of secondary factors as well.

Table A.1: Dominant physical attributes that create ΔSM variability for the 6.4 km support scale

Region	**Dominant physical attribute**
Arizona	Slope
Iowa	% clay
Oklahoma	LAI

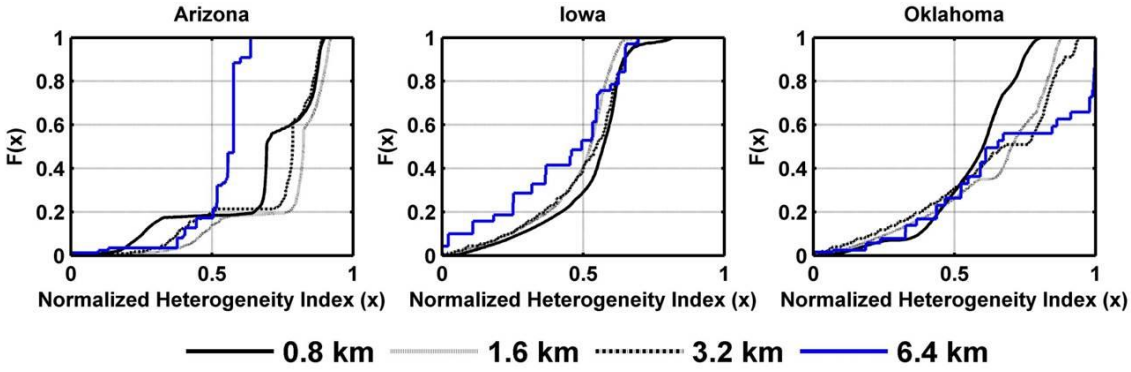

Figure A.1: Cumulative distribution function plots for the heterogeneity indices

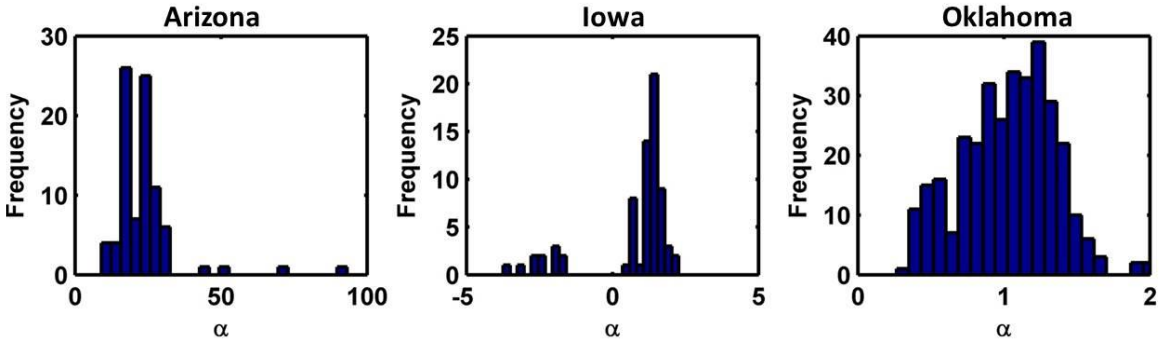

Figure A.2: Histogram of the significant α values for 6.4 km scale for Arizona, Iowa and Oklahoma

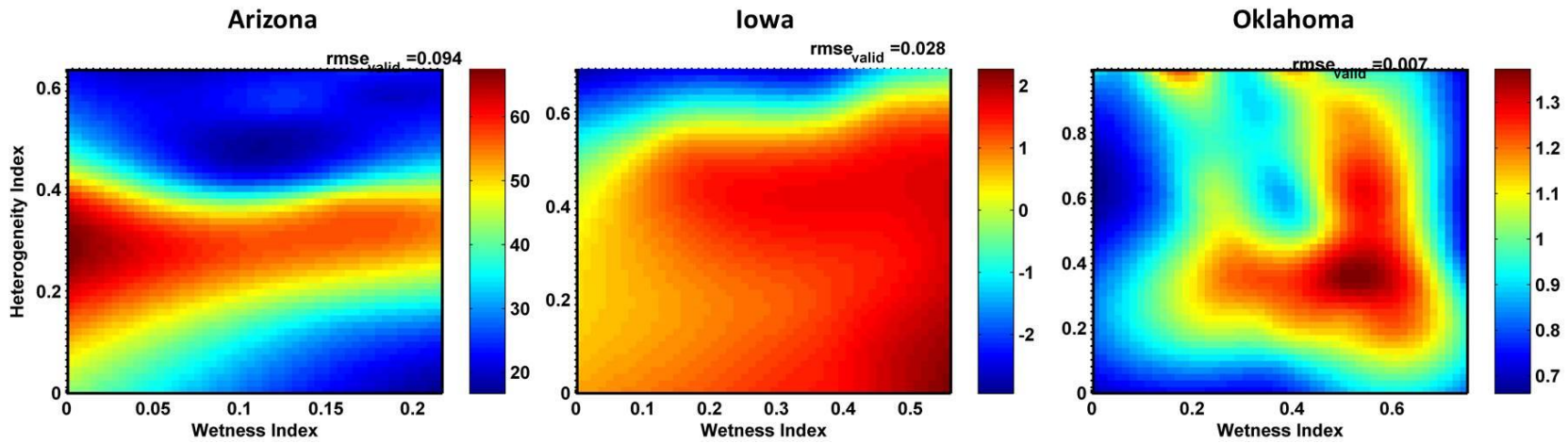

Figure A.3: SWHET cuboid results for 6.4 km support scale